2017

Integration of Shape-Memory Alloys and Self-Healing Microcapsules to Enhance Concrete Durability

Luis Adolfo Bonilla
Louisiana State University and Agricultural and Mechanical College

INTEGRATION OF SHAPE-MEMORY ALLOYS AND SELF-HEALING MICROCAPSULES TO ENHANCE CONCRETE DURABILITY

A Dissertation

Submitted to the Graduate Faculty of the
Louisiana State University and
Agricultural and Mechanical College
in partial fulfillment of the
Requirement for the degree of
Doctor of Philosophy

in

The Interdepartmental Program in Engineering Science

by
Luis Adolfo Bonilla
B.S., Louisiana State University, December 2013
M.S., Louisiana State University, December 2016
August 2017

ACKNOWLEDGEMENTS

I appreciate the guidance and support provided by my advisory committee: Prof. Ursula Emery McClure, Dr. Sherif Ishak, Dr. Ayman Okeil, and, especially, my committee chairman and adviser Dr. Marwa Hassan.

Throughout this experience I have gained not only knowledge, but also friendship with my fellow graduate students who offered practical and moral support. I specially appreciate Max Aguirre's friendship. Several other students have also been helpful over these years including: Jose Milla, Gabriel Arce, and Hassan Noorvand.

My deepest thanks to my parents, Luis Bonilla Pineda and Cecilia Diaz de Bonilla, and my sister, Martha Bonilla, who have always support me in every step of my life, and this dissertation process was not an exception.

TABLE OF CONTENTS

ABSTRACT

Self-healing is a term that has not been used for building material until a few decades ago. The concept of developing a material that mimics what living organisms do, such as identify and repair damage, rather than interesting, constitutes a necessity in today's deteriorated infrastructure. Concrete is one of the main building blocks that support our society's roads, buildings, and dams. Increasing the service life of such structures will have an important socio-economic benefit in our society. Self-healing methods in concrete have been studied in order to minimize human intervention in maintenance procedures. Previous research in this area has provided different self-healing strategies. These strategies include both internally and externally supplied encapsulation of healing agents, internally supplied microcapsules, expansive agent and mineral admixtures, bacteria, and shape memory materials. The presented research evaluated the self-healing effects of integration of microcapsules and shape memory alloys. The combined self-healing mechanisms in concrete were evaluated by developing a procedure to microencapsulate calcium nitrate and integrating them with Shape Memory Alloy (SMA), as a substitution for conventional steel reinforcement. In order to evaluate the structural behavior and healing efficiency, the initial stiffness, peak strength, and deformation were measured and compared with post-healing measurements. Furthermore, the study conducted crack monitoring in order to evaluate crack-healing over time, This procedure would be followed by performance analysis, using Energy-dispersive X-ray spectroscopy (EDX) in order to quantify the healing components in the cracked areas. Lastly, the current research conducted a life cycle cost analysis, using a probabilistic approach to evaluate the long-term economic efficiencies of self-healing concrete pavements as the competing alternatives to conventional pavement.

CHAPTER 1. INTRODUCTION

Deterioration in concrete structures may be categorized by types and causes. Some of these are inclusive of the corrosion of embedded metals, freeze-thaw deterioration, chemical attacks, overload, and impact. Among those listed, corrosion of reinforced steel and other embedded structural components present the leading cause of concrete deterioration [1]. Corrosion of steel causes an increase in the embedded steel volume. thus, increasing the tensile stress in the concrete, which leads to cracking, delamination and spalling [1]. The ASCE 2013 report card for America's infrastructure [2] estimates that one in nine bridges in America can be classified as structurally deficient, which translates in a total inversion to $20.5 billion annually on reparation work in order to achieve optimal levels of serviceability. Similarly, the overall number of high hazard dams has increased to 14,000 in 2012, which requires an investment of $21 billion in reparation work.

Self-healing methods were studied to find methods to efficiently repair concrete cracks automatically, requiring minimal human intervention. Researchers then developed different self-healing strategies. These strategies include both internally and externally supplied encapsulation of healing agents, internally supplied microcapsules, expansive agent and mineral admixtures, bacteria, and shape memory materials. The advantages of using microcapsules among the different strategies is that (1) a healing agent is released based on necessity; in other words, a healing agent is released when cracking occurs, (2) a microcapsules homogenous distribution in concrete matrix allows self-healing capabilities in many locations simultaneously. The major disadvantages of microcapsules are (1) problems and difficulties in encapsulation procedures, (2) a limited amount of healing agent available in the concrete matrix, (3) a negative effect on the mechanical properties in the cement matrix when too many capsules are added to the mix, and (4) a self-healing effect that is limited to small crack-widths [3, 4, 5]. On the other hand, the advantages of using shape

memory alloys consist of (1) an ability to decrease macro-size cracks, (2) efficient recovery effects on mechanical properties and (3) effectiveness under multiple damage events. The major disadvantages of SMAs include (1) an elevated cost of SMAs as a concrete reinforcement material, and (2) difficulties in delivering a heating stimulation which leads to an uncertain behavior of the material [5, 6, 7]. The previous characteristic of the self-healing strategies suggests that an optimal self-healing mechanism could be accomplished by combining microcapsules and SMAs with the ability to heal both micro and macro cracks at various simultaneous locations, as proposed.

1.1 Problem Statement

Enhancement of the autogenous self-healing properties of concrete through the use of microencapsulated self-healing agents is proven to be an effective way to increase the durability of concrete structures [8]. However, the limitation of self-healing by means of microcapsules greatly depends on the crack width [5]. Using Shape memory alloys as a flexural reinforcement can allow crack widths to become closer by using the shape memory effect [5]. Calcium nitrate is known to have hydration incentives properties, and therefore is utilized as an accelerator admixture in the concrete industry. In addition, calcium nitrate also enhances the formation of belite during the hydration product [9].

A limited number of studies were made on the effects of self-healing behavior using microencapsulated calcium nitrate as a healing agent. However, the hydration properties and low cost makes the application of microencapsulated calcium nitrate a suitable candidate for self-healing purposes. The evaluation of a combined self-healing mechanism using calcium nitrate microcapsules and shape memory alloys has not been considered to date.

1.2 Objectives

The main goal of this research is to test hypothesis that the combined self-healing effect of calcium nitrate microcapsules and low-cost shape memory alloys in reinforced concrete can drastically enhanced the self-healing capabilities of concrete while reducing the overall life cycle cost of the structure. In order to test the hypothesis, the following objectives are considered:

- Investigate the structural behavior of plain and reinforced concrete beams with and without microcapsules.
- Investigate the structural behavior of plain concrete, steel reinforced and SMA reinforced beams.
- Study the influence of shape memory effect on the self-healing capabilities of beams
- Quantify Economic benefit of the proposed technology

1.3 Research Approach

Proposed research activities will be organized into three phases and seven tasks as detailed in the following section.

Phase 1: Self-Healing Evaluation on Plain and Steel Reinforced Concrete Beam Using Calcium Nitrate Microcapsules

Task 1: Concrete Beams Production.

In Task 1.1, an experimental program consisting of 20 specimens was devised. The typical beam was a modified modulus of rupture specimen (ASTM C78), in which the span length was increased to 1 m (39.4 in.) to allow for a more typical flexural behavior. The beam matrix is shown in Table 1.1.

Table 1.1. Beam matrix for phase 1

Group	**Plain**	**Plain+MC**	**Steel**	**Steel+MC**
No. of replicas	5	5	5	5
Concrete	Ordinary	Self-healing	Ordinary	Self-healing
Rebar	N/A	N/A	Steel	Steel

Task 2: Structural Testing of Concrete Beams.

In Task 2, a flexural strength test following ASTM C 293 will be conducted. Two of the specimens in each group will be dedicated for strength tests to determine the flexural capacity of the beams, using a three-point bending setup. From these tests, the ultimate load (P_u) of the tested beam will be determined. The remaining three specimens of unreinforced beams will be loaded until cracks are visually observed. For the reinforced beams, a maximum load of 60% of the ultimate load will be applied to develop cracks. During this phase, undamaged and damaged stiffness properties, K_U and K_D, will be calculated using the load-deflection curve. Beams will be left under healing conditions. After the healing period ends, a second round of testing will be conducted on the beam specimens up to the failure point in order to identify any change in structural behavior (healing stiffness) in comparison to the stiffness properties before the curing period.

Task 3: Quantification and Characterization of Self-Healing Products

In Task 3, Optical microscopy will be employed to:

Measure the efficiency and quality control of the self-healing material

- Characterize damage (cracks)
- Assess the degree of self-healing

Image analysis software will be used to calculate and measure the healing efficiency.

The healing efficiency will be calculated, based on Equation (1.1):

$$f_{f=100-\frac{A_t}{A_o}*100} \quad \text{(Eq. 1.1)}$$

where,

f_f= healing efficiency (%);

A_o= Initial area of the cracks; and

A_t = Area of the cracks at the time of analysis.

After allowing the concrete specimens to heal for a period of 28 days, the specimens will be cut and samples will be analyzed, using Environmental Scanning Electron Microscopy (ESEM) equipped with EDX in order to investigate the chemical compositions of the healing products.

Phase 2: Concrete Self-Healing Evaluation of Shape-Memory Alloys

Task 4. Concrete Beams Production

In Task 4, an experimental program consisting of 20 specimens was devised. The typical beam will be a modified modulus of rupture specimen (ASTM C78) in which the span length will be increased to 1 m (39.4 in.) to allow for a more typical flexural behavior. The beam matrix is shown in Table 1.2.

Table 1.2. Experimental matrix of reinforced concrete beams for phase 2

Group ID	**Microcapsules content (% - by weight of cement)**	**Reinforcement type**	**Numbers of specimens**
Steel	0.0	#3 Steel Grade A32	5
MC-Steel	1.0	#3 Steel Grade A32	5
SMA	0.0	7mm Nickel-Titanium Alloy	5
MC-SMA	1.0	7mm Nickel-Titanium Alloy	5

Task 5. Structural Testing

In Task 5, two of the specimens in each group will be dedicated for strength tests to determine the flexural capacity of the beams. From these tests, the ultimate load (P_u) of the tested beam will be determined. Following this determination, the three remaining specimens will be similarly tested in the three-point bending set up used for strength tests. To investigate the structural performance attributes under service conditions, beams will be subjected to a load equal to 60% of the ultimate load ($0.6P_u$). Visible cracks are expected to form, and will be recorded by a digital microscope. After the healing period, a second round of tests will be conducted in order to observe any change in structural behavior, which then will be compared to the behavior of control specimens prior to healing.

Task 6. Crack Width Evaluation and Characterization of Self-Healing Products

In Task 6, all specimens will be placed in deionized water (DI) to accelerate the healing process. A digital light microscope will be used to record the evolution of the cracks after water curing. Images obtained in this period will be analyzed by quantifying and comparing the area difference in all groups. Cracks will be recorded using a digital microscope during loading, immediately after the load is removed, and periodically afterwards, while the cracked beam starts the healing period. Image analysis software will be used to calculate and measure the healing efficiency for each test condition based on Equation (1.1).

Additionally, beams will be placed into an oven in which temperatures will rise until the transition temperature of the shape memory alloys is achieved (60-70 degrees Celsius). Water will be constantly poured into crack areas in order to keep the area hydrated to induce microcapsules to create hydration products. Additionally, to record the effects of SMA recovery, pictures will be captured before and after heating to monitor the changes in crack widths. These results will be

used to capture any changes in the crack dimensions and to provide a reference point for comparison with conditions, immediately after the end of second phase of the tests and after the healing period.

Phase 3: Cost Effectiveness Analysis

Task 7. Evaluate the Economic Performance of Self-Healing SMA Reinforced Concrete and Self-Healing Microcapsules

In task 7, a LCCA will be conducted with the goal of determining the overall cost effectiveness of combining self-healing microcapsules and SMA technologies. The objective of this task is to assess the cost-effectiveness of the concrete beams. This includes initial cost (installation) as well as operation and maintenance over the service life of the structure. Economic analysis will be based on the net present value method by discounting all project costs to the base present year to account for the time effect of money and future costs associated with the concrete structures. A real discount rate will be used based upon guidelines available in the US. The LCCA for this task will consider the expected probability of rehabilitation and its expected rehabilitation cost at a certain age of the concrete structures.

1.4 References

[1] T. PCA, "Causes of Concrete Deterioration," Portland Cement Association, Skokie, Illinois., 2002.

[2] A. W. Herrmann, " ASCE 2013 Report Card for America's Infrastructure," IABSE Symposium Report (Vol. 99, No. 33, pp. 9-10). International Association for Bridge and Structural Engineering, 2013.

[3] B. Boh and B. Šumiga, "Microencapsulation technology and its applications in building construction materials Tehnologija mikrokapsuliranja in njena uporaba v gradbenih materialih.," RMZ–Materials and Geoenvironment , vol. 55, no. 3, pp. 329-344, 2008.

[4] S. K. Ghosh, "1 Functional Coatings and Microencapsulation: A General Perspective," 2006.

[5] M. Wu, B. Johannesson and M. Geiker, " A review: Self-healing in cementitious materials and engineered cementitious composite as a self-healing material," Construction and Building Materials, vol. 28, no. 1, pp. 571-583, 2012.

[6] Y. Sakai, Y. Kitagawa, T. Fukuta and M. Iiba, "Experimental study on enhancement of self-restoration of concrete beams using SMA wire," Smart Structures and Materials, no. International Society for Optics and Photonics., pp. 178-186, 2003.

[7] Y. Kuang and J. Ou, "Self-repairing performance of concrete beams strengthened using superelastic SMA wires in combination with adhesives released from hollow fibers," Smart Materials and Structures, vol. 17, no. 2, p. 025020, 2008.

[8] S. Ge, F. Wan, J. Lu and J. Yu, "Molecular self-assembled microcapsules prepared by in situ polymerization technology for self-healing cement materials," Journal of Inorganic and Organometallic Polymers and Materials, vol. 21, no. 4, pp. 841-846, 2011.

[9] H. &. N. E. C. Justnes, "Technical calcium nitrate as set accelerator for cement at low temperatures.," Cement and concrete research, vol. 25, no. 8, pp. 1766-1774, 1995.

CHAPTER 2. LITERATURE REVIEW

2.1 Introduction

Production hydraulic cement is estimated to be about two billion metric tons per year. This material is sufficient to make about 14-18 billion metric tons of concrete, which presents concrete as the most abundantly manufactured solid material [1]. The manufacturing process of cement involves two major types of activities: 1) the gathering and processing of raw materials, and 2) the manufacture of clinker and finished cement. The principal environmental issue related to these activities involves the CO_2 emissions. The total carbon dioxide emissions, related to the production of cement and inclusive of calcination and combustion emissions, is estimated to be 0.94 tons CO_2/ ton of Clicker [1]. The massive contribution of emissions also estimates to be from 5%-7% of the total CO_2 production in the world [2].

Relative to the environmental impact of concrete in the construction industry, the resultant economic impact is greatly affected by the service life of structures. According to Yunovich et al., the annual cost of reconstructing bridges in the USA estimates to be $5.2 billion. Moreover, indirect costs due to traffic jams, as well as an associated loss of productivity, coupled with ten times the direct cost of maintenance and repair, must be considered as well [3]. The compressive strength of traditional concrete varies between 20-60 MPa, while high-strength concrete can be produced to achieve a compressive strength of 200 MPa. However, concrete can sustain much less tensile loading than compressive loading. As a result, concrete structures loading in bending or in tension can develop cracks easily [2]. Therefore, in order to address the weak tensile strength of concrete, steel reinforcement must be embedded into the concrete matrix, which carries the tensile load, as soon as the first crack appears. Concrete cracking increases the permeability of concrete

by interconnecting flow paths, thereby allowing water and aggressive ions to penetrate into the concrete, thus facilitating the concrete and steel deterioration [4].

The developing of the self-healing mechanism in concrete structures presents not only an effective solution to decrease the environmental effects described earlier, but also by means of self-repairing the cracks developed over time, importantly increases the service life of concrete. Van der Zwaag found a relationship, considering the time elapsed, between structure performances (Figure 2.1). For conventional structures, two approaches may be followed: The first is to invest in a conventional design life, as represented by curve A; the second is to initially invest more money to increase the quality. This would enable the structure to last for a longer time, as represented in curve B; both curves are shown in Figure 2.1a. However, the cost of reparation does become a valid point of concern. For both cases, there is a period of time in which an investment in cost reparation is needed in order to keep the strength of the structure above the required strength line. However, an alternative method in which self-healing technologies become part of the structure design shows a very different behavior in the plots. In Figure 2.1c, the performance of the structure requires no "repair" point in order to keep the performance line above the required strength line, which results in a uniquely constant total cost (Figure 2.1d) [5].

These results clearly suggest a better overall outcome through use of the self-healing approach in building structures. Van Breugel stated that the use of self-healing materials a) increases the service life of structures, b) reduces the amount of waste, c) reduces usage of raw materials, and d) saves energy by reducing building activities for new-built concrete; once self-healing concrete is available, implementation in the building industry is expected to follow [6].

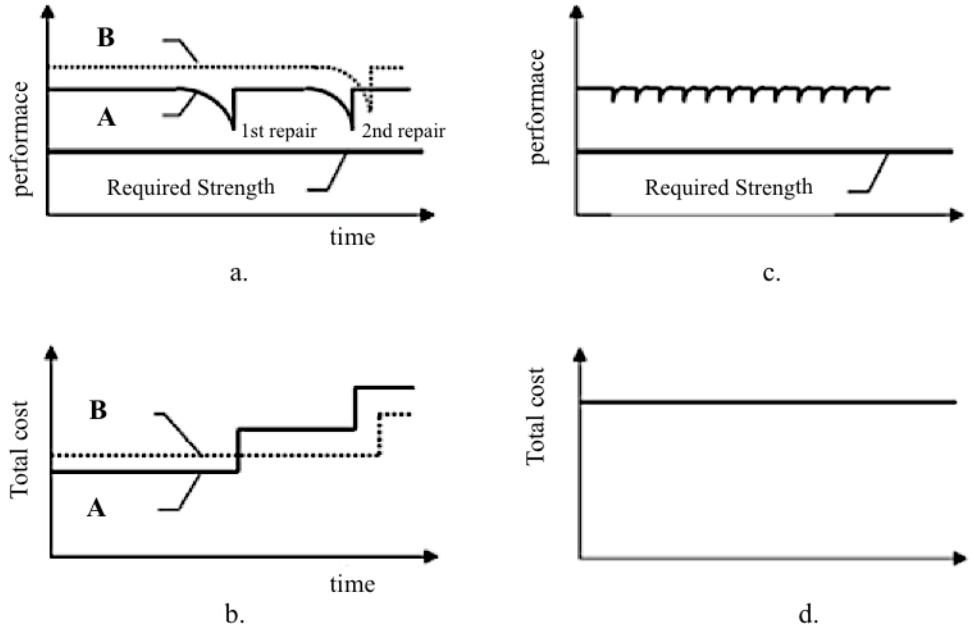

Figure 2.1. Performance (a) and costs (b) with elapse of time for convectional "A" and high quality "B" structures. Performance (c) and cost (d) of a structure made with self-healing concrete with elapse of time [5].

2.2 Self-Healing Phenomena in Cement-Based Materials

The self-healing phenomena of concrete was documented for many years. A number of researchers observed a decrease in the concrete permeability, having studied the flow of water through cracked concrete [7, 8]. Edvardsen attributed the main cause of self-healing to the precipitation of calcium carbonate ($CaCO_3$), in response to the interaction of unhydrated cement and carbon dioxide dissolved in water [7]. Moreover, not only was the permeability of concrete observed to benefit from the presence of water, but also mechanical properties such as stiffness and flexural strength were shown to benefit after the submersion of specimens under water [9,10]. In later studies, the self-healing phenomenon was also associated with the continued hydration of cement within the cracks. Moreover, the main mechanism of the autogenic self-healing in cracks is described as the production of calcium silicate hydrate (C-S-H), which in turn provides strength to hydrated cement

paste. In that manner, the mechanical properties of concrete may be regained [11]. M. de Rooij et al. noted that the formation of C-S-H occurs when tricalcium and dicalcium silicate react with water to form C-S-H and calcium hydroxide. The general equations (Eq. 2.1 and Eq. 2.2) for these reactions are stated as follows:

$$2Ca_2SiO_5 + 6H_2O \rightarrow 3CaO\ 2SiO_2\ 3H_2O + 3Ca(OH)_2 \quad \text{(Eq. 2.1)}$$

$$2Ca_2SiO_4 + 4H_2O \rightarrow 3CaO\ 2SiO_2\ 3H_2O + Ca(OH)_2 \quad \text{(Eq. 2.2)}$$

The natural encapsulation of alite (C_3S) and belite (C_sS) occurs when those particles are not able to react with water, and thus become trapped between C-S-H and CH materials. These un-reactive particles will be capable to heal micro-cracks later, since an exposure to the atmosphere initiates the hydration process [2]. Moreover, Victor Li determined that certain conditions must be met in order to achieve reliable autogenic self-healing [12]. Those conditions are as follows:

- Essential environmental exposure
- Essential chemical species
- Maximum crack width

An environmental condition may range from being fully submerged in water to cyclic wet-dry conditions. This condition is demonstrated to be true in several studies that revealed the high importance of water in autogenic self-healing [7, 8, 13], which in turn corroborates earlier hydration equations. The chemical species required to induced autogenic self-healing are: a) bicarbonate ions, b) carbonate ions, c) free calcium ions, d) unhydrated cement, and e) free chloride ions, which are fully available due to the chemical composition of cementitious materials [12]. Finally, different studies were launched in order to determine the maximum capability of a crack width to heal.

Jacobsen determined that the maximum crack width for self-healing ranges between 5-10 μm [13], while Clear concluded that self-healing capabilities can work, up to 300 μm [14]. The maximum crack width required to successfully show self-healing was estimated to vary in range from 5-300 μm. Hua et al. used the schematic in Figure 2.2 to describe the various factors that may occur in the complicated self-healing phenomena in concrete cracks: 1) Sector "a" in the figure represents the precipitation of calcium carbonate or calcium hydroxide; 2) "b" shows the crack sealing due to lose particles in the concrete crack; 3) "c" displays the further hydration of cement; and 4) "d" represents swelling of calcium silica hydrate [15].

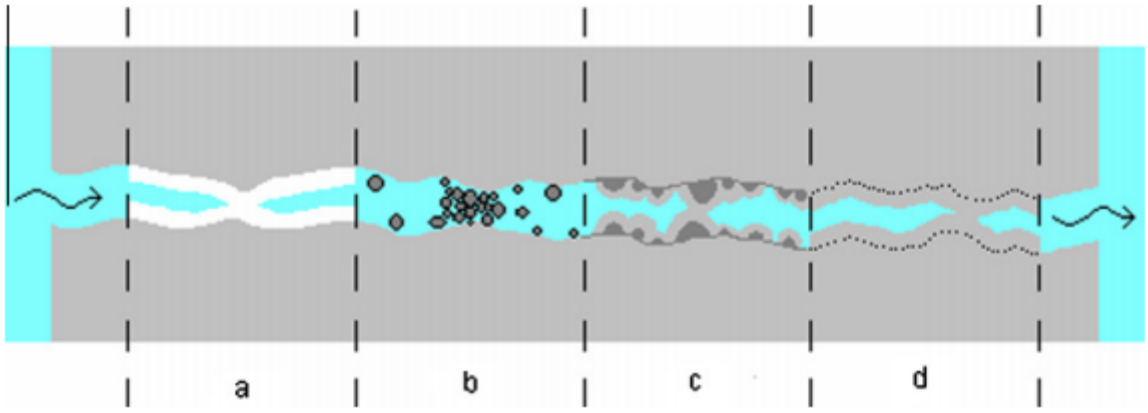

Figure 2.2. Autogenic self-healing mechanism of cementitious materials [15]

2.3 Self-Healing Mechanism in Concrete Structures

Among the research community, the interest increases to both improve and to take advantage of the self-healing capability of concrete. The result has culminated in research and experimental work that optimizes concrete healing by means of different methods and approaches as an ultimate goal. In 1994, Carolyn Dry found that releasing adhesives from glass pipettes under cracking conditions resulted in an increase of flexural toughness for second loading events, as opposed to the decrease of flexural toughness in control samples (without adhesives) [16].

Abd-Elmoaty studied the autogenous healing of polymer modified concrete (PMC), which consists of dispersing organic polymer inside the mixing water of concrete. The researcher reported an increase in the autogenic healing of concrete, orchestrated by increasing the unhydrated cement available in the matrix; in turn, the process would extend healing capabilities for a longer period of time by increasing the service life [17]. Since then, methods of encapsulating different healing materials and the subsequent interactions after cracking were developed by multiple researchers. Victor Li et al. successfully demonstrated that when released into cracks, air-cured polymer would recover the elastic modulus of concrete specimens [18, 19]. The most relevant methods developed will be discussed in the following sub-sections.

2.3.1 Internally Supplied Healing Agents

An internally supplied healing mechanism may be categorized under the autonomic healing concept. White et al. presented an autonomic healing concept by describing a microcapsule healing mechanism in which healing agents are microencapsulated. The microcapsules are further embedded in a structural composite matrix with a required catalyst capable of polymerizing the liquid healing agents. Figure 2.3 shows an illustrated example of this mechanism [20]. Self-healing of concrete using microcapsules proved to increase self-healing capabilities, as well as the durability of concrete. Yang et al. studied the relationship of fatigue strain versus cycling loading in cylindrical mortar specimens containing concrete sealers (MMA and TEB) microcapsules. The results showed a decrease in the strain-increment curve, in which control samples fail at around 5000 cycles, while those with microcapsules failed at around 22500 cycles. The main reason for this behavior was attributed to inhibition during the initiation and propagation of the crack in the mortar matrix [21].

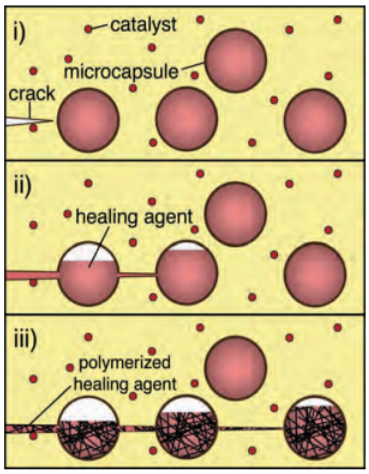

Figure 2.3. (i) Cracks start forming in the matrix. (ii) The path of the crack passes through the microcapsules, releasing the healing agent into the open crack space. (iii) The healing agent reacts with the catalyst in the matrix and polymerization reactions trigger [20].

The selection of a healing agent represents an important factor in the overall self-healing capabilities of the mix. For example, Cailleux and Pollet studied the effects of using tung-oil, calcium hydroxide ($Ca(OH)_{2)}$, and bisphenol-F epoxy as encapsulated healing components of spherical microcapsules. Results showed that some of the capsules were broken in the mixing procedure. Tung-oil was shown to react with air, calcium hydroxide with carbon dioxide, and finally the epoxy resin was activated in contact with a hardener. Even though a similar process was used for all three healing agents, the most effective and efficient agent was found to be epoxy resin, which was able to adhere to fracture surfaces of beam specimens [22]. Wang et al. studied the effects of microcapsules containing bacterial spores. The results displayed a better healing ratio in specimens containing bio-microcapsules (48%-80%), compared to the control samples (18%50%), and coupled with an overall decrease in permeability and an increase in maximum crack width healing [23]. Moreover, Huang and Ye introduced an encapsulated sodium silicate (Na_2SiO_3) solution into spherical capsules with a diameter of 5mm, which were further sealed with wax. The fragility of these capsules necessitated a hand-mixed procedure in order for the capsules to survive.

After cracking occurred, the release of sodium silicate, following a rupture of the capsules, then reacted with calcium hydroxide (naturally present in concrete) to form calcium silica hydrate, which in turn healed the crack; However, a negative impact was shown by decreasing the compressive strength of the specimens containing these capsules [24]. In a similar study performed by Pelletier et al., sodium silicate was encapsulated in smaller size capsules ranging from 40 to 800 μm. Most of these microcapsules resisted the mixing design while maintaining the compressive strength, thus remaining unaffected. Pelletier also observed that the microcapsules released the healing agent after a cracking of the specimen, thereby healing the crack by the formation of C-S-H. Further testing of the flexural strength of samples showed an improved healing efficiency of samples containing microcapsules by yielding a 26% recovery in contrast to control samples, showing only a 10% recovery [25].

A major problem that researchers face is the ability of released healing agents to react with a catalyst in order to seal crack openings. For example, Mihashi et al. tested urea formaldehyde formalin shell microcapsules containing two types of epoxy resin. However, the epoxy had difficulty hardening, due to the lack of mixing components in the crack [26]. In another study using a similar encapsulation procedure involving a urea formaldehyde shell and two epoxy healing agents, the researchers activated a hardening of the epoxy by diluting and thus modifying the resin. This procedure decreased the viscosity and thereby allowed an improved mix of the components inside the crack area [27].

Different encapsulated, internally-supplied mechanisms have also been studied over the years. Yang et al. developed a procedure in which a silica gel shell was used to encapsulate triethylborane (TEB) and methyl methacrylate resin (MMA); these hold a viscosity similar to water that facilitates a migration into micro cracks though the capillary action when capsules rupture

[28]. Similarly, White el al. first tried the effects of embedding hollow fibers filled with a liquid adhesive dicyclopentadine (DCPD) into a cement based matrix. The method proved to be an effective procedure to deliver healing material through the crack. White et al. also mentioned a microencapsulation process of DCPD, in which an in-situ polymerization of urea with formaldehyde containing an acid-catalyzer was used to form the capsule walls [20]. Moreover, Brown et al. improved the microencapsulation procedure to achieve high-quality microcapsules of a urea formaldehyde shell with a DCPD core by performing the in-situ procedure in an oil-in-water emulsion [29]; the process is described in Figure 2.4. Brown et al. also developed a linear correlation between the agitation rate and the diameter of the microcapsules created in the process that ranged from 1000 μm at 200 rpm to 10 μm at 2000 rpm.

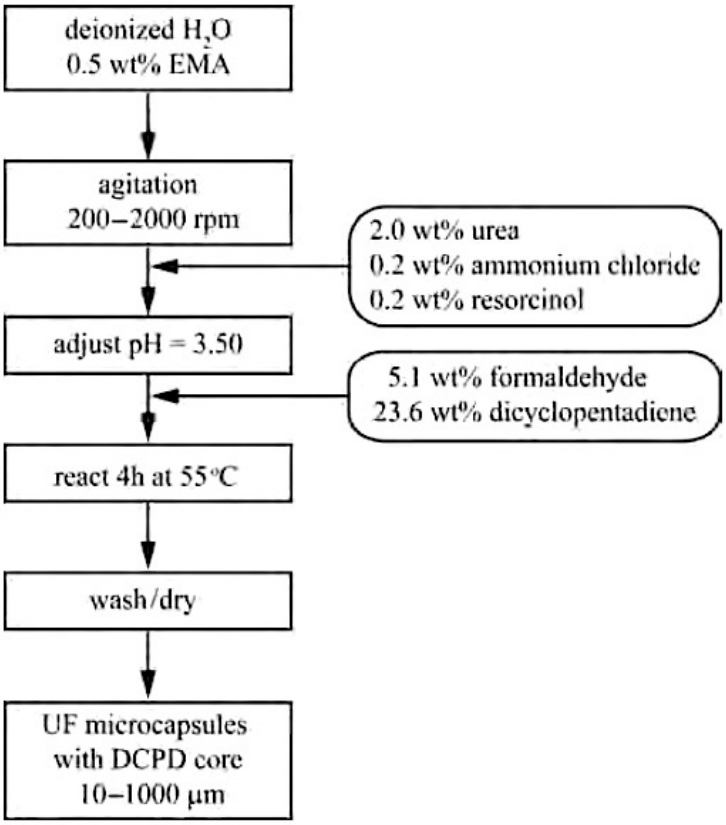

Figure 2.4. Microencapsulation process using in situ polymerization of urea formaldehyde [29]

Hassan et al. applied an in-situ polymerization process in order to encapsulate calcium nitrate ($Ca(NO_3)_2$. The effects of these microcapsules in concrete showed both a higher modulus of elasticity and a lower surface permeability in comparison with control samples [30]. Additionally, Milla et al. studied the effects of calcium nitrate microcapsules by testing the before and after healing of concrete cylinders. The results showed an overall decrease in the compressive strength of the concrete microcapsules. However, the microcapsules improved the self-healing capabilities of the concrete after curing for specimens by increasing the modulus of elasticity at a concentration of 1% microcapsules by weight of cement [31].

A study performed by Wu et al. on the different effects of microcapsule use, based the main strategy for inducing self-healing on the following conclusions. Microcapsules hold an advantage by releasing a healing agent when necessary, which not only is effective in reaching many locations in the cementitious matrix, but also is shown to be effective under multiple damaging scenarios. On the other hand, the main disadvantages are that 1) the microencapsulation process is not only difficult, but also yields a limited amount of healing agent; 2) The bond between the microcapsules and the cement matrix is a point of concern; and 3) An overall decrease on the mechanical properties of the matrix might occur if too many capsules were added to the mix [32].

2.3.2 Externally Supplied Healing Agents

A different delivery method to introduce healing agents into cracks requires an external application. Nishiwaki et al. proposed a system with self-diagnosis composites and an organic film pipe that applies the repair agent around the cracking area. The mechanism consists of increasing the temperature in the heating device (Self-diagnosis composite) in order to induce a melting of

the embedded organic film pipe, which in turn will release the repair agent to harden and heal the crack opening [33]. This self-healing mechanism is illustrated in Figure 2.5.

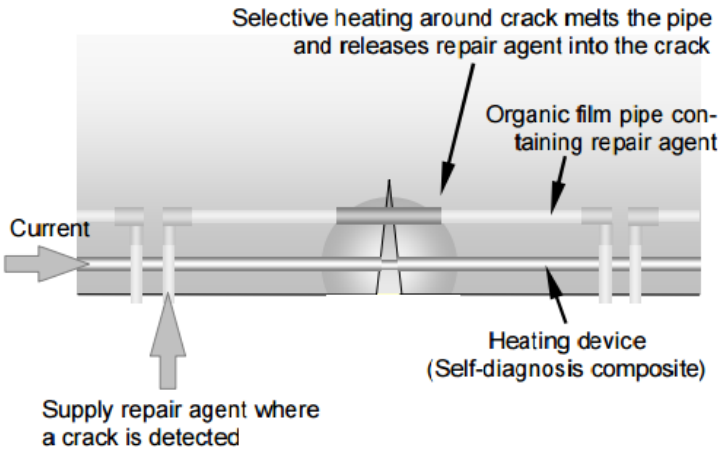

Figure 2.5. Externally applied self-healing mechanism [33]

Another approach taken by Joseph et al. consisted of building reinforced concrete beams, installed with four hollow capillary tubes. An end-opening to the atmosphere was placed to prevent negative pressure from releasing the healing agent − in this case, cyanoacrylate [34, 35]. The parameters studied by Joseph et al. took into consideration the effects of the loading rate, the reinforced level, and the specimen age on self-healing. After conducting a three-point, bending, loading test to induce cracking and allow specimens to heal for 24-hours, the researchers concluded that a lower loading rate allows the healing agent to have a greater time to bond with the matrix, thus resulting in an increase of self-healing stiffness. Moreover, a higher reinforcement level similarly allows crack growth to form more slowly than a low level of reinforcement, and also allows cyanoacrylate to propagate throughout the crack; this would permit more healing time. Finally, the effect of the specimen's age reflects no negative trend on the healing capabilities of the hollow tube containing samples, in contrast to the autogenic, self-healing capabilities of concrete, which depend heavily on the specimen age [34].

A different approach was used by Dry et al., who determined that having an external reservoir of healing agent, and delivering the healing agent after cracking occurs, fills the generated crack [36]. Sangadj and Schlangen applied the same concept by delivering an external healing agent from a reservoir. However, the researchers proposed placing a hollow network though porous concrete, by building specimens with a solid outer layer and an inner spongy layer, thus imitating the nature of human bones. The healing agent then is delivered by a pump in the inner layer after sensors detect damage. As shown in Figure 2.6, the healing agent was able to reach the crack opening, due to the high network connectivity of the matrix and by this means, further healed the crack opening.

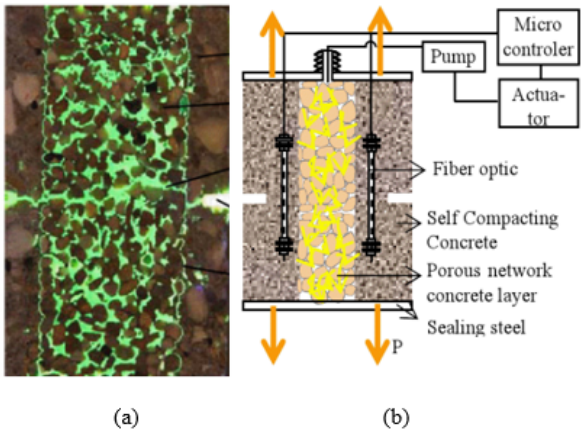

Figure 2.6. (a) Porous concrete network connectivity, (b) Self-healing mechanism

Wu et al., in a comprehensive review regarding an externally supplied system of self-healing mechanisms, found that the major advantages were that the healing material is released upon necessity. Further, the healing amount is not limited as in the internal supplies (microcapsules), but was adjusted, depending on the necessity of the cement base structure. However, this strategy also presented challenges in casting procedures. Further, negative effects could become problematic in the mechanical properties of cement matrix, should too many hollow fiber/pipes be embedded into the matrix [32].

2.3.3 Self-Healing of Cementitious Material Using Bacteria

The main idea of using bacteria for self-healing purposes in cementitious materials is based on the ability of some bacteria to produce (precipitate) calcium carbonate [37]. Dick et al. applied a mechanism that involved microbial hydrolyses of urea to obtain a calcite layer to restore and protect degraded limestone. Further studies done by Stocks-Fischer et al. followed the same principle, in which a hydrolysis of urea in the bacteria would yield carbonate and ammonium, while calcium ions are surrounded in the cell wall, in order to allow the formation of ureolytic carbonate precipitates on the bacterial cell [38]. Ramachandran et al. investigated micro-organisms (S. pasteurii and P. aeruginosa) that induced mineral precipitation in a cement matrix that increased the compressive strength of Portland cement mortar cubes from 55 MPa to 65MPa. However, as the dead-biomass increased over time, a reduction in the compressive strength was attributed to the increase in the mix porosity. Nevertheless, the presence of bacteria resulted in an increased concrete resistance against alkali, sulfate, freeze thaw cycles, and drying shrinkage. These benefits were attributed to the formation of a calcite layer on the surface of the specimen, thereby lowering the permeability of the mortar [39].

Bang et al. studied the effects of immobilizing bacillus pasteurii bacteria by means of apolyurethane foam in concrete cubes. Although the results showed an increase in the compressive strength, no considerable change was evidenced in the elastic modulus or the tensile strength of the specimen. The researchers concluded that the calcite precipitated by the bacteria was not bonded to the matrix, but rather was precipitated into the cracked space [40]. In more recent studies, researchers have considered the durability aspect more than the mechanical properties. For example, Jonkers et al, directly applied bacterial spores to a cement paste mixture. The bacteria were found to be viable up to a period of four months. Further analysis revealed evidence that

cement stones with bacillus bacteria are able to convert calcium lactate to calcium-carbonate-based precipitates upon the intrusion of water after cracking, thereby decreasing the overall permeability [41]. Wu et al. mentioned that the principal advantage of using bacteria as a self-healing strategy in concrete was that the process created a pollution-free and natural way to heal cementitious materials. However, the major disadvantages were that 1) extraordinary measures must be taken in order to protect the bacteria in concrete, and 2) the recovery of mechanical properties is not efficient in addressing multiple damaged conditions [32].

2.3.5 Shape-Memory Alloys

Lagoudas defined shape memory alloys (SMAs) as a unique, active material, capable of recovering the original shape when the temperature is increased, even though high loads may be applied to the material [42]. The two transformation phases of SMAs are martensite (M), which occurs at low temperatures, and austenite (A), that occurs at high temperatures. The change in shape when temperature is changed is due to shear lattice distortion. This phenomenon is termed *martensitic transformations* [42]. The shape memory effect (SME), is exhibited when an SMA undergoes deformation (loading) while in the twinned martensitic phase, which is an orientation formed by a combination of self-accommodated martensitic variants, unloaded while at a temperature below the austenitic start temperature (As).

When the alloy temperature increases above the austenitic finish temperature (Af), the SMA will regain the original shape by returning to the parent austenitic phase. These transformation phases may be better understood and visualized in Figure 2.7 [42].

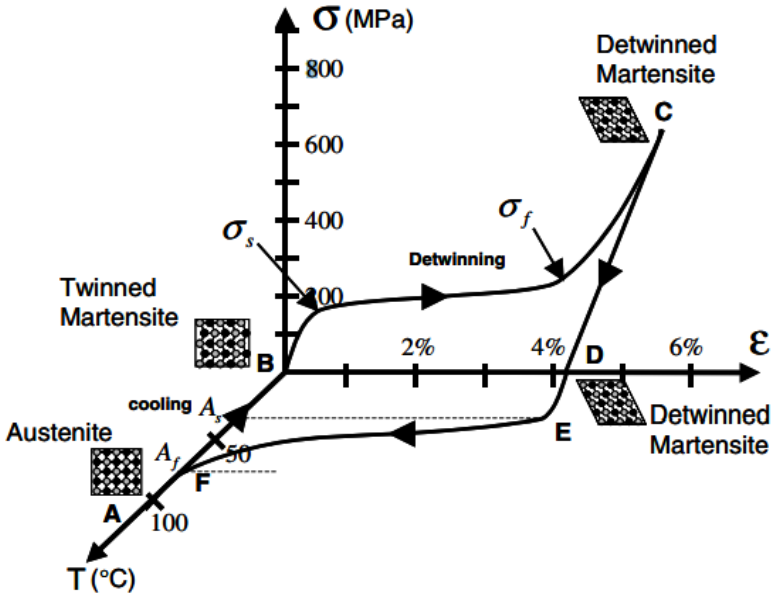

Figure 2.7. Stress-strain-temperature SME for a uniaxial loading of nickel-titanium shape memory alloy [42]

Several applications in civil structure are being studied by researchers at present. A study developed by Song et al. indicated that SMAs may be used for active, semi-active, and passive civil applications. In active applications, the term *intelligent reinforced concrete* is introduced. This active mechanism consists of embedding SMA wires as the flexural reinforcement in concrete beams. By monitoring the electric resistance of the wires, the strain distribution of concrete may be determined; upon crack generation due to a sudden high loading (explosion or earthquake), an electric current is induced to the wires to increase the temperature above the auntensitic finish temperature. Upon contact, the current reduces the crack-width of the structure [43]. A study by McGaving and Guerin provided an example of a semi-active application of SMAs in an experiment where the resonant frequency of a steel structure was adjusted by an SMA actuator installed in the structure; the SMA actuator increased the stiffness of the structure, so that the vibrating frequency could be reduced to as much as 32% lower [44]. Lastly, SMAs may be used for passive civil

applications by embedding the SMA actuators for energy dissipation purposes. Clark et al. developed a set of SMA braced reinforced structures, in which 210 loops of Nickel-Titanium wires (NiTi) were wrapped around two cylindrical supports. The configuration showed great versatility, a self-centering capability, high stiffness for small displacement, and good energy dissipation [45].

Jefferson et al. utilized the SME property by implanting a shape memory polymer into a prismatic mortar specimen. By thermally activating the polymers, Jefferson induced an axial shrinkage force of up to 34 MPa. Further, the effects of heating by means of curing cycles from four to eight days increased the overall strength of the mortar by 25% [46]; the proposed schematic is shown in Figure 2.8.

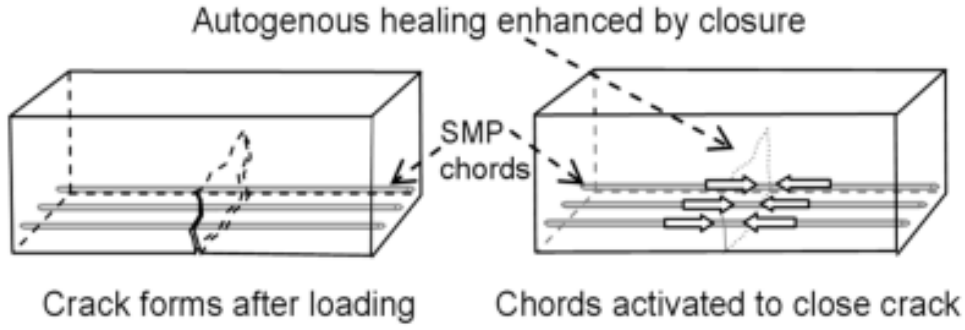

Figure 2.8. Shape-memory polymer-cementitious composite [46]

Similarly, Saiidi et al. discussed the behavior of the SME of NiTi when used as the main reinforcement of concrete beams. The conclusion drawn from the experiments revealed that the average residual displacement for the NiTi beams was less than 20% of those beams reinforced with a regular steel reinforcement. Moreover, the NiTi beams also showed super elastic behavior in the recovery strain, by achieving several times the yield strain of the material, while the residual strain of the steel averaged 4.25 in greater values. However, the stiffness of the NiTi beams became considerably lower, due to the lower modulus of elasticity compared to steel [47].

Kuang and Ou studied the effect of using SMA wires and fiber containing adhesives to evaluate the potential self-repairing capacity of concrete. The beam dimension used for this experiment consisted of a quadratic 100x100 mm cross-section by 400 mm in length, using SMAs as the main reinforcement as well as a singular two mm in diameter, in order to improve the bonding between the concrete and the nitinol wires; steel blocks then were attached to both ends on the beam where the SMAs were fixed [48]. Kouan and Ou found that the concrete beams containing SMAs added a self-restoration capacity to the beams, resulting in an almost-completed crack closure after unloading the specimens. Moreover, the combined effect of SMA and the fibers containing adhesives showed a considerable improvement in the crack healing. Reloading of these specimens resulted in newly appearing crack sectors, while previously cracked areas remained closed. Figure 2.9 shows the different stages of the cracked area [48].

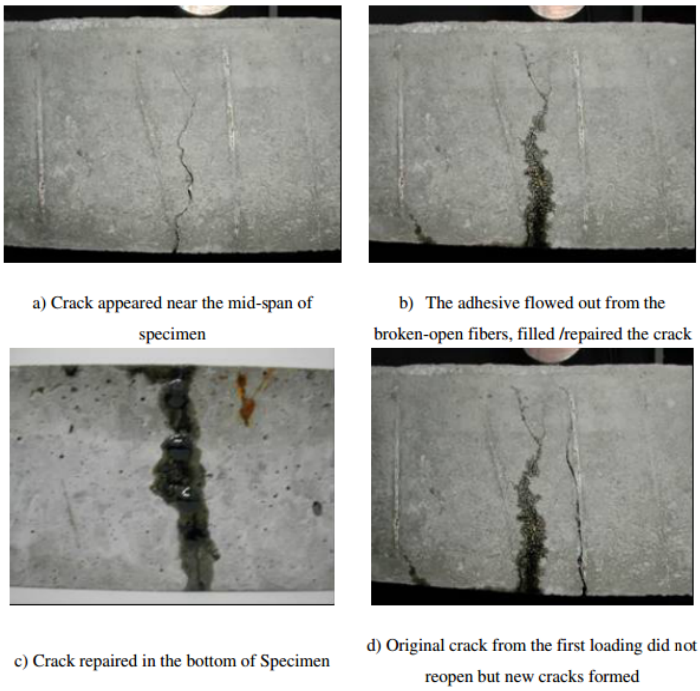

Figure 2.9. Crack evolution for SMA-fibers concrete beams [48]

Wu et al. mentioned that the major advantages of using shape memory alloys for a self-healing application was that SMA wires are able to close macro-sized cracks. Moreover, the mechanical properties of specimens show higher mechanical properties in healing than other self-healing strategies. SMA wires are also effective when dealing with multiple damage scenarios to specimens. On the other hand, the major disadvantages include a high cost needed to properly reinforce specimens in comparison with commercially used material such as steel, as well as the difficulties and uncertainties of a heating mechanism when used to stimulate a shape memory effect and hence, the self-healing of concrete [32].

2.4 Techniques Used to Analyze Self-Healing of Cracks in Concrete

Several techniques have been used to verify and quantify the effects of self-healing technologies on mortar and concrete. These techniques are applied in order to verify that concrete has been repaired or sealed, and to quantify the effectiveness of healing in terms of the mechanical properties of concrete. The following subsections will discuss the application of research techniques on self-healing, cementitious materials.

2.4.1 Optical Microscopy and Scanning Electron Microscopy

Microscopy technologies used for several decades are now in concrete applications. For example, Katherine Mather used light microscopy to study concrete petrology, mineralogy, and chemistry properties [49]. At present, both optical microscopy and electron microscopy are widely used in concrete and cement research. SEM displays several major advantages over optical microscopy, which reveal much higher quality productions in resolution images and X-ray detection capabilities, as well as an increased depth of field focus.

On the other hand, optical microscopy also holds advantages over SEM, which include an ability to obtain color images, as well as to increase the field of view for qualitative distribution analysis [50]. A later usage of light microcapsules was accomplished by Nijland et al., who assessed a microcopy analysis of historic mortar. In his findings, the formation of self-healing products was visible solely on the samples containing lime, while on those structures where a cement-based binder was applied, no self-healing was visible, leading to the finding that a free lime source becomes indispensable for self-healing. Moreover, the self-healing hydration products in specimens containing lime were most likely caused by the formation of calcium carbonate ($CaCO_3$) or portlandite ($Ca(OH)_2$) [51]. Moreover, Kishi et al. used optical microscopy to assess the degree of self-healing when combining photomicrography with a quantitative image analysis in concrete, together with expansive agents. Wiktor and Jonkers also used this technique to observe and quantify crack healing on bacterial concrete, a study in which cracks were observed to have self-healing capabilities up to a 160 μm crack-width [52].

Further investigations by Wiktor and Jonkers on bacterial concrete revealed that by combining two components of bio-chemical agents (bacterial spores and calcium lactate), the crack-healing capabilities could be increased up to 460 μm. The main reason for the self-healing phenomena was attributed to a bacterial metabolic conversion of calcium lactate to calcium carbonated minerals [53]. Both studies by Wiktor and Jonkers show a time-lapse of the crack healing process, in which a white residue may be observed to seal the crack over time, seen in Figure 2.10. In a similar study, Ahn and Kishi used expansive agents, geo-materials, and chemical agents in order to test the self-healing properties of concrete cylinders. Concrete cylinders were damaged to achieve crack-widths ranging between 0.1mm to 0.3 mm. After allowing specimens to cure for 28 days, a rehydration product was clearly observed on the light microscopy images.

Further image analysis revealed the effectiveness of self-healing on cracks up to 2 mm wide. In this case, the self-healing phenomenon was attributed to the crystallization of aluminosilicate with calcium ions [54].

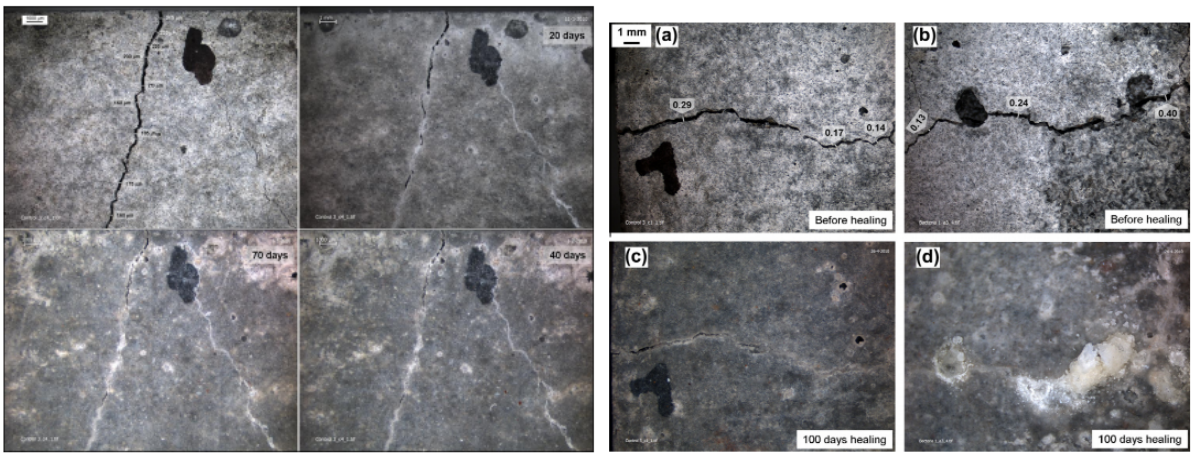

(a) **(b)**

Figure 2.10. Optical microscopy images of self-healing bacterial concrete (a) Crack sealing capabilities up to 160 μm crack width; (b) Crack sealing capabilities up to 460 μm. [52, 53]

Efficiency and quality control problems in the self-healing of concrete may be addressed by using an environmental electron microcopy (ESEM). For instance, Jonkers [55] used ESEM to characterize and compare the sample with B. Cohnii spores, both before and after cracking. ESEM images showed an overall decrease in the diameters of spore and an increase in the hydration products in the form of minerals that sealed micro cracks. Metchtcherine and Lieboldt [56] performed an ESEM imaging both before and after water curing on concrete specimens, which served to reveal a new, crystal-like formation around cracking areas. The accuracy and quality of ESEM technology allowed the author to accurately quantify the self-healing efficiency, as well as to identify the calcium carbonate crystals that close the crack.

De Muynck's investigation of the bacterial carbonate precipitation in concrete showed that SEM holds capabilities to identify hydration products, as well as calcium carbonate crystals on

mortar specimens treated with bacillus sphaericus bacteria. [57].Zhengxian et al. [21] implemented the design of microcapsules with an oil core and a silica gel shell containing methyl methacrylate (PMMA) monomer and triethylborane (TEB), applied as both the healing agent and the catalyst.

The self-healing effects were confirmed using an optical and field emission, scanning electron microscope (FESM), coupled with an energy-dispersive X-ray analyzer (FESEM/EDX). The optical microscope was used to identify the encapsulation of the oil phase. including the healing agents and the catalyst which were combined by means of a special fluorescent dye. Using image analysis tools, the team measured microcapsules, concluding that an average microcapsule diameter consisted of 4.15 μm. Figure 2.11a shows optical images of PMMA and TEB microcapsules. Moreover, specimens were loaded to 80% of the ultimate compressive strength.

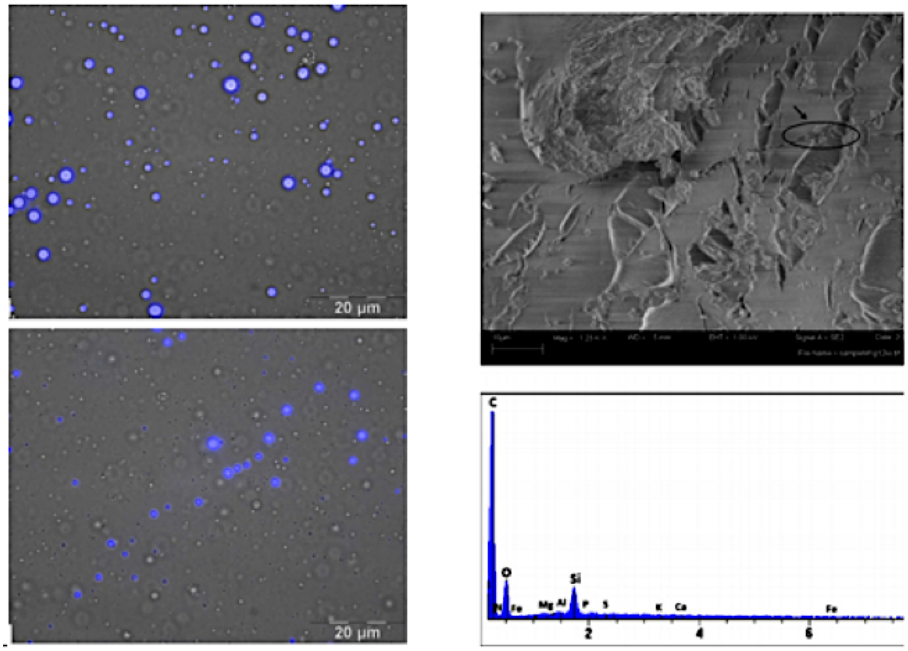

(a) **(b)**

Figure 2.11. Self-healing cementitious mechanism (a) Optical microscopic image of microcapsules; (b) FESEM image of crack surface and EDX spectrum of filled crack void [21]

Using FESEM/EDX, the study observed that ruptured capsules filled surface voids of cracks. An EDX analysis revealed that the chemical composition of the filled void area mainly consisted of C, O, and Si, indicating that the voids were sealed by PMMA and silica gel shell. Figure 2.11b shows an FESEM image of the cracked surface area and an EDX spectrum of the filled void.

Quian et al. [58] investigated the deflection recovery of pre-cracked, fiber-reinforced beams containing a blast furnace slab (BFS) and limestone powder (LP). Beams were tested by using a four-point bending test in order to pre-crack the specimens at 28 days. Results showed that specimens left for water curing recovered a deflection capacity of 65-105%, which was lower than the air-cured beams that showed only a 40-60% recovery. Further observation and analysis using ESEM and EDX confirmed that cracks of beam submerged in water were filled with calcium carbonate; in addition, healing products formed and grew from the sides or faces of the cracks.

Moreover, in order to address the self-healing behavior of the material, Kan et al. investigated the crack characteristics, resonant frequency recovery, and effect of the wet-dry cycles of engineering cementitious composites. Kan et al. utilized an environmental scanning electron microscope, coupled with an energy dispersive spectroscopy system, transmission electron microscopy (TEM), fourier transform infrared spectroscopy (FTIR), and X-ray difraction (XRD), in order to characterize the self-healing products in the specimens. The result showed that the main composition of the healing products consisted of calcium silica hydrate and calcite. These hydration products closed cracks up to 50 μm. Crack widths below 15 μm were confirmed to be filled mostly by C-S-H, while crack widths between 15-30 μm were found to have a combination of C-S-H and calcium carbonate. Wet and dry cycles significantly contributed to the self-healing effect.

2.4.2 X-Ray Diffraction

X-ray diffraction phenomenon occurs when the atomic planes of a crystal cause incidental beams of x-rays to interfere with one another as the beams leave the crystalline material. The recoding of x-rays spectrums allows a determination of the spacing between the layers or rows of atoms, thus permitting the crystal structure of an unknown material to be determined [50]. Ahn and Kishi studied autogenous, self-healing, concrete behavior using various geo-materials as admixtures, which resulted in the overall decrease of concrete cracks. Cracks below 0.15mm wide self-healed in the first three days of the curing period. Crack widths greater than 15 mm decreased considerably in size after 33 days. Ahn and Kishi [59] used the XRD analysis over time to identify the evolution of the main hydration products. The results indicated that for specimens containing expansive agents and geo materials, AFt phases peak in the XRD spectrum, decrease after three days, and begin to disappear after seven, which indicates that these phases may be transferred from hydrated aluminate phases to Stratlinite.

Perez et al. [60] utilized silica microcapsules containing the epoxy sealing compound (CAP), together with amine-functionalised nonsilica (NS) particles, to enhance self-healing capabilities in Portland cement pastes. By X-ray diffraction analysis, Perez et al. [60] described the hydration behavior of cement pastes with no additives (REF) where spectrum is illustrated in Figure 2.12. The behavior of the REF group showed a decrease in the contribution of anhydrous alite, belite, and aluminate phases, and an increase contribution of the portlandite phase. The XRD spectrum of cement pastes containing a low proportion of CAP and NS (MIX5) showed that a slight decrease of the anhydrous phases tends to peak at 28 days, showing a clearer decrease as the portlandite phases peak. Lastly, a mixture containing a double dose of microcapsules (MIX10) in the cement matrix showed similar results, with a single variability in the portlandite phase peak

behavior. Perez et al. [60] concluded that the different behavior in the specimen with microcapsules must relate to the consumption of portlandite phase by means of a pozzolanic reaction induced by the healing agents.

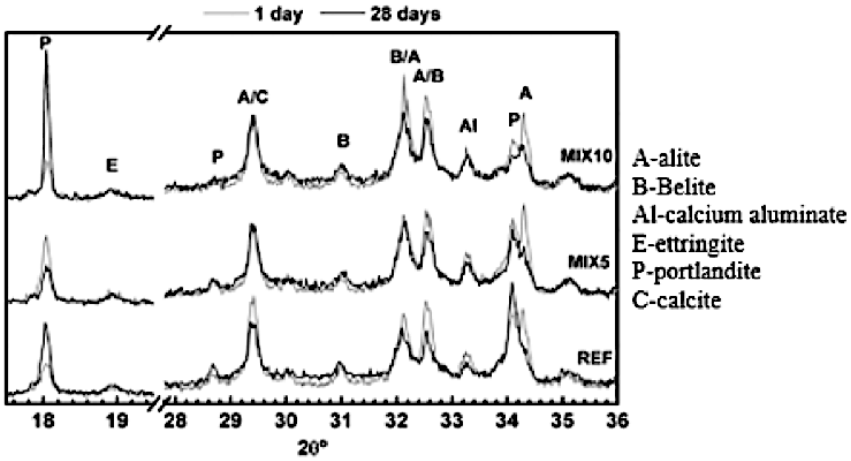

Figure 2.12. XRD of REF, MIX5 and MIX10 at 1 and 28 of hydration [60]

2.4.3 EDS Analysis on Cementitious Materials

Sidney Diamond [61] applied significant research to identify hydrated cement constituents using an electron dispersive x-ray spectrometer (EDS); the researcher accomplished the task by analyzing the ratios of calcium oxide to silicon, sulfur, and aluminum oxides. Diamond concluded that the K-peak heights of calcium, when compared to silicon, sulfur, and aluminum, establish linear functions of the corresponding ratios; in addition, the observed CaO/SiO_2 ratios identify as calcium silica hydrate (C-S-H). In a more recent study, Huang et al. investigated the effects of self-healing due to further hydration in cement paste. The EDS analysis revealed that the chemical composition of the crystals showed a much higher Ca/Si ratio in comparison to the gel-like healing product. Ca/Si ratios of the crystal-like products range from 9-16, while the gel-like healing products range from 2-3; these findings reveal a completely different chemical composition between both products. The ratio plot of the healing products is shown in Figure 2.13.

Palin et al. [62] performed a study on the autogenous self-healing of ordinary Portland cement concrete (OPC) and blast-furnace slag (BFS) cement mortar, when submerged in both fresh water and sea water. After submerging the specimen in fresh-water, Palin et al. [62] conducted an ESM/EDX analysis, which revealed a formation of a 10μm layer of calcium, oxygen, and carbon in specimens of OPC samples, while BFS samples formed a similar chemical-wise layer of 5 μm. Based on the chemical composition of the layer, the study identified an association with the formation of calcium carbonate, as given by Equation 2.3.

$$CO_2 + Ca(OH)_2 \rightarrow Mg(OH)_2 + CaCl_2 \quad \text{(Eq. 2.3)}$$

On the other hand, the specimen submerged in sea-water developed a double layer: a lower layer largely formed from magnesium composites, and an outer layer similar to one formed from fresh-water specimens. Palin et al. [62] observed that after 56 days, BFS samples submerged in sea-water healed 100% of the cracks with a crack-width of up to 104 μm; for OPC specimens, the maximum width was 592 μm. On the other hand, BFS samples submerged in fresh-water healed up to 408 μm crack-widths, while OPC specimens only healed 168 μm cracks.

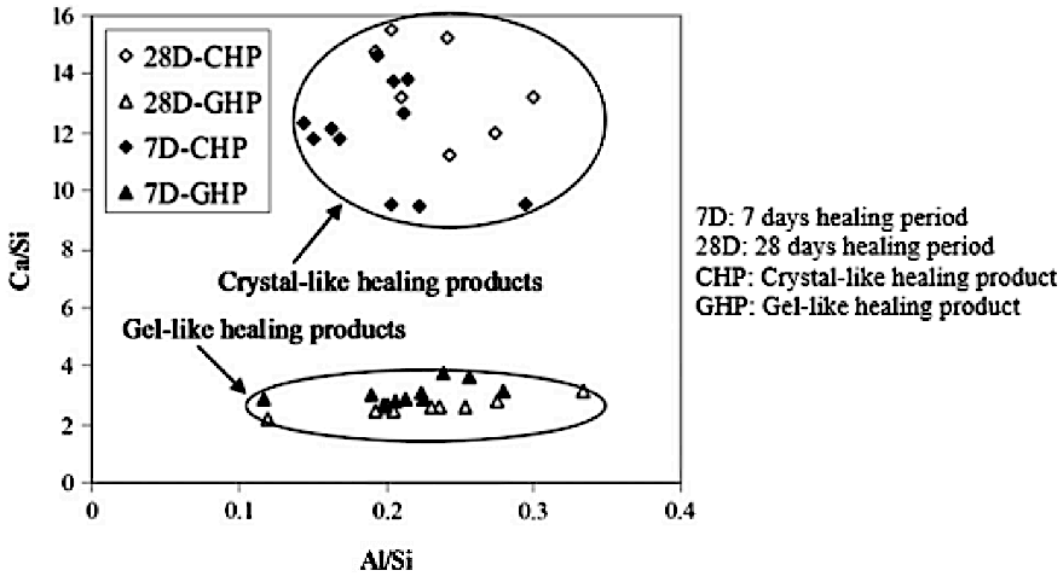

Figure 2.13. Ca/Si vs. Al/Si ratio plot of healing products [61]

2.4.4 Water Permeability of Concrete

When concrete structures are exposed to extreme loading events and/or weathering actions, the permeability of concrete is increased by the interconnection of flow paths due to cracking. Moreover, the increase in permeability further deteriorates the internal component of the structure, due to an aggressive chemical such as the oxidation of a steel internal reinforcement [63]. Therefore, the permeability recovery of self-healing concrete constitutes a good method to determine the self-healing effectiveness in concrete, while a decrease in concrete permeability suggests a decrease in the cracking-interconnection of the structure.

In order to test the water permeability of a controlled-crack concrete specimen, Nishiwaki et al. [64] adapted a permeability test in which the interface gab between a pipette funnel and a concrete plate specimen was sealed with silicone gel. The permeability test showed that specimens containing a healing agent stopped water leakage for up to a 2.5 mm maximum crack width. Meanwhile, untreated concrete samples showed a linear relationship between the quantity of water leakage and the maximum crack width induced in the samples.

Reinhardt and Jooss [8] performed a study on the effects of temperature regarding crack-width, relative to the permeability of self-healing in cracked concrete. The permeability test was set up to develop test cells, and consisted of an aluminum housing, a contact pressure tube, a seal pressure sleeve, and a capillary measuring instrument in the inlet and outlet ends. A schematic of the test cell is shown in Figure 2.14. The results showed that cracks exposed to higher temperatures enhance self-healing concrete capabilities, also confirming that smaller cracks heal faster than larger cracks.

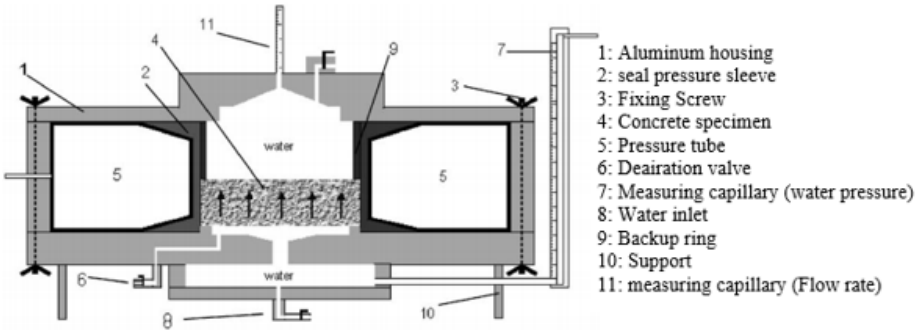

Figure 2.14. Test cell for Permeability test in self-healing concrete [8]

Wang et al. [65] investigated the healing efficiency of bacterial self-healing concrete by measuring the water permeability of samples after a controlled cracking test. The permeability instrumentation set up consisted of a low-pressure water permeability test. Results showed that the permeability coefficient (k) on samples containing the healing agent were of $6x10^{-11}$, while the reference (untreated) specimen yielded a k value of $7x10^{-6}$.

2.4.5 Stiffness and Strength recovery

Previous methods in the evaluation of the self-healing of concrete structures focused on the ability of healing agents to close and seal open crack voids. Sealing of open cracks improved the durability of concrete by decreasing the exposure of internal structural components to the open environment. Yet the ability of healing agents to restore the mechanical properties of structures as well is of great interest to the research community. Structural mechanical properties, such as stiffness and the compressive strength of concrete, can be tested to determine the self-healing effects of concrete structures. Victor Li et al. [18] conducted an experiment in which a three-point bending set up was used on concrete beams with the dimensions of a 203.2 mm span length, 38.1mm width, and a 76.2mm height. Results showed a regain from the flexural stiffness of damaged specimens with healing agents, followed by water curing for two weeks, thus validating the re-healing effects.

Ter Heide and Schlangen [66] implemented a study on crack healing in hydration concrete to investigate the necessary conditions in which early-staged cracks can self-repair. In order to evaluate this, the author built prismatic concrete specimens to be tested at an early age under a three-point bending set up that created controlled crack widths. Next, the beams were water cured for several weeks, both with and without compressive loads. A retesting of water-cured beams showed that the age when the first cracking occurs determines the strength recovery capabilities. Importantly, as the concrete age increases, the ability for strength recovery decreases. Moreover, the amount of compressive strength applied in the curing period does not affect strength recovery. Figure 2.15 shows the stress-displacement curves for the beams specimen after water curing.

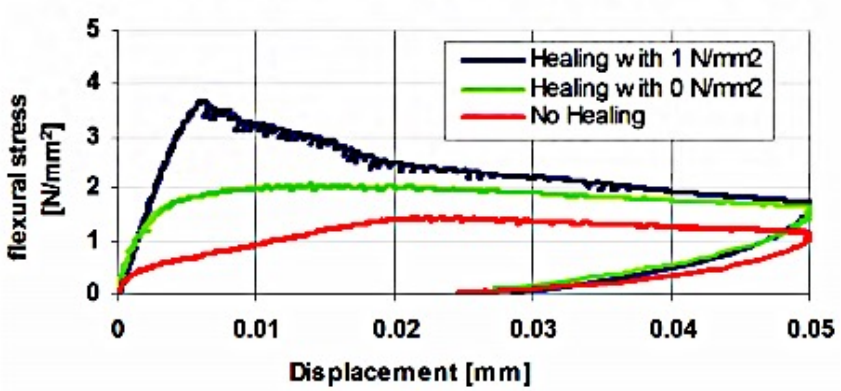

Figure 2.15. Stress-displacement curve with and without compressive strength [66]

Pang et al. [67] built a large scaled concrete structure in which encapsulated microcapsules were mixed into the concrete matrix. Beams with dimensions of 125 mm x 200 mm x 2000 mm were tested, using a three-point bending set up. The results showed a flexural-stiffness recovery of 84% of the initial stiffness. Moreover, Van Tittelboom et al. [68] researched the effects of encapsulated healing agents (polyurethane Meyco MP 355 1k), embedded in a concrete matrix of self-healing properties. Mortar beams and mortar cylinders were cast in order to evaluate the mechanical properties and water permeability. The regain of the mechanical strength of the treated

samples were subsequently compared with the control group. The results found an overall recovery of 80% of the original strength, together with a recovery of 60% of the original stiffness of the specimen treated with microcapsules. Figure 2.16 shows the regain in strength and stiffness plots for the different specimens, tested under different loading conditions.

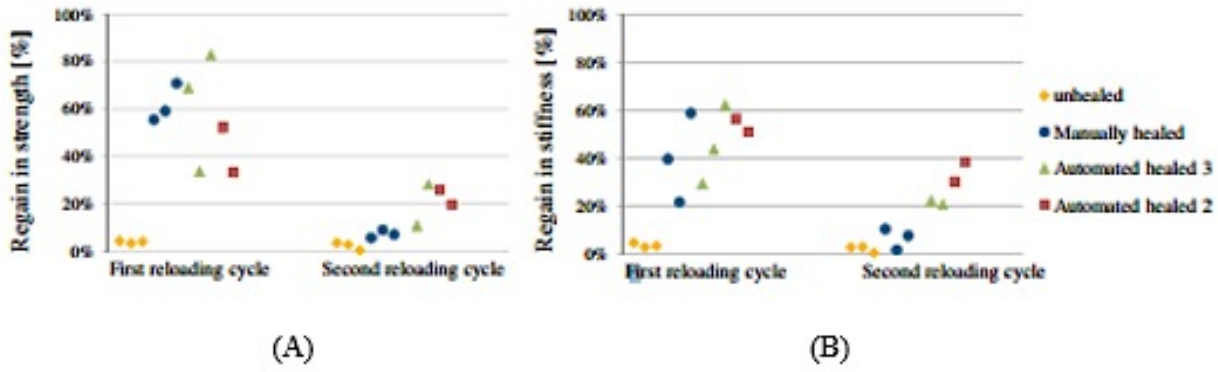

Figure 2.16. (A) Straight recovery (B) Stiffness recovery [68]

2.5 References

[1] H. G. Van Oss, "Background facts and issues concerning cement and cement data," 2005.

[2] M. de Rooij, K. Van Tittelboom, N. De Belie and E. Schlangen, Self-Healing Phenomena in Cement-Based Materials., 2014.

[3] M. Yunovich and N. G. Thompson, Corrosion of highway bridges: Economic impact and control methodologies, Concrete International, 25(1), 52-57., 2003.

[4] S. P. Shah and K. Wang, "Concrete cracking and durability.," International Conference on Advances in Concrete and Structures (pp. 3-10), 2003.

[5] S. Zwaag, "Self healing materials: an alternative approach to 20 centuries of materials science," Springer Science+ Business Media BV, 2008.

[6] K. Van Breugel, "Is there a market for self-healing cement-based materials," Proceedings of the first international conference on self-healing materials, 2007.

[7] Edvardsen, "Water permeability and autogenous healing of cracks in concrete," ACI Mater J, p. 96:448–455, 1999.

[8] H. W. Reinhardt and M. Jooss, "Permeability and self-healing of cracked concrete as a function," Cement and Concrete Research, pp. 33(7), 981-985., 2003.

[9] S. Granger, G. Pijaudier-Cabot and A. Loukili, "Mechanical behavior of self-healed ultra high performance concrete: from experimental evidence to modeling," The 6th international conference on fracture mechanics of concrete and concrete structures. Vol. 1722, 2007.

[10] N. Ter Heide, E. Schlangen and K. Van Breugel, "Experimental study of crack healing of early age cracks," Proceedings Knud Højgaard conference on Advanced Cement-Based Materials, 2005.

[11] H. F. W. Taylor, "Cement chemistry," 1997.

[12] V. C. Li and E.H. Yang, "Self healing in concrete materials," in Self healing materials, Springer Netherlands, 2007, pp. 161-193.

[13] S. Jacobsen, J. Marchand and H. Hornain, "SEM observations of the microstructure of frost deteriorated and self-healed concretes," Cement and Concrete Research, no. 25(8), pp. 1781-1790, 1995.

[14] C. A. Clear, "The effects of autogenous healing upon the leakage of water through cracks," No. Tech Rpt. 559.

[15] X. Hua, K. van Breugel, G. Ye, P. C. J. Hoogenboom and I. L. Houben, "Self-healing of engineered cementitious composites (ECC) in concrete repair system," Doctoral dissertation, Master thesis, Delft University of Technology, 2010.

[16] C. Dry, "Matrix cracking repair and filling using active and passive modes for smart timed release of chemicals from fibers into cement matrices," Smart Materials and Structures, 1994.

[17] A. M. Abd-Elmoaty, "Self-healing of polymer modified concrete," Alexandria Engineering Journa, pp. 171-178.

[18] V. C. Li, Y. M. Lim and Y.-W. Chan., "Feasibility study of a passive smart self-healing cementitious composite," Composites Part B: Engineering, pp. 819-827, 1998.

[19] J. Y. Lee, G. A. Buxton and A. C. Balazs, "Using nanoparticles to create self-healing composites," The Journal of chemical physics, vol. 121(11), pp. 5531-5540, 2004.

[20] S. R. White, N. R. Sottos, P. H. Geubelle, J. S. Moore, M. Kessler, S. R. Sriram and S. Viswanathan, "Autonomic healing of polymer composites," Nature, 409(6822), pp. 794-797, 2001.

[21] Z. Yang, J. Hollar, X. He and X. Shi, "A self-healing cementitious composite using oil core/silica gel shell microcapsules," Cement and Concrete Composites, vol. 33, no. 4, pp. 506-512, 2011.

[22] E. Cailleux and V. Pollet, "Investigations on the development of self-healing properties in protective coatings for concrete and repair mortars," Proceedings of the 2nd International Conference on Self-Healing Materials, vol. 28, 2009.

[23] J. Y. Wang, H. Soens, W. Verstraete and N. De Belie, "Self-healing concrete by use of microencapsulated bacterial spores," Cement and Concrete Research, vol. 56, no. 2014, pp. 139-152, 2014.

[24] H. Huang and G. Ye, "Application of sodium silicate solution as self-healing agent in cementitious materials," International RILEM conference on advances in construction materials through science and engineering, no. RILEM Publications SARL, pp. 530-536, 2011.

[25] M. Pelletier, R. Brown, A. Shukla and A. Bose, "Self-healing concrete with a microencapsulated healing agent," Cement and Concrete Research, 2011.

[26] H. Mihashi, Y. KANEKO, T. Nishiwaki and K. Otsuka, "Fundamental study on development of intelligent concrete characterized by self-healing capability for strength," Transactions of the Japan Concrete Institute, vol. 22, pp. 441-450, 2001.

[27] F. Xing, Z. Ni, N. Han, B. Dong, X. Du, Z. Huang and M. Zhang, "Self-healing mechanism of a novel cementitious composite using microcapsules," Proceedings of the International Conference on Durability of Concrete Structures, vol. 2627.

[28] Z. Yang, J. Hollar, X. He and X. Shi, "Laboratory assessment of a self-healing cementitious composite," Transportation Research Record: Journal of the Transportation Research Board, vol. 2142, pp. 9-17, 2010.

[29] E. N. Brown, M. R. Kessler, N. R. Sottos and S. R. White, "In situ poly (urea-formaldehyde) microencapsulation of dicyclopentadiene," Journal of microencapsulation, vol. 20, no. 6, 2003.

[30] M. M. Hassan, J. Milla, T. Rupnow, M. Al-Ansari and W. H. Daly, "Microencapsulation of Calcium Nitrate for Concrete Applications.," Transportation Research Record: Journal of the Transportation Research Board, no. 2577, pp. 8-16, 2016.

[31] J. Milla, M. M. Hassan, T. Rupnow, M. Al-Ansari and G. Arce, "Effect of Self-Healing Calcium Nitrate Microcapsules on Concrete Properties," Transportation Research Record: Journal of the Transportation Research Board, vol. 2577, pp. 69-77, 2016.

[32] M. Wu, B. Johannesson and M. Geiker, "A review: Self-healing in cementitious materials and engineered cementitious composite as a self-healing material," Construction and Building Materials, vol. 28, no. 1, pp. 571-583, 2012.

[33] T. Nishiwaki, H. Mihashi, B. K. Jang and K. Miura, "Development of self-healing system for concrete with selective heating around crack," Journal of Advanced Concrete Technology, vol. 4, no. 2, pp. 267-275, 2006.

[34] C. Joseph, A. D. Jefferson, B. Isaacs, R. J. Lark and D. R. Gardner, "Experimental investigation of adhesive-based self-healing of," Magazine of Concrete Research, vol. 62, no. 11, pp. 831-843, 2010.

[35] C. Joseph, A. D. Jefferson and M. B. Cantoni, "Issues relating to the autonomic healing of cementitious materials," Proceedings of the 1st International Conference on Self-Healing Materials, no. CD-ROM, 2007.

[36] C. Dry and M. Corsaw, "A comparison of bending strength between adhesive and steel reinforced concrete with steel only reinforced concrete," Cement and Concrete Research, vol. 33, no. 11, pp. 1723-1727, 2003.

[37] E. Boquet, A. Boronat and A. Ramos-Cormenzana, "Production of calcite (calcium carbonate) crystals by soil bacteria is a general phenomenon," 1973.

[38] S. Stocks-Fischer, J. K. Galinat and S. S. Bang, "Microbiological precipitation of CaCO 3," Soil Biology and Biochemistry, vol. 31, no. 11, pp. 1563-1571, 1999.

[39] V. Ramakrishnan, R. K. Panchalan, S. S. Bang and R. City, "Improvement of concrete durability by bacterial mineral precipitation," Proceedings of 11th International Conference on Fracture, pp. 20-25, 2005.

[40] S. S. Bang, J. K. Galinat and V. Ramakrishnan, "Calcite precipitation induced by polyurethane-immobilized Bacillus pasteurii," Enzyme and microbial technology, vol. 28, no. 4, pp. 404-409, 2001.

[41] H. M. Jonkers, A. Thijssen, G. Muyzer, O. Copuroglu and E. Schlangen, "Application of bacteria as self-healing agent for the development of sustainable concrete," Ecological engineering, vol. 36, no. 2, pp. 230-235, 2010.

[42] D. C. Lagoudas, Shape memory alloys, Science and Business Media, LLC., 2008.

[43] G. Song, N. Ma and H. N. Li, "Applications of shape memory alloys in civil structures," Engineering structures, vol. 28, no. 9, pp. 1266-1274, 2006.

[44] G. L. McGavin and G. Guerin, "Real-time seismic damping and frequency control of steel structures using Nitinol wire," SPIE's 9th Annual International Symposium on Smart Structures and Materials, no. International Society for Optics and Photonics., pp. 176-185, 2002.

[45] P. W. Clark, I. D. Aiken, J. M. Kelly, M. Higashino and R. Krumme, "Experimental and analytical studies of shape-memory alloy dampers for structural control," Smart Structures & Materials' 95, no. International Society for Optics and Photonics., pp. 241-251, 1995.

[46] A. Jefferson, C. Joseph, R. Lark, B. Isaacs, S. Dunn and B. Weager, "A new system for crack closure of cementitious materials using shrinkable polymers," Cement and Concrete Research, vol. 40, no. 5, pp. 795-801, 2010.

[47] M. S. Saiidi, M. Sadrossadat-Zadeh, C. Ayoub and A. Itani, "Pilot study of behavior of concrete beams reinforced with shape memory alloys," Journal of materials in civil engineering, vol. 19, no. 6, pp. 454-461, 2007.

[48] Y. Kuang and J. Ou, "Self-repairing performance of concrete beams strengthened using superelastic SMA wires in combination with adhesives released from hollow fibers," Smart Materials and Structures, vol. 17, no. 2, 2008.

[49] K. Mather, "Applications of light microscopy in concrete research," Symposium on Light Microscopy. ASTM International, 1953.

[50] O. Çopuroğlu, E. Schlangen, T. Nishiwaki, K. Van Tittelboom, D. Snoeck, N. De Belie and M. R. de Rooij, "Experimental Techniques Used to Verify Healing," in Self-Healing Phenomena in Cement-Based Materials, Netherlands, Springer , 2013, pp. 19-63.

[51] T. G. Nijland, J. A. Larbi, R. P. van Hees, B. Lubelli and M. de Rooij, "Self healing phenomena in concretes and masonry mortars: a microscopic study," Proc. 1st Int. Conf. on Self Healing Materials, vol. 1, pp. 1-9, 2007.

[52] V. Wiktor and H. M. Jonkers, "Bio-chemical self-healing agent to prevent reinforcement corrosion in concrete," 2nd International Conference on Self-healing Materials, p. 118, 2010.

[53] V. Wiktor and H. M. Jonkers, "Quantification of crack-healing in novel bacteria-based self-healing concrete," Cement and Concrete Composites, vol. 33, no. 7, pp. 763-770, 2011.

[54] T. H. Ahn and T. Kishi, "The effect of geo-materials on the autogenous healing behavior of cracked concrete," Proceedings of 2nd International Conference on Concrete Repair, Rehabilitation and Retrofitting, pp. 24-26, 2008.

[55] H. M. Jonkers, "Self healing concrete: a biological approach," in Self Healing Materials, Springer Netherlands, 2007, pp. 195-204.

[56] Mechtcherine, Viktor, and Matthias Lieboldt. "Permeation of water and gases through cracked textile reinforced concrete." Cement and Concrete Composites 33, no. 7 (2011): 725-734

[57] W. De Muynck, K. Cox, N. De Belie and W. Verstraete, " Bacterial carbonate precipitation as an alternative surface treatment for concrete.," Construction and Building Materials, vol. 22, no. 5, pp. 875-885, 2008.

[58] S. Qian, J. Zhou, D. R. M. R., E. Schlangen, G. Ye and K. Van Breugel, "Self-healing behavior of strain hardening cementitious composites incorporating local waste materials," Cement and Concrete Composites, vol. 31, no. 9, pp. 613-621, 2009.

[59] T. H. Ahn and T. Kishi, " Crack self-healing behavior of cementitious composites incorporating various mineral admixtures," Journal of Advanced Concrete Technology, , vol. 8, no. 2, pp. 171-186, 2010.

[60] Perez, G., E. Erkizia, J. J. Gaitero, I. Jimenez, and A. Guerrero. "Effect of different amounts of innovative self-healing additions on the microstructure of cement pastes." In Proceedings of the 1st Ageing of Materials & Structures conference, pp. 628-634. 2014.

[61] S. Diamond, "Identification of hydrated cement constituents using a scanning electron microscope energy dispersive X-ray spectrometer combination," Cement and Concrete Research, vol. 2, no. 5, pp. 617-632, 1972.

[62] D. Palin, V. Wiktor and H. M. Jonkers, "Autogenous healing of marine exposed concrete: characterization and quantification through visual crack closure," Cement and Concrete Research, vol. 72, no. 2015, pp. 17-24, 2015.

[63] K. Wang, D. C. Jansen, S. P. Shah and A. F. Karr, "Permeability study of cracked concrete," Cement and Concrete Research, vol. 27, no. 3, pp. 381-393, 1997.

[64] K. Wang, D. C. Jansen, S. P. Shah and A. F. Karr, "Permeability study of cracked concrete," Cement and Concrete Research, vol. 27, no. 3, pp. 381-393, 1997.

[65] J. Wang, K. Van Tittelboom, N. De Belie and W. Verstraete, "Use of silica gel or polyurethane immobilized bacteria for self-healing concrete," Construction and building materials, vol. 26, no. 1, pp. 532-540, 2012.

[66] Ter Heide and E. Schlangen, "Self-healing of early age cracks in concrete," First international conference on self healing materials, 2007.

[67] S. D. Pang and T. Diep., "ST: Self-healing concrete structural elements," 3rd International Conference on Self-healing Materials, pp. 322-323, 2011.

[68] K. Van Tittelboom and N. De Belie, "Self-healing concrete by means of encapsulated polymers," 13th International Congress on Polymers in Concrete (ICPIC-2010), no. Oficinas Graficas de Barbosa & Xavier, Lda., pp. 681-688, 2010.

CHAPTER 3. SELF-HEALING EVALUATION OF REINFORCED CONCRETE BEAMS WITH CALCIUM NITRATE MICROCAPSULES

3.1 Introduction

Concrete structures are known to be susceptible to many sources of damage. Cracks develop internally and in areas where the presence of cracks can potentially cause major corrosion problems to the structure. Other sources for major damage to concrete include freeze/thaw cycles, extreme loads, chemical attacks, and severe environmental conditions. To combat cracking damage, significant funds are spent regularly on maintenance and rehabilitation activities [1].

Self-healing phenomena in concrete originate from a complex combination of chemical and physical processes. Wu identified the main possible causes responsible for self-healing mechanisms: a) formation of calcium carbonate or calcium hydroxide; b) sealing of crack due to impurities accumulation delivered by water flow through the crack area; c) loose concrete particles resulting from crack spalling; d) hydration of unreacted cement or cementitious materials; and e) expansion of the hydrated cementitious matrix in the crack flanks [2]. The main process responsible for these mechanisms is assumed to be related to the crystallization of calcium carbonate [3]. This statement is supported by precipitated calcium-carbonate that is usually found around crack surfaces as a white residue [4].

In order to improve self-healing efficiency on cementitious materials, several strategies have been developed as a way to provide and deliver the necessary products (healing agents) for cracks to self-repair. Some of these strategies are: (a) embedding hollow fibers filled with functional components; (b) microencapsulation of healing agents; (c) expansive agents and mineral admixtures; (d) biological repair using bacteria; and (e) shape memory materials [5]. An advantage offered by microencapsulation is that the treatment may be delivered to multiple locations, due to

the agents being dispersed inside the concrete matrix [6]. The present study evaluated the healing efficiency and mechanical behaviors of concrete beams prepared with microcapsules filled with calcium-nitrate.

3.2 Objectives and Scope

This study had two main objectives: (1) to evaluate the self-healing efficiency of microcapsules filled with calcium-nitrate in concrete beams; and (2) to investigate the structural behavior of concrete beams with and without microcapsules. To evaluate the structural behavior and healing efficiency, the initial stiffness, peak strength, and deformation were measured and compared with post-healing measurements. Furthermore, the study conducted crack monitoring in order to evaluate crack-healing over time, followed by characterization analysis using Energy-dispersive X-ray spectroscopy (EDX) in order to quantify the healing components in the cracked areas.

3.3 Background

The American Society of Civil Engineers (ASCE) estimate that $2.2 trillion dollars will be needed to repair and retrofit the egregious amount of deteriorated infrastructures. In a study of the autogenous healing of concrete, Edvarsen noted that autogenous healing is caused mainly by a precipitation of calcium carbonate crystals on the crack surface [3]. Furthermore, results indicated that the growth rate of these crystals show a dependency on crack widths and water pressure, i.e., narrower cracks under higher pressures experience a higher healing rate. Enhancing the autonomous healing properties of concrete has long provided a topic of high interest for the scientific community. The last decade has seen the concept of developing smart materials that require no human intervention to address and repair damaged infrastructure increase in popularity in the research community [7].

One method to develop a self-healing concrete is known as microencapsulation. White explained the self-healing concept mechanism of microencapsulation as follows [6]: Microcapsules are embedded in the concrete matrix; once a crack ruptures these microcapsules, a healing agent is released into the crack faces by means of capillary action. The crack is then sealed due to the polymerization of the healing agent on the crack faces. Huang and Ye [8] successfully encapsulated a sodium silicate solution into spherical capsules with a diameter of 5 mm, sealed with wax. The release of the solution at the crack locations reacted with calcium hydroxide $Ca(OH)_2$ present in the concrete to form calcium silica hydrate or CSH, which sealed the crack. White et al. mentioned the microencapsulation process of with liquid adhesive dicyclopentadine (DCPD), in which in situ polymerization of urea with formaldehyde containing an acid-catalyzed was used to form the capsules wall [6]. Moreover, Brown et al, further improve the microencapsulation procedure to achieve high-quality microcapsules of urea formaldehyde shell with DCPD core by performing the in-situ procedure in an oil-in-water emulsion [20]. Brown et al, also developed a linear correlation between the agitation rate and the diameter of the microcapsules created in this process that resulted from 1000 μm at 200 rpm to 10 μm at 2000 rpm.

Hassan et al. developed a synthesis for production of urea-formaldehyde microencapsulation of calcium nitrate [9]. The authors evaluated the self-healing efficiency in concrete as the modulus of elasticity increased after healing on all specimens containing microcapsules. The incorporation of microcapsules also increased the surface resistivity of those samples, thereby, reducing the permeability of the concrete. Milla et al. [10] investigated the effects of encapsulation of calcium nitrate as a healing agent. The study evaluated the compressive strength and elastic modulus of concrete, admixed with microcapsules at various percentages by

weight of cement. The results indicated a decrease in compressive strength, when compared to the control samples; yet, results showed that a concentration of 0.5 to 1% yielded the best results for recovery of the concrete modulus of elasticity.

Rooij cited Carolyn Dry [17], who developed a frame structures test in which a structural damage location was properly controlled by releasing high modulus adhesives; the adhesives allowed the samples to regain stiffness, thereby preventing future damage to that location. The researcher repeated the experiment using low modulus adhesives. Results indicated that even though the crack was sealed, no increase occurred to the member stiffness [11].

Li evaluated the self-healing mechanism of "passive smart self-healing engineered cementitious composites" or PSS-ECC, containing self-healing agents carrying fibers embedded in the concrete matrix by a regain in material stiffness; the damage was inflicted by a mechanical load in a three-point bending test setup [12]. Stiffness values were normalized by the initial stiffness (uncracked). The researcher demonstrated that while most specimens containing healing agents either recovered or surpassed the initial stiffness, the control samples showed a drop in stiffness from 10 to 40%.

Various techniques were developed in order to examine crack healing at the microscopic levels. Some of these techniques include microscopy (optical and electron), X-ray diffraction, EDX, and Raman spectroscopy. Optical microscopy was employed by Wiktor and Jonker in order to observe self-healing of cracks up to 160 μm in bacterial concrete [13]. The researchers identified healing products developed by bacteria as "white crystalline precipitates." In turn, Yang utilized both optical and electron microscopy to study the self-healing of concrete through wet and dry cycles [14]. When the optical microscope showed the sealing of a crack with a white

precipitation, Yang used the EDX spectra to identify the chemical composition of the healing products, which was mostly calcite.

3.4 Experimental Program

3.4.1 Self-Healing Microcapsules

Previous research by the authors successfully developed procedures for encapsulating calcium-nitrate [9, 10]. The microcapsules developed in this study followed the same procedure, in which the production parameters were as follows: (a) heating temperature of 40ºC, (b) heating time of 1.5 hours, (c) 0.6 g of sulfonic acid, (d) agitation rate of 800 rpm. Figure 3.1 illustrates the morphology and dimensions of the prepared microcapsules based on the developed procedure.

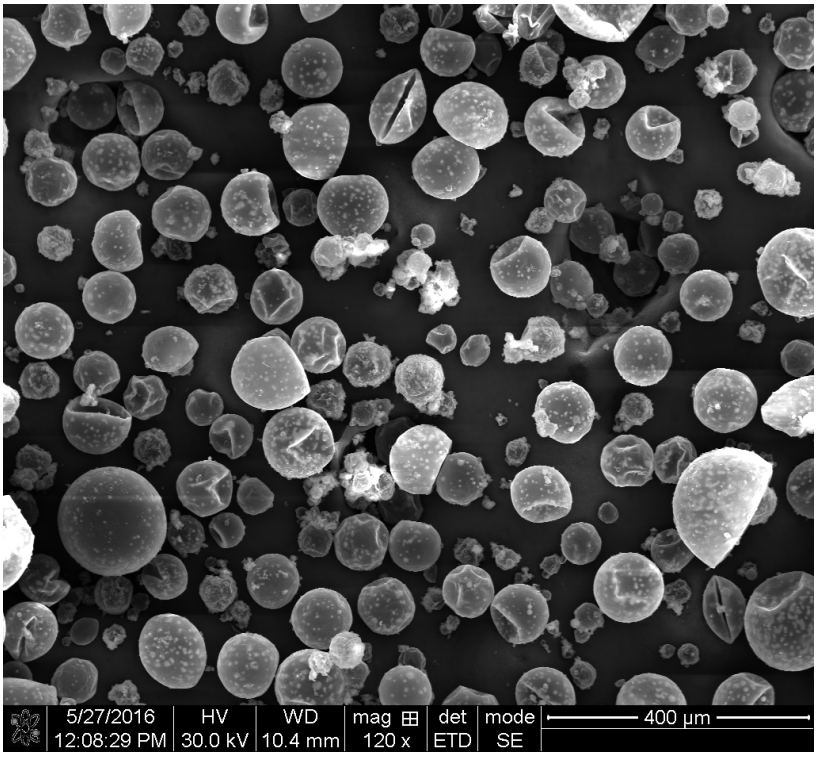

Figure 3.1 Microcapsules morphology using scanning electron microscopy (SEM)

3.4.2 Concrete Beams Matrix

Prepared beam specimens were divided into four groups, control, microcapsules, steel, and microcapsules-steel. Control specimens were prepared with no microcapsules and no reinforcement. The microcapsules group contained 1% by weight of cement of calcium nitrate microcapsules. The steel group was reinforced with two #3 steel grade A32 bars. Finally, the microcapsules-steel group contained both flexural steel reinforcements and microcapsules. Five specimens were prepared in each category to allow for different types of test to assess strength and recovery. Table 3.1 lists the attributes of the beams prepared for this study and designations for each group.

Table 3.1. Experimental test factorial

Group ID	**Microcapsules content (% - by weight of cement)**	**Reinforcement type**	**Numbers of specimens**
Control	0.0	N/A	5
Microcapsules	1.0	N/A	5
Steel	0.0	#3 Steel Grade A32	5
Microcapsules-Steel	1.0	#3 Steel Grade A32	5

3.4.3 Concrete Mix Design

The selected mix design was based on a typical mix used in Louisiana for road applications; the expected compressive strength is 41.4 MPa and the water-cement ratio is 0.48. The coarse aggregates used were limestone, where the maximum aggregate size was 19 mm. Sand was used as a fine aggregate with a maximum particle size of 4.76 mm. Microcapsules were dispersed into one-third of the water used prior to the mix procedure. The mix procedure involved three minutes of mixing coarse aggregate with two-thirds of the water content, followed by the addition of

cement, fine aggregates, and one-third of the water for another three minutes. Next, the mix was left to cure for a three-minute period. Finally, the contents were mixed again for three minutes before pouring followed by performing slump test and air content according by pressure method according ASTM C 143 [18] and ASTM C 231 [19]. Table 3.2 shows the details of the concrete mix design. Concrete beams were cast into a modified ASTM C 293 rectangular beam with dimensions of 39.4 in. x 4in. x 4in. [16].

Table 3.2. Concrete mix design

Material description		**Proportion (kg/m^3)**
Aggregate 1	Sand, Dennis Mills, LA	789
Aggregate 2	#67 Limestone, Martin Marietta	1118
Cement	Holcim Type I	297
Water	Mixing Water	141
Air (%)		5.0%
Admixtures		**Dosage**
Air Admixture	N/A	0.00
Admixture 1	Glenium 7500	15.00 (ml/batch)
Admixture 2	Microcapsules	1% (by weight of cement)

3.4.4 Structural Testing of Self-Healing Concrete

Flexural strength of concrete beams was tested per ASTM C 293 [16]. The flexural strength was also used to estimate the appropriate load levels for serviceability tests. Two of the specimens in each group were dedicated for strength tests to determine the flexural capacity of the beams, using a three-point bending setup.

The load – deflection ($P - \Delta$) relationship was obtained for each of the tested beams up to the failure point. From these tests, the ultimate load (P_u) of the tested beam was determined.

Ultimate load test results were utilized in order to plan the second phase of testing. On the second phase, three specimens were tested for each group. For the unreinforced beams, the specimens were loaded until cracks were visually observed. For the reinforced beams, the maximum load applied was 60% of the ultimate load. Undamaged and damaged stiffness properties, K_U and K_D, were calculated using the load-deflection curve during this phase. Beams were left under healing conditions. The healing conditions consisted of submerging the specimens in deionized water for seven days. Deionized water was used as a replacement of regular tap water in order to avoid and eliminate unwanted mineral contaminants that are present in regular water. After the healing period ended, a second round of testing was conducted on the beam specimens up to the failure point. Retesting the beams allowed for identifying any change in structural behavior (healing stiffness) in comparison to the stiffness properties before the curing period.

3.4.5 Quantification and Characterization of Self-Healing Products

Various techniques were utilized to evaluate crack healing; these techniques include microscopy (optical and electron), X-ray diffraction, and Raman spectroscopy. Microscopy was employed in this study to (a) measure the efficiency and quality control of the self-healing material; (b) characterize damage (cracks); and (c) assess the degree of self-healing [11]. After the conclusion of the second phase of testing; i.e., serviceability tests, all specimens were placed in DI water to accelerate the healing process. Furthermore, visible cracks were observed using a digital microscope during loading, immediately after the load was removed, and periodically after that, while the cracked beam started the healing period.

Image analysis software was used to calculate and measure the healing efficiency for each test condition. The healing efficiency was calculated, based on Equation (3.1):

$$f_{f=100-\frac{A_t}{A_o}*100} \quad \text{(Eq. 3.1)}$$

where,

f_f= healing efficiency (%);

A_o= Initial area of the cracks; and

A_t = Area of the cracks at the time of analysis.

After allowing the concrete specimens to heal for a period of 28 days, the specimens were cut, allowing the cracked areas to be exposed. Samples were analyzed using Environmental Scanning Electron Microscopy (ESEM) equipped with EDX in order to investigate the chemical compositions of the healing products. Atomic ratio plots were developed as part of the quantification analysis. The environmental scanning electron microscope utilized in this research was a FEI Quanta 3D dual beam SEM/FIB.

3.5 Results and Analysis

3.5.1 Concrete Properties

The slump test did not show a significant variability with microcapsule batches between the control and the concrete. However, there was a significant change in the air content of the two cases. Batches containing microcapsules yielded two times more air content than the control batch, 8.5% air content for 1% microcapsules concentration versus 4.5% air content for the control batch.

3.5.2 Beam Flexural Strength

Table 3.3 presents the details of the flexural strength test results. Results of the flexural test of concrete beams showed that the strength capabilities of the control specimens were significantly greater than the samples containing microcapsules. Control beams averaged an ultimate load (P_u) of 3.9 kN, while the beams with microcapsules yielded an average P_u of 2.1 kN. The steel group averaged an ultimate load of 23.9 kN, while the microcapsules-steel yielded an average ultimate load of 15.1 kN. The microcapsules group yielded a decrease in strength of 46.2%, and similarly the steel-microcapsule group showed a decrease of 36.8%. These results suggest that microcapsules have a direct effect on decreasing the flexural strength of the concrete beams due to the high air content. On a study conducted by Milla et al. [10], the compressive strength for the concrete cylinders containing calcium nitrate microcapsules also showed a decrease of 32.9% from the control specimens. Based on these results, there exists a strong correlation between the decrease of flexural and compressive strengths and the addition of microcapsules to the concrete matrix. While this decrease appears related to the addition of microcapsules, it is in fact related to the increase in air voids in the specimens with microcapsules and not the microcapsules themselves.

Table 3.3. Concrete beams flexural strength properties

Group ID	**# Specimen**	**Ultimate load, Pu (kN)**	**Average ultimate load (kN)**
Control	1	4.04	3.9
	2	3.67	
Microcapsules	1	2.09	2.1
	2	2.19	
Steel	1	23.03	23.9
	2	24.7	
Microcapsules-Steel	1	15.59	15.1
	2	14.67	

3.5.3 Stiffness Properties

Undamaged and Damaged Flexural Stiffness

Concrete beams were subjected to a center-point flexural strength test in order to obtain the undamaged and damaged stiffness. The undamaged stiffness was calculated before the cracking of the specimens, while the damaged stiffness occurred after cracking. The highest stiffness values were recorded for the undamaged stiffness of the steel group, K_0 =7,179 N/mm, followed by the control group, K_0 =6,258.5 N/mm. Both groups containing microcapsules exhibited significantly lower averaged values. These results were expected given that the beams with microcapsules yielded lower flexural strength values. For damaged stiffness, the group with steel reinforcements showed higher stiffness than the group with no reinforcements. The steel group exhibited the highest values for damaged stiffness, K_D=5,912.4 N/mm. Strain gages installed in steel reinforcement revealed that most of the rebars exhibited strains greater than 0.002, and have therefore, yielded.

Healing Recovery of Beams

By comparing the damaged stiffness with the recovery stiffness, one can determine the recovery stiffness after healing. Table 3.4 shows stiffness properties for undamaged and damaged, as well as healed for all tested specimens. These results show a positive stiffness recovery for all groups, with and without microcapsules or steel. Stiffness changes are presented in Figure 3.2(a) for all groups. Figure 3.2(b) shows the averaged stiffness recovery for all groups. From these figures, it may be seen that the control group was the poorest performing group in terms of healing recovery, yielding only a 2% recovery after being damaged.

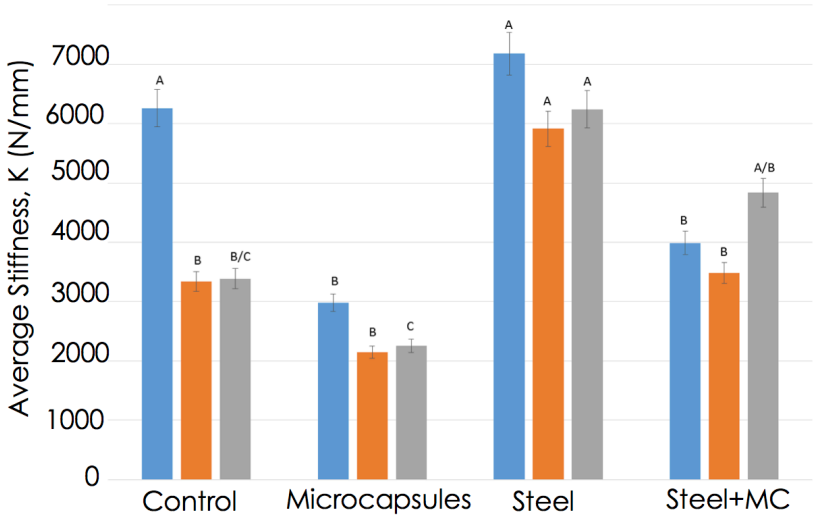

(a)

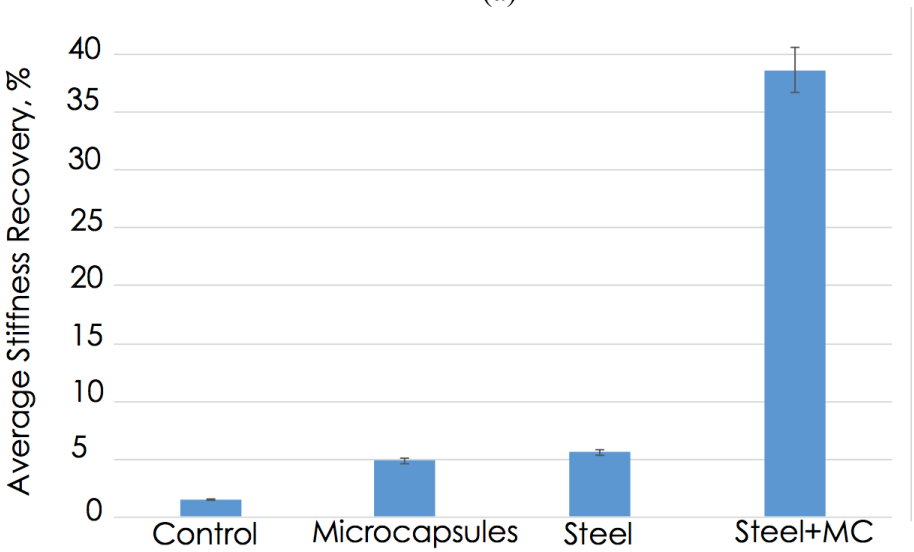

(b)

Figure 3.2. (a) Average stiffness of undamaged, damaged, and healed beam specimens and (b) Average stiffness recovery

On the other hand, the group with microcapsules yielded significantly better results, having a recovery stiffness of 5%. The steel group showed a healing recovery similar to the microcapsules group, having a stiffness recovery of 6%. However, the microcapsules-steel group showed great improvement on stiffness healing capabilities, having a stiffness recovery of 38%. These results show that microcapsules have a positive influence on recovering stiffness capabilities. It is noted

that the microcapsules-steel displayed a much greater healing efficiency than the microcapsules group, due to the ability of the reinforced beams to draw the faces of the cracks closer together allowing for greater recovery. This effect allows water to interact with anhydrate cement and the calcium nitrate released by the broken microcapsules allowing for greater healing efficiency.

Table 3.4. Stiffness properties for undamaged samples

Group ID	Average Stiffness (N/mm)		
	Undamaged, K_0	Damaged, K_D	Healing, K_H
Control	6258.5	3341.6	3390
Microcapsules	2979.6	2147.6	2252.4
Steel	7179.0	5912.4	6242.5
Steel-Microcapsules	3990.6	3487.1	4835.3

3.5.4 Image Analysis

After cracking the specimens, light microscope images of each crack on each specimen were acquired. The specimens were then subjected to a 7-day healing period (water-cured). Specimens were placed under open containers filled with deionized water under constant controlled temperature of 23 ± 2 °C. During the healing process, a digital light microscope was utilized to acquire images of the specimens at three and seven days. Table 3.5 shows the evolution of the cracks before and after the healing period. Formation of healing products were observed in all groups. The healing products for the concrete beams without microcapsules may be attributed to the unhydrated cement product present on the beams; the healing products for beams containing microcapsules may be due to the combined effect of unhydrated cement and the release of calcium nitrate from the microcapsules.

Table 3.5. Crack area before and after healing

Control	
Before Healing	After Healing
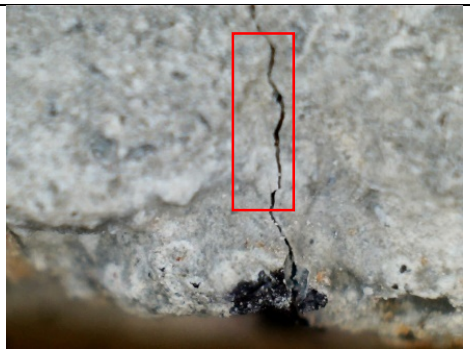	
Microcapsules	
Before Healing	After Healing
	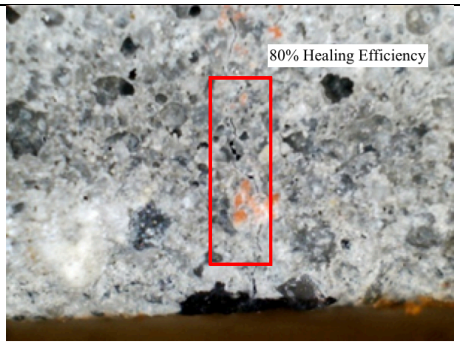
Steel	
Before Healing	After Healing
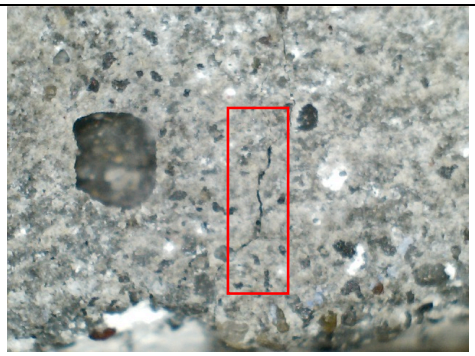	

(Table 3.5 continued)

Steel-Microcapsules	
Before Healing	After Healing
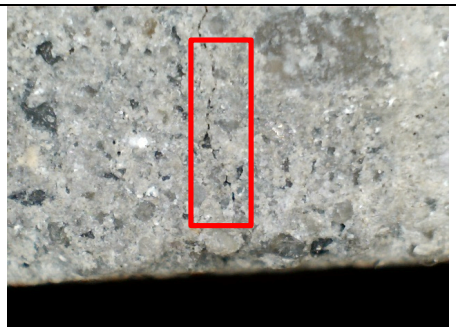	

Larger crack widths did not completely heal on the control samples, achieving only partial closure. On the other hand, similar crack widths were able to heal more efficiently on the concrete beams with microcapsules.

In order to quantify the healing efficiency, an analysis of the crack areas was conducted using imaging software. The healing efficiency was calculated according to Equation (3.1). The healing area analysis revealed that all of the groups exhibited crack healing. Most of the healing occurred within the first three days of curing, further showing a small increase at seven days. The control group was the worst performing group while having 65% of the initial cracks healed. Similarly, the steel group showed a cracked heal area of 67% after 7 days. The best performing groups were the ones containing microcapsules. For the microcapsules group, crack areas of 80% were healed after 7 days of the healing period. On the other hand, the best performing group of the study was the microcapsules-steel, which yielded 100% healing of the cracks. The microcapsules-steel specimens completely sealed the crack area, while the microcapsules group did not achieve the same results.

This outcome was due to the fact that the crack widths ranges developed in the unreinforced group were much wider than in the reinforced beams, thereby resulting in a reduction of the interfacial transition zone (ITZ) between crack widths for the reinforced group. Figure 3.3 shows a summary of the healing efficiency results.

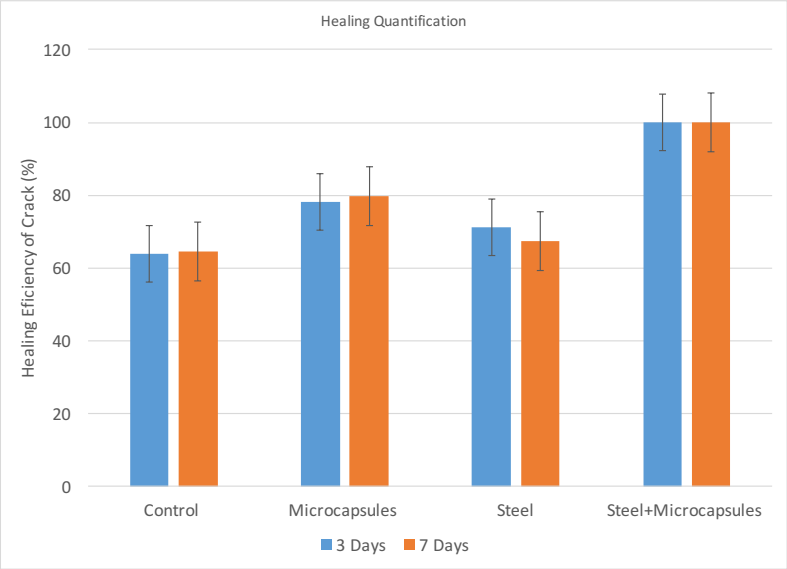

Figure 3.3. Healing efficiency of cracks

3.4.5 Healing Products Characterization

After a healing period of seven days, three specimens from the control group and three from the microcapsules group were cut using a diamond saw and small sections were analyzed using ESEM. Using EDX microanalysis, the study investigated healing products located in the crack opening by utilizing an environmental pressure of 0.6 Mbar and an accelerating voltage of 20 kV. An EDX spectrum was collected by using the spot mode in different locations of the crack where the healing products were observed. The procedure analyzed 80 individual spots in which the spectrum was allowed to collect for 30 seconds for the control and microcapsules groups. In order to visualize the chemical nature of the healing products generated by both groups, an Al/Ca vs. Si/Ca and S/Ca vs. Al/Ca ratios plots were generated, as shown in Figure 3.4.

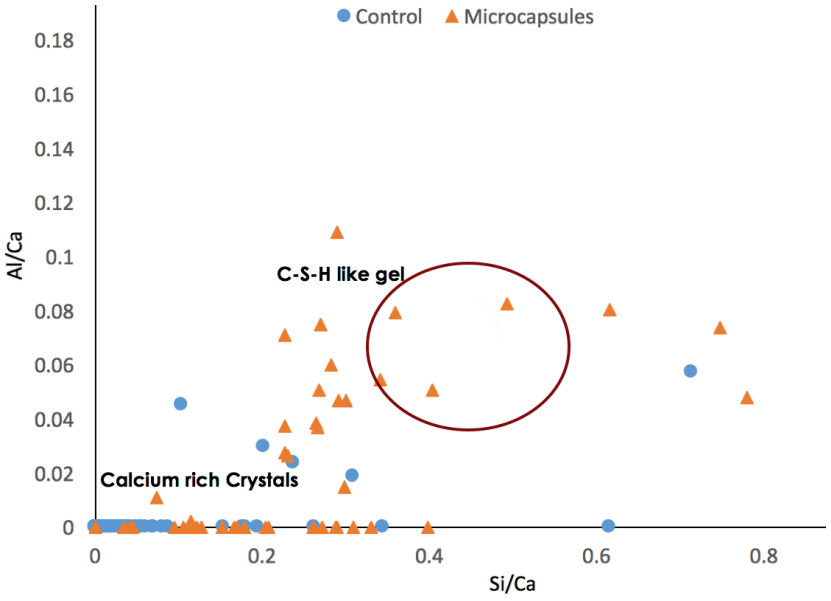

(a)

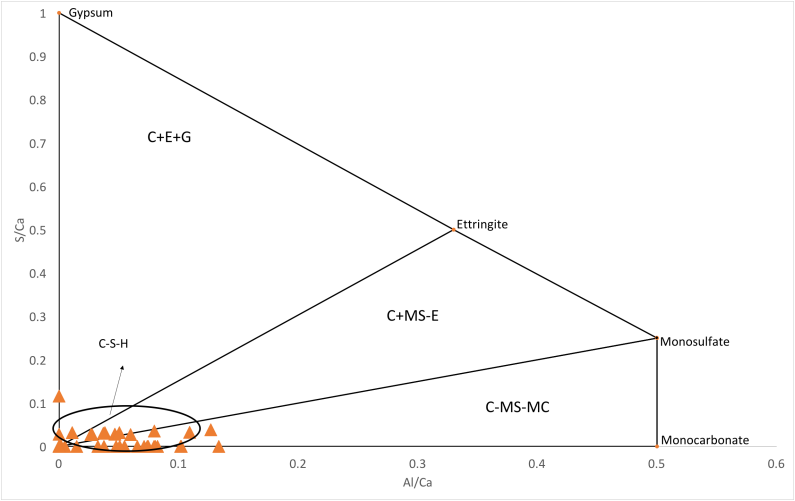

(b)

Figure 3.4. Healing products (a) Al/Ca vs. Si/Ca ratio plot, (b) S/Ca vs. Al/Ca ratio plot

Figure 3.4(a) revealed that most points for the control group, located close to the origin, were positioned where calcium rich crystals-like CH (Calcium hydroxide) or calcite ($CaCO_3$) usually locate [15]. On the other hand, the specimens containing microcapsules showed different results where some points plotted under the C-S-H region between 0.45 to 0.55 Si/Ca and 0.04 to

0.08 Al/Ca. Microcapsules also revealed mixtures of C-S-H and CH and some points near the lines of AFm (Alumina, Ferric oxide, Mono-sulfate), and AFt (Alumina, Ferric oxide, Tri-sulfate). Figure 3.4(b) presented that most of the AFm phases were a mixture of mono-sulfates and mono-carbonate. These findings suggest a possible presence of hydration products, due to the healing agents inside the microcapsules. The control group plotted no points on the S/Ca vs. Al/Ca atomic ratio plot, suggesting that no healing agents were formed for this group.

3.4.6 Statistical Analysis

A statistical analysis was performed to compare the results of similar mixes (i.e., Control and Microcapsules, etc.) and to determine whether the differences in undamaged, damaged, and healing stiffness were significant. Table 3.6 presents the normalized mean and the statistical ranking of the mixtures for different stiffness of samples for undamaged, damaged, and healing. Letters A, B, C, etc., are assigned to rank the statistical results for each group. The letter A is used for the highest average of each group, followed by the other letters in proper order. Double letters (e.g., B/C) indicate that there is no significant difference in the mixtures performance for two different groups. Results of the statistical analysis of undamaged stiffness indicate that the steel and control groups, Rank A, are significantly different from mixtures with microcapsule. The performance relationship for damaged stiffness between samples is presented in Table 3.6. It may be observed that only the steel group, Rank A, is significantly different in damaged stiffness from the other groups. The performance of the other mixtures, in terms of damaged stiffness, is equal for control, microcapsule, and Steel-microcapsule, Rank B. Finally, healing stiffness shows different statistical analysis. There is no significant difference on steel and steel-microcapsule group. However, steel group is significantly different to those of control and microcapsule groups.

Moreover, steel-microcapsule group has a significant difference with microcapsule, while there is no significant difference between control and microcapsule groups. It is also observed that there are significant differences between microcapsule with steel in the presence and absence of microcapsule.

Table 3.6. Statistical ranking of mixtures

Group ID	**Undamaged**		**Damaged**		**Healing**	
Mixture Type	Normalized Mean	Rank	Normalized Mean	Rank	Normalized Mean	Rank
Control	6258.5	A	3341.6	B	3390	B/C
Microcapsules	2979.6	B	2147.6	B	2252.4	C
Steel	7179	A	5912.4	A	6242.5	A
Steel-Microcapsules	3990.6	B	3487.1	B	4835.3	A/B

3.6 Summary and Conclusions

This study evaluated the self-healing efficiency of microcapsules filled with calcium-nitrate in concrete beams and investigated the structural behavior of concrete beams with and without microcapsules. The following conclusions may be drawn from the results of the experimental program:

- Air content in samples containing microcapsules were two times higher than the control sample, with an 8.5% air content for 1% microcapsules concentration versus 4.5% air content for the control batch.
- Addition of microcapsules lowered the flexural strength of concrete beams in comparison to those of the control samples. The results showed that microcapsules had a direct effect on reducing the flexural strength of the concrete beams due to the high air content.

- Undamaged stiffness for the steel group showed the highest value, while incorporation of microcapsules decreased the average stiffness significantly, which agrees with flexural strength values. The average damaged stiffness exhibited the same trend as the undamaged stiffness.
- A positive stiffness recovery was recorded for all groups, with and without microcapsules or steel. Control samples showed the lowest stiffness recovery, with a 2% recovery after being damaged. An incorporation of microcapsules and steel increased the stiffness recovery by 5% and 6%, respectively. However, the use of steel with microcapsules presented a superior healing efficiency and improved stiffness recovery significantly by 38%.
- Results from image analysis showed that crack widths did not completely heal for the control samples, while utilizing microcapsules allowed the cracked widths to heal more efficiently. The best observed performance was for the microcapsules-steel group, which yielded 100% healing of the crack.
- Atomic ratio plots suggested the possible presence of hydration products, due to the healing agents inside the beams with microcapsules. In contrast, the control group revealed the formation of calcium hydroxide (CH) as a healing product; however, the study did not find any C-S-H product or any points on the S/Ca vs. Al/Ca atomic ratio plots for the control group suggesting that no phases were formed for this group.

3.7 References

[1] M. M. Pelletier, R. Brown, A. Shukla, and A. Bose, "Self-healing concrete with a microencapsulated healing agent," Univ. Rhode Island, Kingston, No. C, 2010.

[2] M. Wu, B. Johannesson, and M. Geiker, "A review: Self-healing in cementitious materials and engineered cementitious composite as a self-healing material," Construction and Building Materials, vol. 28, no. 1. pp. 571–583, 2012.

[3] C. Edvardsen, “Water permeability and autogenous healing of cracks in concrete,” ACI Mater. J., vol. 96, no. 4, pp. 448–454, 1999.

[4] S. Qian, J. Zhou, M. R. de Rooij, E. Schlangen, G. Ye, and K. van Breugel, “Self-healing behavior of strain hardening cementitious composites incorporating local waste materials,” Cem. Concr. Compos., vol. 31, no. 9, pp. 613–621, 2009.

[5] M. Wu, B. Johannesson, and M. Geiker, “A review: Self-healing in cementitious materials and engineered cementitious composite as a self-healing material,” Construction and Building Materials, vol. 28, no. 1. pp. 571–583, 2012.

[6] S. R. White, N. R. Sottos, P. H. Geubelle, J. S. Moore, M. R. Kessler, S. R. Sriram, E. N. Brown, and S. Viswanathan, “Autonomic healing of polymer composites,” Nature, vol. 409, no. 6822, pp. 794–797, 2001.

[7] V. C. Li and E. Herbert, “Robust Self-Healing Concrete for Sustainable Infrastructure,” J. Adv. Concr. Technol., vol. 10, no. 6, pp. 207–218, 2012.

[8] H. Huang and G. Ye, “Application of sodium silicate solution as self-healing agent in cementitious materials,” Int. RILEM Conf. Adv. Constr. Mater. Through Sci. Eng., no. 1993, pp. 530 – 536, 2011.

[9] M. Hassan, J. Milla, T. Rupnow, M. Al-Ansari, and W. Dayly, “Micro-Encapsulation of Calcium Nitrate for Concrete Applications.” 95th Transportation Research Board Annual Meeting, Washington, D.C., 2016.

[10] J. Milla, M. Hassan, T. Rupnow, M. Al-Ansari, and G. Arce, “Evaluation of the Effect of Self-Healing Calcium Nitrate Microcapsules on Concrete Properties.” 95th Transportation Research Board Annual Meeting January 10-14, 2016, Washington, D.C.

[11] M. Rooij, K. van Tittelboom, N. Belie, and E. Schlangen, Self-Healing Phenomena in Cement-Based Materials: State-of-the-Art Report of RILEM Technical Committee. 2013.

[12] V. C. Li, Y. M. Lim, and Y.-W. Chan, “Feasibility study of a passive smart self-healing cementitious composite,” Compos. Part B Eng., vol. 29, no. 6, pp. 819–827, 1998.

[13] V. Wiktor and H. M. Jonkers, “Bio-chemical self-healing agent to prevent reinforcement corrosion in concrete,” in 2nd International Conference on Self-healing Materials, 2010.

[14] Y. Yang, M. D. Lepech, E. H. Yang, and V. C. Li, “Autogenous healing of engineered cementitious composites under wet-dry cycles,” Cem. Concr. Res., vol. 39, no. 5, pp. 382–390, 2009.

[15] N. Winter, Scanning Electron Microscopy of Cement and Concrete. WHD 25 Microanalysis Consultants Ltd, 2012.

[16] ASTM C293 / C293M-16, Standard Test Method for Flexural Strength of Concrete (Using Simple Beam with Center-Point Loading), ASTM International, West Conshohocken, PA, 2016, www.astm.org.

[17] Dry, C., "Improvement in reinforcing bond strength in reinforced concrete with self-repairing chemical adhesives.". SPIE, pp. 44–50, 1997

[18] ASTM, C. "143/C 143 M: Standard test method for slump of hydraulic-cement concrete." Annual Book of ASTM Standards 4 (2010).

[19] ASTM, C. "231, Standard test method for air content of freshly mixed concrete by the pressure method." In American Society for Testing and Materials. 2000.

[20] Brown, Eric N., et al. "In situ poly (urea-formaldehyde) microencapsulation of dicyclopentadiene." Journal of microencapsulation 20.6 (2003): 719-730.

CHAPTER 4. SELF-HEALING EVALUATION OF REINFORCED CONCRETE BEAMS WITH CALCIUM NITRATE MICROCAPSULES

4.1 Introduction

In recent years, many approaches and methods were introduced to utilize self-healing materials in reinforced concrete. Self-healing processes may be divided into two categories: (1) non-automated materials, which require an external trigger, and (2) automated materials, which require no external trigger. In addition, self-healing material may be categorized as extrinsic and intrinsic. The extrinsic subclass consists of healing additives, such as microcapsules, that are embedded into the concrete matrix to allow the material to self-heal. The intrinsic subclass requires no healing agents but rather, it requires physical interaction between the interfaces of the crack, for example, the activation of shape memory alloys (SMA) wires in concrete beams [1]. Li Sun et al. studied the effect of SMAs embedded in concrete beams and observed that SMA wires closed crack up to 4.0 mm in width [2].

Microcapsules have gained interest as an effective method to enhance the self-healing capabilities of concrete under certain conditions; however, the effectiveness of this method is limited to micro-cracks. As the crack width becomes larger (> 0.3 mm), the healing agent in the microcapsules does not interfere with the crack faces. As a result, only healing of small crack width may be achieved [3].

In this study, the automatic and non-automatic self-healings of concrete were evaluated under both extrinsic and intrinsic mechanisms. The healing of concrete cracks was achieved by embedding microcapsules containing calcium nitrate as a healing agent into the concrete matrix. Microcapsules would break and release healing agents under high stresses that occur during

cracking formation. Moreover, conventional structural reinforcement was replaced by shape memory alloys, which were triggered by induced heat; this process was expected to hold the crack interfaces together in order to allow microcapsules to heal the concrete section.

4.2 Objectives and Scope

This study had three main objectives: (1) evaluate the self-healing effectiveness of calcium nitrate microcapsules on steel and SMA reinforced-concrete beams; (2) evaluate the structural behavior and stiffness recovery of beams after damage under water curing conditions; and (3) study the influence of shape memory effect on the self-healing capabilities of concrete beams. In order to study structural behavior and healing efficiency, an experimental program consisting of 20 specimens was planned. Beam dimensions were modified from ASTM C 293 specimen dimensions in order to allow for a more typical flexural behavior. The undamaged and damaged stiffness, peak strength, and deformation were measured and compared with post-curing time values. Moreover, crack monitoring was conducted in order to evaluate the crack-healing over the curing time, and an Energy Dispersive X-Ray Spectroscopy (EDX) analysis was conducted in order to quantify the healing components in the cracked areas.

4.3 Background

Concrete is the most widely used building material in the world while cement is used to make approximately 2.5 metric tons of concrete per person per year [4]. Moreover, the production of Portland cement generates nearly one ton of CO_2 when the emissions attributed to calcination are paired with fuel combustion [4]. In addition, the cost of bridge reconstruction has been estimated at $200 billion in the US alone [5]. In fact, technologies to increase the service life of concrete would reduce the demand of new structures. Hence, the choice to repair in-place concrete

construction not only would directly reduce pollution and maintenance cost, but also energy consumption and CO_2 emissions as well. To this end, self-healing concrete has been proposed as one method to achieve this goal, and it has received significant interest by the research community over the last decade [6].

Different approaches were studied to improve the self-healing properties of concrete. Among these approaches, the embedment of microcapsules containing healing agents in the concrete mix has been proposed by different researchers. Huang et al. [5] and Pelletier [6] successfully encapsulated sodium silicate solution into spherical capsules. In Pelletier's study, the compressive strength of the concrete was not compromised by the addition of the capsules but Huang reported a decrease in strength. Following concrete cracking, the capsules released the healing agent (Na2SiO3), which reacted with the calcium hydroxide naturally presented on concrete; the reaction formed calcium silica hydrate (CSH), which sealed the crack [7, 8]. In another approach by Mihai [9], spherical capsules were prepared using a urea formaldehyde formalin (UFF) shell, containing a two-component epoxy resin. Mihashi reported that the two-component epoxy had difficulties in hardening, due to a mixing complication. However, a similar approach developed by Feng et al. [10] using a modified epoxy resin hardened when optimal conditions were provided for the epoxy.

Shape Memory Alloys (SMA) were also used as a way to repair concrete cracks. In a study developed by Sakai et al. [11] and Kuan and Ou [12, 13], the super elastic property of SMAs embedded in concrete allowed induced cracks to completely close. A research group in Cardiff University [14, 15, 16,17, 18] embedded shrinkable polymer tendons into cementitious materials. Heating these tendons activated a shape memory effect that allowed autonomic crack closure, thus enhancing an autonomous self-healing. In a study conducted by Saiidi et al., the researchers

conducted several test procedures to evaluate the yield load and ultimate load on both steel and Nickel-Titanium (SMA) reinforced beams. The results showed that those specimens containing SMA generated lower values for both yield and ultimate load; in addition, beams with SMAs showed a 60% decrease in stiffness, which was attributed to the relative lower modulus of elasticity of SMAs, compared to steel [19].

4.4 Experimental Program

4.4.1 Self-Healing Microcapsules

Calcium nitrate is known to have hydration incentives properties, and therefore is utilized as an accelerator admixture in the concrete industry. In addition, calcium nitrate also enhances the formation of belite during the hydration product [24]. Previous research by the authors developed methods for encapsulating calcium-nitrate [20, 21]. The microcapsules developed in this study followed the same procedure, in which the production parameters were as follows: (a) heating temperature of 40ºC, (b) heating time of 1.5 hours, (c) 0.6g of sulfonic acid, and (d) agitation rate of 800 rpm. Figure 4.1 illustrates typical microcapsules morphology and dimensions from the adopted procedure.

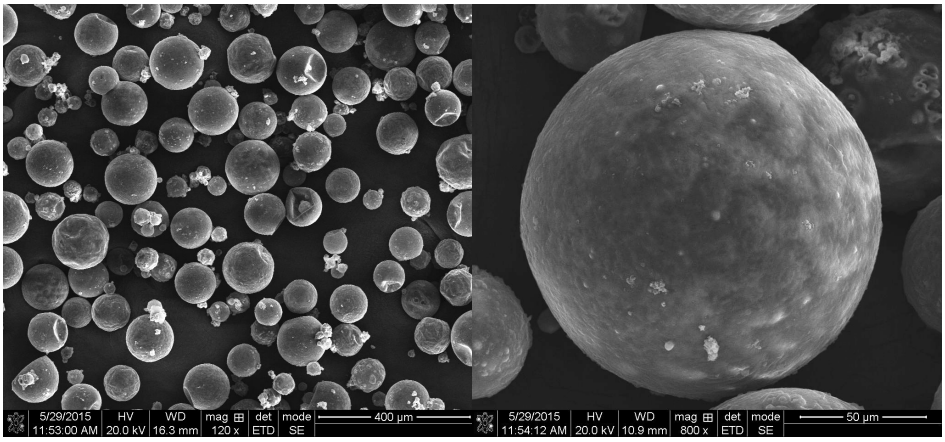

Figure 4.1. Calcium-Nitrate microcapsules morphology

4.4.2 Experimental Beam Matrix

The experimental program encompassed beams with two reinforcement types (conventional steel bars and SMA bars) and concrete mixes (with and without microcapsules). The experimental program was divided into two main groups: control and self-healing. Control specimens were prepared with no microcapsules in the concrete mix to serve as reference. Beams in the self-healing group (MC group) included calcium nitrate microcapsules (1% by weight of cement). For both control and healing agent test conditions, steel reinforced and SMA-reinforced beams were used leading to four different test conditions as shown in Table 4.1. Five specimens were prepared for each test condition to allow for different tests and to provide replicas. The reinforcement of the beams was designed to fail in flexure by overdesigning the beams in shear. Table 4.1 presents the characteristics of the different test conditions.

Table 4.1. Experimental matrix of beams

Group ID	**Microcapsules content (% - by weight of cement)**	**Reinforcement type**	**Numbers of specimens**
Steel	0.0	#3 Steel Grade A32	5
MC-Steel	1.0	#3 Steel Grade A32	5
SMA	0.0	7mm Nickel-Titanium Alloy	5
MC-SMA	1.0	7mm Nickel-Titanium Alloy	5

4.4.3 Beams Design

Figure 4.2 presents the reinforcement details for a typical beam in the experimental program and the loading setup used for testing. It should be noted that because of the small, cross-sectional dimensions of the tested beams, bending the bars caused the corners to be free of reinforcement at the ends where the beam is supported. To avoid the potential for premature failure at these corners, additional L-shaped bars of a smaller diameter were added at the corners.

These bars overlapped with the main reinforcement for about 15.2 mm (6in.) but were not extended to the critical test region at mid-span. Concrete beams were cast into a modified ASTM C 293 rectangular beam with dimensions of 39.4 in. x 4in. x 4in. [22].

(a) (b)

Figure 4.2. (a) Reinforcement setup in forms and (b) Placement set up under loading

4.4.4 Concrete Mixture Design

The concrete mix design was based on a typical mix used in Louisiana for road applications with an expected compressive strength at 41.4 MPa and with a water-cement ratio of 0.48. The coarse aggregates were limestone, in which the maximum aggregate size was 19 mm. Sand was used as a fine aggregate with a maximum particle size of 4.76 mm. Microcapsules were dispersed into one-third of the water used prior to the mix procedure. The mix procedure involved three minutes of mixing coarse aggregate with the other two-thirds of the water content, followed by the addition of cement, fine aggregates, and one-third of the water for another three minutes. Afterwards, the mix was left for rest for a three-minute period. Finally, the contents were mixed again for three minutes before pouring. Table 4.2 presents the details of the concrete mix design.

Table 4.2. Concrete mix design

Material description		**Proportion (kg/m^3)**
Aggregate 1	Sand, Dennis Mills, LA	789
Aggregate 2	#67 Limestone, Martin Marietta	1118
Cement	Type I	297
Water	Mixing Water	141
Air (%)		5.0%
Admixtures		**Dosage**
Air Admixture	N/A	0.00
Admixture 1	Glenium 7500	15.00 (ml/batch)
Admixture 2	Microcapsules	1% (by weight of Cement)

4.4.5 Structural Testing

The first phase of testing was conducted to understand the structural behavior of beams constructed with advanced materials up to the failure point. Determining the flexural strength from these tests also allowed for determining the appropriate load levels for the second phase of testing. Two of the specimens in each group were dedicated for strength tests to determine the flexural capacity of the beams using a three-point bending setup. The load – deflection relationship was obtained for each of the tested beams up to the failure point. From these tests, the ultimate load (P_u) of the tested beam was also determined.

The test procedure in the second phase of testing was like the first phase of testing; however, beams were only subjected to a load equal to 60% of the ultimate load ($0.6P_u$), as determined from the first phase. Visible cracks were analyzed using light microscopy during loading, immediately after the load was removed, and then periodically afterwards, while the cracked beam started the water-curing period.

After the healing period, a second round of testing was conducted on the beam specimens, which were tested up to failure. Retesting the beams allowed one to observe any change in structural behavior in comparison to the behavior of the control specimens and prior to healing.

4.4.6 Crack Monitoring and Curing Conditions

After the conclusion of the second phase of testing, all specimens were placed in Deionized water (DI) to accelerate the healing process. A digital light microscope was used to study the evolution of the cracks after three and seven days of water curing. Images obtained in this period were analyzed by quantifying and comparing the cracked area in all groups. Furthermore, visible cracks were monitored during the healing period using a digital microscope. Image analysis software was used to calculate and measure the healing efficiency for each test condition. The healing efficiency was calculated, based on Equation (4.1):

$$f_{f=100-\frac{A_t}{A_o}*100} \quad \text{(Eq. 4.1)}$$

where,

f_f= healing efficiency (%);
A_o= Initial area of the cracks; and
A_t = Area of the cracks at the time of analysis.

Beams were then placed in an oven in which temperatures would rise until the transition temperature of the shape memory alloys was achieved. The transition temperature for the particular SMAs used in this research was between 60-70 ^{o}C. However, for a more practical used in real structures the transition temperature can be lowered. Water was constantly poured into the cracked areas in lapses of one hour for 3 days in order to keep the area hydrated and to induce microcapsules and unhydrated cement to create hydration products. Additionally, to record the effects of SMA recovery, pictures were captured before and after heating to monitor the changes

in crack widths. These results were used to capture any changes in the crack dimensions and to provide a reference point for comparison with conditions immediately after the end of the second phase and after the healing period.

4.5 Results and Analysis

4.5.1 Concrete Properties

The slump test did not exhibit a significant variability with the use of microcapsule. However, there was a significant change in air content with the use of microcapsules. Batches containing microcapsules generated two times more air content than the control batch, 8.5% air content for 1% microcapsules concentration versus 4.5% air content for the control batch.

4.5.2 Beams Flexural Strength

Table 4.3 presents the details of the flexural strength test results. Results of the flexural test showed that the strength capabilities of the control groups, e.g., Steel and SMA, were significantly greater than the samples containing microcapsules. Steel beams averaged an ultimate load (P_u) of 23.9 kN, while the MC-Steel beams yielded an average P_u of 15.1 kN. The SMA group averaged an ultimate load of 10.5 kN, while the MC-SMA specimens yielded an average ultimate load of 7.1 kN. The MC-Steel group experienced a decrease in strength of 36.6% relatively to the beams without microcapsules, and similarly the MC-SMA group showed a decrease of 31.9% as compared to the SMA group. These results suggest that microcapsules negatively affected the flexural strength of concrete beams, which may be attributed to the high air content. Based on these results, there exists a strong correlation between the decrease of flexural and compressive strengths and the addition of microcapsules to the concrete matrix. The authors are currently

evaluating a new microencapsulation preparation procedure to address the decrease in strength associated with calcium nitrate microcapsules.

Table 4.3. Concrete beams flexural strength properties

Group ID	**# Specimen**	**Ultimate load, Pu (kN)**	**Average ultimate load (kN)**
Steel	1	23.03	23.87
	2	24.7	
MC-Steel	1	15.59	15.13
	2	14.67	
SMA	1	10.84	10.45
	2	10.05	
MC-SMA	1	6.66	7.12
	2	7.58	

4.5.3 Stiffness Properties

Undamaged and Damaged Flexural Stiffness

In order to obtain the undamaged and damaged stiffness (K_u and K_d), beam specimens were subjected to a three-point bending flexural test. A loading of 60% of the ultimate load for each group, obtained from the flexural strength test, was used as the maximum load. The undamaged and damaged stiffness were measured before and after cracking of the samples, respectively. Table 4.4 shows the results of this testing phase. The SMA groups were found to have the highest, undamaged stiffness values followed by the steel cases. It was observed that groups containing microcapsules yielded substantially lower values for undamaged stiffness. These results were expected, due to the lower flexural strength values of the specimens containing microcapsules. The decrease of undamaged stiffness values of specimens containing microcapsules may be attributed to the fact that microcapsules hinder the hydration process before cracking. In fact, the efficiency

of microcapsules was observed after cracking of the specimens. For the damaged stiffness, the highest stiffness values were recorded for the steel groups, followed by the MC-Steel case.

The reason for higher damaged stiffness values for the steel groups, in comparison with the SMA groups, could be related to the higher bonding strength between steel and concrete, which was studied using digital image analysis.

Table 4.4. Stiffness properties for undamaged, damaged and healing samples

Group ID	**Average stiffness (N/mm)**		
	Undamaged, K_0	**Damaged, K_D**	**Healing, K_H**
Steel	7179.0	5912.4	6242.5
MC-Steel	3990.6	3487.1	4835.3
SMA	9410.9	2451.2	2649.3
MC-SMA	4962.1	1890.8	2289.0

Healing Recovery of Beams

Recovery of stiffness (K_H) after the curing period was calculated by comparing the undamaged and damaged stiffness. Figure 4.3a illustrates the stiffness properties for undamaged, damaged, and healed, for all tested specimens. The results showed a positive trend for stiffness recovery for all groups; however, there was a notable difference in stiffness recovery between the four groups. The average healing recovery for all groups are presented in Figure 4.3b. Results showed that steel and SMA groups had a stiffness recovery of 5.6% and 8%, respectively. On the other hand, addition of microcapsules to both steel and SMA increased the healing efficiency considerably by 38.7% and 21.1%, respectively. This indicates that using microcapsules for both steel and SMA resulted in a better performance in terms of stiffness recovery. This may be attributed to the release of calcium nitrate as a healing agent into the cracked areas.

It was also observed that the beams reinforced with steel performed better than those reinforced with SMA, possibly due to the stronger bonding between steel and concrete. Deformed steel rebars were provided with lugs and ribs, which had better mechanical-anchoring than the smooth and flat-shaped memory alloy rebars. The shape and surface of the steel bars resulted in a stronger bonding between the steel and the concrete paste than those of the SMA bars. Stronger bonding of steel reinforcement helped developed cracks to stay closer together which permitted the better interaction of unhydrated cement products with calcium nitrate as it was released from the microcapsules further promoting hydration.

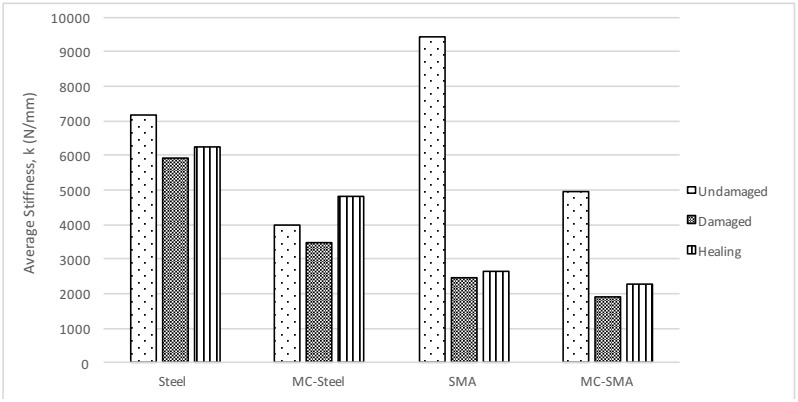

(a)

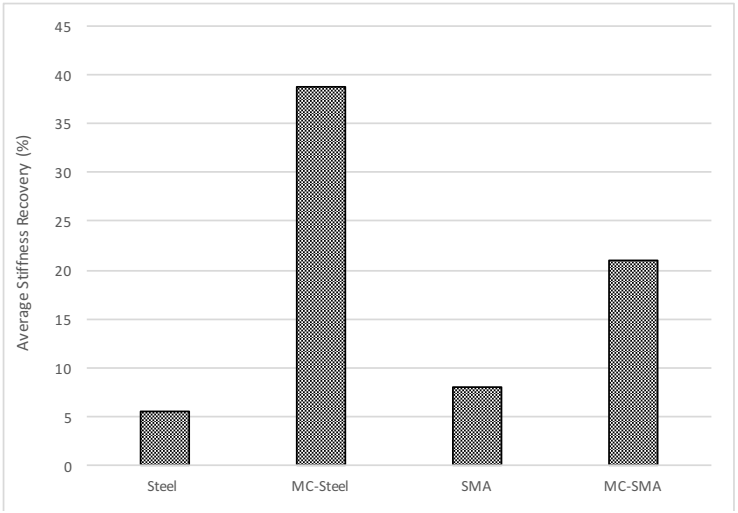

(b)

Figure 4.3. Undamaged, damaged and healing of (a) average stiffness and (b) average stiffness recovery

4.5.4 Image Analysis

Water Curing

Upon cracking of the beams, all specimens were submerged into water for curing. In order to avoid results variabilities caused by using tap water impurities (chlorides, sulphates, sodium bicarbonates, magnesium, chloride and iron), deionized water (DI) was used in order to avoid any unwanted particles from contaminating the cracked areas. Microscopic images of selected cracked regions were recorded in periods of one and three days; at day one, the initial, unhealed cracks were used as a reference point. An area analysis was used to identify and quantify the evolution of the cracked areas over the healing time. Figure 4.4 shows the results obtained from this analysis. From this figure, it is noted that all of the cases yielded a positive healing efficiency, meaning that partial or total cracks' closure occurred. In addition, Table 4.5 presents a comparison of the cracks before and after water curing.

As shown in Figure 4.4, the group that exhibited the best results were the beams reinforced with steel and containing microcapsules (MC-Steel), in which total closure of the cracks was observed. On the other hand, the steel beams without microcapsules healed with an efficiency of only 71%. Beams reinforced with SMA and microcapsules showed a healing efficiency of 54%, while SMA with no microcapsules yielded only 32% healing efficiency. It should be noted that the crack widths developed in the beams reinforced with SMA were noticeably wider than the ones with steel reinforcement, even though the beams were loaded consistently at 60% of the ultimate load. Strain gages data installed in the tension reinforcement revealed that both steel and SMA yielded allowing cracks to remain open when the loading was removed.In addition, the number of cracks developed by the steel beams were higher (between 4-6 cracks per beam) compared to the SMA beams (1-2 cracks per beam).

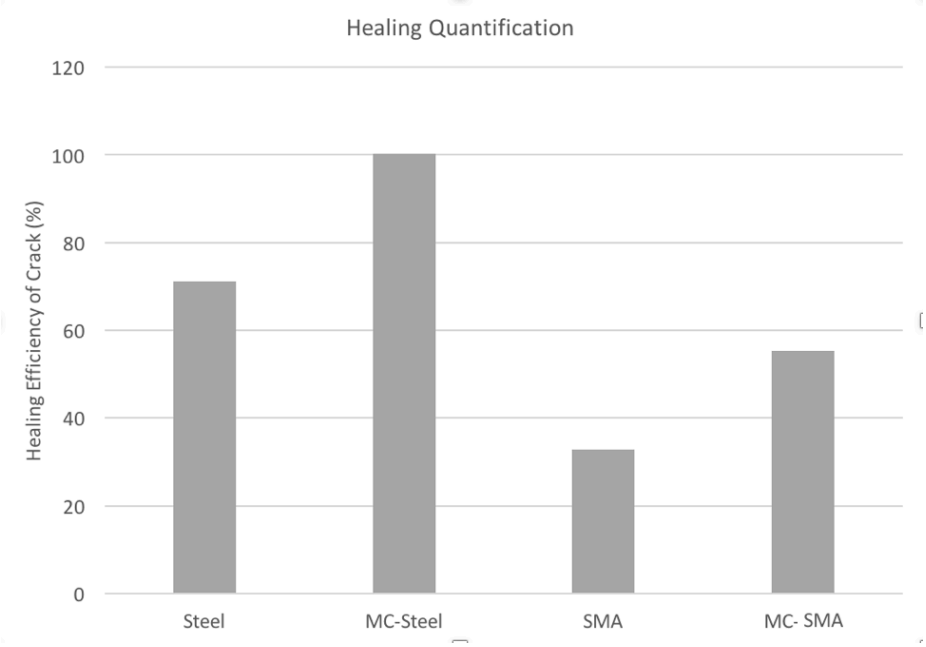

Figure 4.4. Healing efficiency of cracks

Table 4.5. Crack before and after water curing for 3 days

Day 1	**Day 3**
SMA	
	
SMA-Microcapsules	
	

(Table 4.5 continued)

Day 1	Day 3
Steel	
	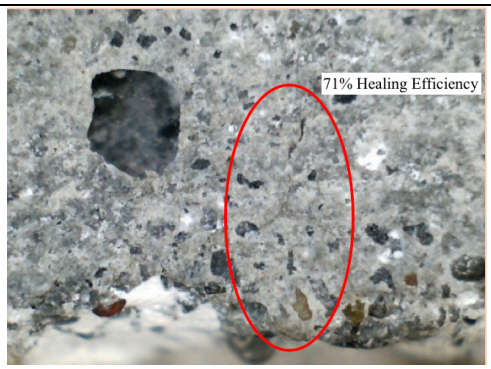
Steel-Microcapsules	
	

Activation of Shape Memory Effect

At the end of the water curing period, microscopic pictures for the analyzed area were recorded, and the beams were then subjected to a reloading of 40% of the ultimate load, in order to reopen the cracks for SMA activation. The beams were kept in an oven to maintain high temperatures (60-70^{o}C), thus activating– the shape memory effect. Figure 4.5a presents the average crack width results of the specimen after damaged and after healing period of 3 days, measured by light microscope images. Different crack widths of the samples containing steel and SMA with and

without microcapsules were evaluated. Generally, crack widths of the mixtures in the steel groups tended to be smaller than those of the SMA groups. As stated before, the surface characteristics between SMA and steel bars were quite different.

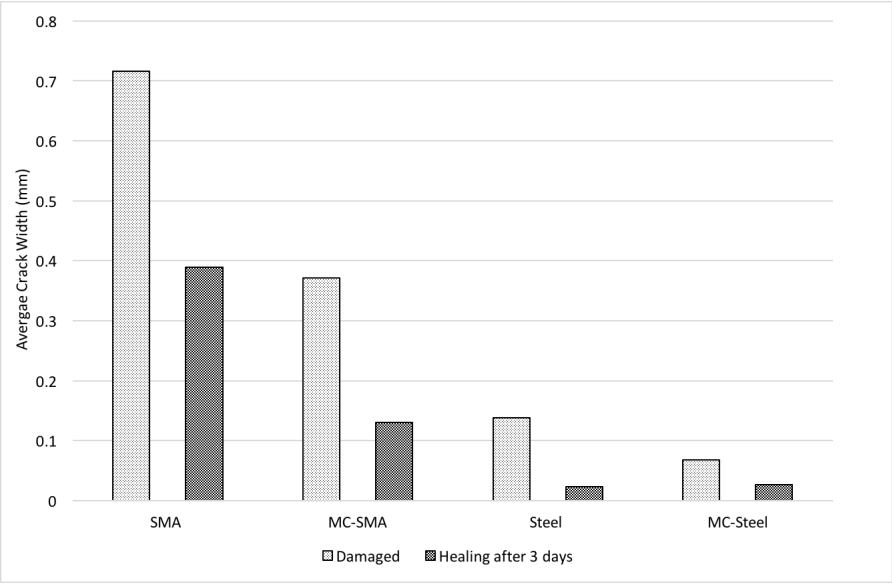

(a)

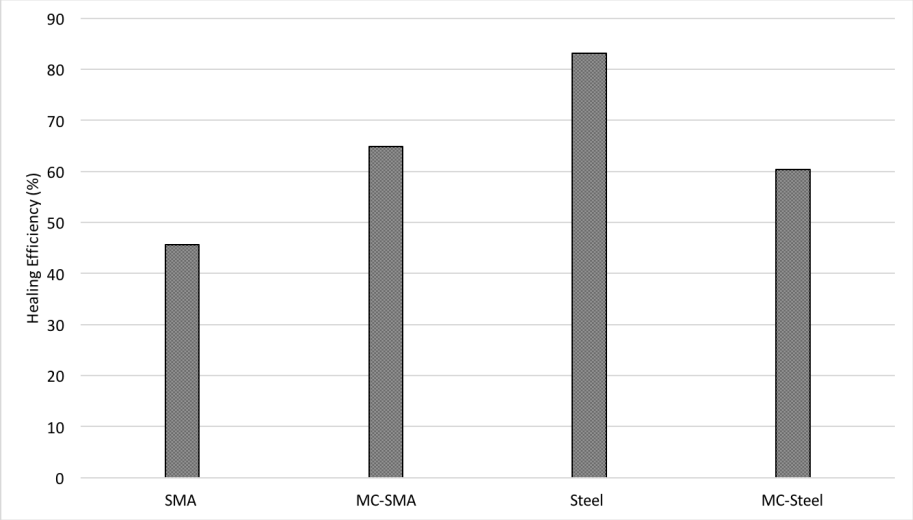

(b)

Figure 4.5. (a) Average crack widths of sample with steel and SMA in the presence and absence of microcapsules: after damaged and after healing for 3 days (b) Crack healing efficiency

The surface of the SMA bars was smooth while steel rebar contained ribs. This characteristic resulted in the bonding between SMA and concrete to be weaker than for steel. Czaderski et al. [25] investigated different coatings of SMA reinforcement, with the objective of increasing the pullout strength. In the present study, wider cracks were observed on SMA beams, which can be attributed to the weak bonding between SMA and the concrete paste. Figure 4.5b shows healing efficiency for 3 days. Specimens in the Steel group experienced the highest crack efficiency in this process, yielding 83% efficiency. The healing efficiency of MC-SMA group achieved 65%. Specimens in the MC-Steel group and SMA yield 60% and 46% respectively.

Table 4.6 presents a comparison of the cracks before and after healing. Developed crack widths under loading conditions were observed and recorded during the loading period. Beams were then unloaded and evaluated during the healing time. Images in table 4.6 show that the incorporation of microcapsules reduced the cracks widths notably, while the SMA without microcapsules displayed larger crack widths. Arce et al. investigated the healing agent release mechanism of calcium-nitrate microcapsules on mortar samples. Arce et al. observed broken microcapsules in the crack surface [26]. The same mechanism was observed to occur in this study, which was confirmed by EDX microanalysis of the formation of additional healing products in the presence of microcapsules**.** On the other hand, the effectiveness of microcapsules to heal crack was not as pronounced in the steel groups, due to the small crack size in these groups. This was confirmed through statistical analysis, which showed no statistical difference between the samples of the Steel and Steel-Microcapsules. In contrast, the groups with SMA revealed that there was a significant difference between SMA samples with and without microcapsules.

Table 4.6. Developed cracks before and after healing for 3 days

Before Healing	After Healing
SMA	
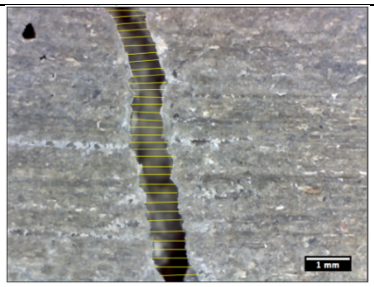 Zoom x10	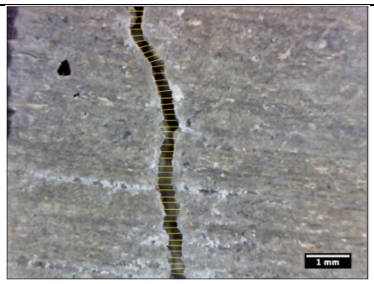 Zoom x10
SMA-Microcapsules	
 Zoom x10	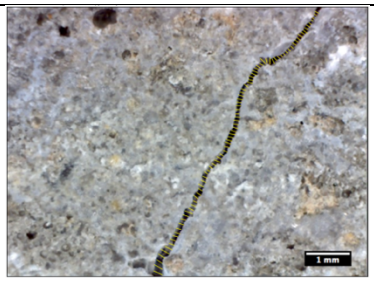 Zoom x10
Steel	
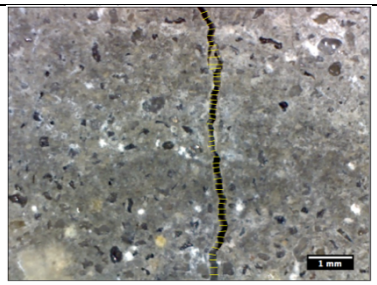 Zoom x10	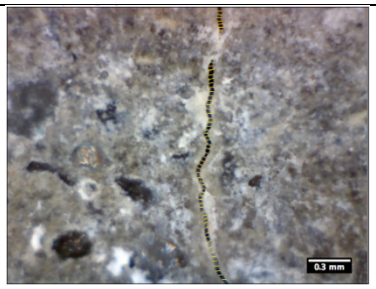 Zoom x150
Steel-Microcapsules	
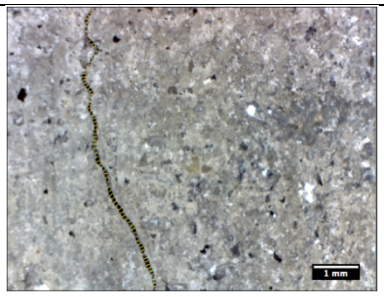 Zoom x10	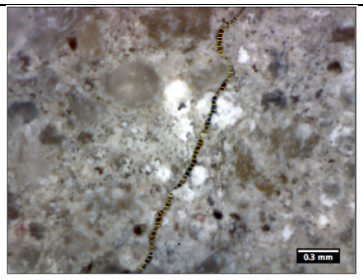 Zoom x150

4.6 Statistical Analysis

A Tukey's test statistical analysis was performed using 96 cracks sections (24 for each testing groups) to compare the results of similar mixes (i.e., Steel and Steel-Microcapsules, etc.) and to determine whether the differences in healing through heating were significant. Table 4.7 presents the normalized mean and the statistical ranking of the mixtures for different crack widths. Letters A, B, C, etc., were assigned to rank the statistical results for each group. The letter A is used for the highest average of crack widths, followed by the other letters in proper order. Double letters (e.g., B/C) indicate that there is no significant difference in the mixtures performance. Results of the statistical analysis under loading indicate that the SMA group, Rank A, was significantly different in crack widths from all other mixtures. Yet, the MC-SMA was equal in performance with the Steel group, while the Steel group was equal with MC-Steel, which ranked B/C. Although the MC-Steel group was different in crack widths with SMA and MC-SMA, Steel and MC-Steel were equal; therefore, the grouping was classified as Rank C.

Table 4.7. Statistical ranking of mixtures

Group ID	**Prior to healing**		**After healing**	
	Normalized mean	**Rank**	**Normalized mean**	**Rank**
Steel	0.138	B/C	0.023	B
MC-Steel	0.068	C	0.025	B
SMA	0.716	A	0.326	A
MC-SMA	0.371	B	0.116	B

The performance relationship for crack widths between samples after healing of 3 days is presented in Table 4.7. It may be observed that only the SMA group, Rank A, was significantly different in cracks widths from the other groups. The performance of the other mixtures, in terms of crack widths, was equal for MC-SMA, Steel and MC-Steel, Rank B. This suggests that

microcapsules did not significantly affect the crack widths of steel rebars. However, reinforcing concrete with SMA revealed that there is a significant difference between SMA samples with and without microcapsules.

4.7 Healing Products Characterization

After the healing period, cracked sections in the concrete specimens were cut using a diamond saw, and were analyzed using EDX microanalysis; the study inspected healing products located at the crack opening. An EDX spectrum was collected by using the spot mode in different locations of the crack, where the healing products were observed or were most likely to form. The procedure consisted of analyzing 50 individual spots, in which the spectrum was allowed to collect for 30 seconds for the Steel, MC-Steel, SMA, and MC-SMA groups. In order to visualize the chemical nature of the healing products generated by all groups, an Al/Ca vs. Si/Ca ratio plot was generated as shown in Figure 4.6.

Results show that the majority of points generated by the Steel group were closely located at or on the Si/Ca axis, which indicates a strong presence of calcium-hydroxide. Some locations were plotted close to the CH+C-S-H line, which indicates a combination of calcium-hydroxide with calcium-silica-hydrate. The group that plotted the most locations under the pure phase of C-S-H, which is approximately on the range (0.45-0.55, 0.04-0.008) [23], or a combination compound of CH and C-S-H, is the MC-Steel group, which indicates the formation of healing products. This trend is in agreement with the self-healing results presented in this study. The SMA groups showed results similar to the Steel groups, by showing points on the Si/Ca axis, with a few points dispersed on the CH and AFm lines. The groups containing microcapsules and SMA plotted points close to the origin (0, 0), which indicated the pure phase of CH.

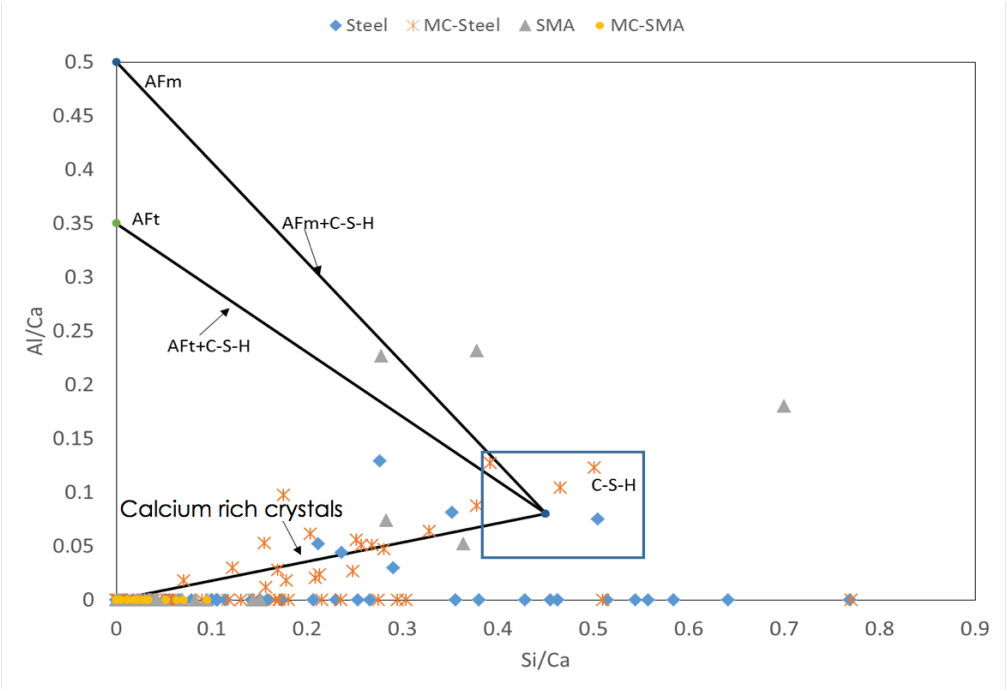

Figure 4.6. Al/Ca vs Si/Ca ratio plot

4.8 Conclusions

The following conclusions may be drawn from the results of the experimental program:

- Experimental results suggest that microcapsules have a direct effect on decreasing the flexural strength of concrete beams. This result was attributed to the high air content when microcapsules are used.
- Even though microcapsules lowered the flexural strength of the beams, it was observed that the stiffness recovery value for MC-Steel group was the highest, followed directly by the MC-SMA group.
- An image analysis conducted for the groups after the water curing period revealed that the specimens with microcapsules showed the best crack healing efficiency whether steel or SMA was used.

- Statistical analysis showed that upon shape memory effect activation, similar mixtures (i.e., Steel and Steel-Microcapsules, etc.), showed no statistical difference between samples with Steel and Steel-Microcapsules. However, reinforcing concrete with SMA revealed that there was a significant difference between SMA samples with and without microcapsules.

4.9 References

[1] M. D. Hager, P. Greil, C. Leyens, S. Van Der Zwaag, and U. S. Schubert, "Self-healing materials," Adv. Mater., vol. 22, no. 47, pp. 5424–5430, 2010

[2] Li, Sun, et al. "Analysis on Factors Affecting the Self-Repair Capability of SMA Wire Concrete Beam." Mathematical Problems in Engineering (2013): 1-6. Academic Search Complete. Web. 25 July 2016.

[3] Ter Heide, N.,"Crack healing in hydrating concrete. MSc thesis, Delft University of Technology", p. 128 (2005)

[4] van Oss, H.G, " Background facts and issues concerning cement and cement data", Open-file report 2005-1152, US Dept. of the Interior & US Geological Survey (2005)

[5] Yunovich, M., Thompson, N.G.," (Van Oss 2005)" Concrete Int. 25(1), 52–57 (2003)

[6] V. C. Li and E. Herbert, "Robust Self-Healing Concrete for Sustainable Infrastructure," J. Adv. Concr. Technol., vol. 10, no. 6, pp. 207–218, 2012.

[7] Huang, H., Ye, G., "Application of sodium silicate solution as self-healing agent in cementitious materials", International Conference on Advances in Construction Materials through Science and Engineering, Hong Kong, China (2011)

[8] Pelletier, M., et al. "Self-healing concrete with a microencapsulated healing agent" (2010)

[9] Mihashi, H., et al.: Fundamental study on development of intelligent concrete characterized by self-healing capability for strength. Transactions of the Japan Concrete Institute 22, 441–450 (2000)

[10] Feng, X., et al., "Self-healing mechanism of a novel cementitious composite using microcapsules", International Conference on Durability of Concrete Structures, Hangzhou, China, pp. 195–204 (2008)

[11] Sakai, Y., et al. “Experimental study on enhancement of self-restoration of concrete beams using SMA wire”, Conference on Smart Structures and Materials, San Diego, California, pp. 178–186 (2003)

[12] Kuang, Y., Ou, J. “Self-repairing performance of concrete beams strengthened using super elastic SMA wires in combination with adhesives released from hollow fibers”, Smart Materials and Structures 17, 1–7 (2008)

[13] Kuang, Y., Ou, J., “Passive smart self-repairing concrete beams by using shape memory alloy wires and fibers containing adhesives”, Journal of Central South University Technology 15, 411–417 (2008)

[14] Isaacs, B., et al. “Enhancement of self-healing in cementitious materials, posttensioned with shrinkable polymers”, White, S., Bond, I. (eds.) 2nd International Conference on Self-Healing Materials, Chicago, USA, p. 102 (2009)

[15] Isaacs, B., et al., “Enhancement of self-healing in cementitious materials”, Bond, I., Varley, R. (eds.) 3rd International Conference on Self-healing Materials, Bath, UK, pp. 119–120 (2011)

[16] Lark, R.J., et al. “Active confinement of cementitious composites with shape memory plastics”, 2nd International Conference on Self-healing Materials, Chicago, USA, p. 138 (2009)

[17] Joseph, C., et al. “Experimental investigation of adhesive-based self-healing of cementitious materials”, Magazine of Concrete Research 62(11), 831–843 (2010)

[18] Jefferson, A., et al. “A new system for crack closure of cementitious materials using shrinkable polymers”, Cement and Concrete Research 40(5), 795–801 (2010).

[19] Saiidi, M. Saiid, et al. “Pilot study of behavior of concrete beams reinforced with shape memory alloys.” Journal of materials in civil engineering 19.6 (2007): 454-461.

[20] M. Hassan, J. Milla, T. Rupnow, M. Al-Ansari, and W. Dayly, “Micro-Encapsulation of Calcium Nitrate for Concrete Applications.” 95th Transportation Research Board Annual Meeting, Washington, D.C., 2016.

[21] J. Milla, M. Hassan, T. Rupnow, M. Al-Ansari, and G. Arce, “Evaluation of the Effect of Self-Healing Calcium Nitrate Microcapsules on Concrete Properties.” 95th Transportation Research Board Annual Meeting January 10-14, 2016, Washington, D.C

[22] ASTM C293 / C293M-16, Standard Test Method for Flexural Strength of Concrete (Using Simple Beam with Center-Point Loading), ASTM International, West Conshohocken, PA, 2016, www.astm.org.

[23] N. Winter, Scanning Electron Microscopy of Cement and Concrete. WHD 25 Microanalysis Consultants Ltd, 2012.

[24] Justnes, H., & Nygaard, E. C. (1995). Technical calcium nitrate as set accelerator for cement at low temperatures. Cement and concrete research, 25(8), 1766-1774.

[25] Czaderski, Christoph, Bernd Hahnebach, and Masoud Motavalli. "RC beam with variable stiffness and strength." *Construction and Building Materials* 20, no. 9 (2006): 824-833.

[26] Arce, Gabriel A., Marwa M. Hassan, Louay N. Mohammad, and Tyson Rupnow. "Characterization of Self-Healing Processes Induced by Calcium Nitrate Microcapsules in Cement Mortar." *Journal of Materials in Civil Engineering* 29, no. 1 (2016): 04016189.

CHAPTER 5. COMPARATIVE STUDY OF SELF-HEALING CONCRETE TECHNOLOGIES: LIFE CYCLE COST ANALYSIS

5.1 Introduction

Self-Healing of cementitious materials is a topic that has received considerable attention in the last 20 years, mainly due to the potential benefit of increasing the durability of concrete infrastructure. Self-healing could be an important factor on increasing the service-life of structures. For instance, it is well known that an elevated concentration of chloride in reinforced concrete causes corrosion in embedded steel. The buildup of corrosion products over time generates internal cracking around the reinforcing bars with damaging consequences, as these cracks propagate to the surface [1]. De Rooij et al. [2] observed a reduction in the chloride diffusion coefficient in marine concrete structures, due to self-healing of microcracks over time, as well as the diminishing damage due to corrosion. Van Breugel [3] found that gradual deterioration in the infrastructure occurs until it reaches a moment in time when urgent rehabilitation action is needed to meet the design requirements. However, a second rehabilitation procedure is often needed shortly after the first procedure. Van Breugel [3] reported that the ideal case for infrastructure maintenance is one that has no cost associated with it. This could be achieved by using materials that are able to self-repair.

Different methods to achieve improvement on self-healing capabilities in cementitious materials include embedding microcapsules containing healing agents and using shape memory alloys (SMA) as a substitution for convectional steel reinforcement [4, 5, 6, 7, 8]. In order to quantify the real cost benefit of using the available self-healing technologies, a life cycle cost analysis should be conducted. Frangopol and Jung Kong [9] stated that the construction cost, the maintenance cost, the user cost, and the failure cost should be considered in a life cycle cost

analysis (LCCA) of deteriorating infrastructures. This concept may be applied on conducting a comparative LCCA, in which the main parameter of evaluation consists of self-healing methods.

In this paper, a comparative LCCA is conducted for self-healing concrete pavements containing calcium-nitrate microcapsules, using SMA, a concrete containing both microcapsules and SMAs. For this study, the construction, material, and maintenance cost were the main categories considered, with the assumption that the user cost and failures cost would be constant among all the cases. Furthermore, the LCCA method was based on the expected probability of rehabilitation at a certain infrastructure age and the expected maintenance cost.

5.2 Objectives and Scope

The objective of this study is to conduct an economic analysis to evaluate the long-term economic efficiencies of self-healing concrete pavements as a competing alternative to conventional concrete. In order to conduct this analysis, the main parameters considered by the LCCA are the initial cost of the alternatives and the cost of the rehabilitation at a certain age of the pavement. The LCCA also considered the expected probability of rehabilitation, together with its expected rehabilitation cost at a certain age of the pavement.

5.3 Background

The decision in selecting a specific alternative for an infrastructure project is a complex process that should consider various parameters. If all these parameters can be represented in monetary terms, the best alternative would be the one with the least cost over the service life of the structure. According to James Walls III and Michael Smith [10], LCCA is an analysis technique that supports more informed investment decisions and can be applied to a wide variety of investment-related decisions to evaluate the economic worth of alternatives. LCCA involves economic analysis over

long period of time. The federal highway administration (FHWA) recommends the minimum time for an LCCA for a pavement project to be no less than 35 years. AASTHO also recommends that for heavy-duty pavement, the minimum analysis period should be at least 50 years [11]. In order to conduct a reliable cost calculation, dollars spent in the future should be considered. The dollars spent in the future may be converted to present value dollars, using a specific discount rate. FHWA recommends using a present value approach (PV), which converts initial and future cost to present worth [12]. The net present value formula for keeping pavements above the minimum serviceability threshold is defined by James Walls III and Michael Smith [10] as follows:

$$NPV = Initial\ Cost + \sum_{k=1}^{N} Rehabilitation\ Cost_k \left[\frac{1}{(1+i)^{n_k}}\right] \quad \text{(Eq. 5.1)}$$

where: i=discount rate

n=year of expenditure

Discount rates are driven by several socio-economic factors and the prediction becomes more difficult over long periods of time. Real discount rates reflect the true time value of money, excluding the effects of the general rate of inflation. However, the general methodology with life cycle studies is to ignore the effects of inflation, based on the assumption that all cost will inflate at the same rate [13]. Current practices of LCCA for infrastructures are based on the OMB Circular A-94 and use a discount rate between 3% to 5% [12].

LCCA may be conducted using two types of approaches. The first approach is a deterministic methodology, in which input variables such as maintenance and rehabilitation are fixed and distinct at the time of occurrence and in cost. Such inputs are based on a historical database for previous similar projects and on professional judgment [13]. The major advantage of using a deterministic approach is that calculations are usually simple and straightforward.

However, this approach does not consider the uncertainty in the input variables, meaning that the results are very sensitive to any misassumption made in the analysis. The second approach is the probabilistic methodology, which uses probabilistic distribution for discount rate, maintenance cost, time of rehabilitation procedures, etc. The major disadvantages of using a probabilistic approach are that calculations gets exponentially higher as more variables are included in the analysis. However, the results in using this approach would determine the likelihood that a particular LCC forecast would actually occur [14].

One of the variables that must be considered in conducting LCCA is rehabilitation procedures. According to Hall et al., pavement rehabilitation consists of "structural or functional enhancement of a pavement which produces a substantial extension in service life, by substantially improving pavement condition and ride quality [15]" which also includes restoration treatments and overlays. Different pavement alternatives may have different expected rehabilitation times. A typical example is shown in Figure 5.1(a) in which two pavement alternatives are compared, one with a long-term rehabilitation time and one with a shorter rehabilitation time.

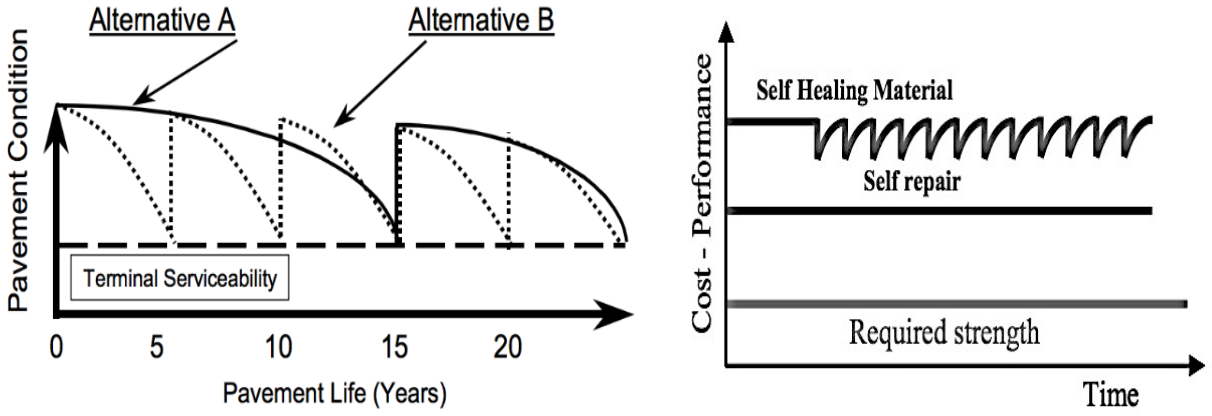

(a) (b)

Figure 5.1. (a) Conventional strategies [10], (b) Self-healing ideal model [16]

As discussed, the ideal case for a rehabilitation treatment is one that will not have a significant cost, while maintaining the minimum requirement of serviceability.

Using self-healing materials in pavements could cause a noticeable change to the conventional performance vs. rehabilitation strategy. The new performance curve is illustrated in Figure 5.1(b).

5. 4 Methodology

5.4.1 Selecting Alternatives

The potential cost benefits of self-healing concrete can be quantified by conducting a life-cycle cost analysis. This first step towards conducting a case study should be to select the type of structures in which that technology is best suited. Previous studies have shown that self-healing efficiency of calcium-nitrate microcapsules increase with the presence of water, hence selecting a concrete pavement, which is constantly subjected to a rain event in most areas, which can in turn be a reliable option [17]. Moreover, per the AASTHO guide for design of pavement structure, "the purpose of distributed steel reinforcement in reinforced pavements is not to prevent cracking, but to hold tightly closed any cracks that may form [18]." Hence, if steel reinforcement is substituted for SMA reinforcement, it could be a better material choice, due to its super-elastic property and shape memory effects. Therefore, the present study will conduct a LCCA on continuously reinforced concrete pavement (CRCP).

The base alternative for this study will be a conventional CRCP, using longitudinal steel reinforcement, from now on abbreviated as "*Steel*". The considered alternatives will be: (1) CRCP with calcium-nitrate microcapsules, from now on abbreviated "*Steel-MC*", (2) CRCP using SMA longitudinal reinforcement, from now on abbreviated as (*SMA*), (3) CRCP with both calcium-nitrate microcapsules and SMA longitudinal reinforcement, from now on abbreviated as (*SMA-*

MC). (4) CRCP with SMA fibers, from now on abbreviated as (*SMA Fibers*) and (5) CRCP with SMA fibers and calcium nitrate microcapsules, from now on abbreviated as (*SMA Fibers-MC*).

5.4.2 Initial Cost

Obtaining a good estimate of the initial cost of concrete-reinforced concrete pavement requires a survey of historical bids of similar construction projects. To obtain a good initial estimate, however, it is necessary to base our study on an initial hypothetical design that takes into account important cost parameters. These parameters should include material cost and labor, equipment, and overhead cost. The Texas A&M Transportation Institute [19] developed a spreadsheet tool for calculating cost, based on the several design inputs. The design assumptions and corresponding cost estimates using this tool are summarized in Table 5.1. Similar to the California DOT database, the estimated initial cost for the assumed base alternative resulted to be $256.28/CY.

Table 5.1. Construction cost calculation [19]

Description	**Unit**	**CRCP**		
Total Project Length	mile	1		
Pavement Thickness	inch	9		
Pavement Width	feet	24		
Reinforcement, Tie Bar and Dowel Bar Volume	%	0.79		
Concrete Volume	CY	3492		
Transverse Reinforcement Bar Volume	CY	4.5		
Longitudinal Reinforcement Bar Volume	CY	22.7		
Pavement Volume	CY	3520		
Construction cost				
Description	**Unit**	**Quantity**	**Unit cost**	**Total cost**
Coarse Aggregate for Concrete	ton	2,924	$30.05	$87,860
Concrete w/o Coarse Aggregate	CY	3,492	$45.00	$157,143
Total Concrete Cost	CY	0	$0.00	$245,003
Dowel Bar	each	5,280	$4.96	$0
Sawcutting	lane-feet	5,280	$1.97	$26,189
Joint Clean and Seal	lane-feet	184.96	$2,125	$10,402
Steel Reinforcement (#5, #6, Tie Bars)	ton	14,080	$16.16	$393,046

(Table 5.1 continued)

Description	Unit	Quantity	Unit cost	Total cost
Labor, Equipment & Overhead	SY			$227,533
Total Construction Cost				$902,172
Unit Construction Cost	SY			$64.07
Unit Construction Cost	CY			$256.28

The calculation of the manufacturing cost of calcium nitrate microcapsules was based on small scale laboratory production costs. Mass production of microcapsules should drive the cost down significantly. However, laboratory cost was used in the present analysis. Total steel reinforcement percentage for the assumed pavement resulted in a required 0.79% of the total pavement volume. This percentage includes all reinforcement types (Transverse, longitudinal, and tie bars). However, the alternative pavements containing SMA would only substitute for longitudinal reinforcement on the pavement, therefore a percent reinforcement of 0.65% was assumed and was used to calculate the cost per cubic yard of the SMA alternatives. For the case containing SMA fibers, the assumed percentage that should be used in pavement is 5% of the volume of steel reinforcement; therefore, the percentage used for this alternative is 0.65%x0.05=0.0325%. The breakdown of self-healing additives cost is presented in Table 5.2. It is important to notice the price difference per CY between SMA bars and SMA fibers.

The manufacturing cost of SMA's bars increase significantly as the thickness increases, and as a result, drives the massive increase of price per cubic yard of SMA bars versus SMA fibers. Based on the initial costs of the base alternative ($256/CY), the alternatives in which microcapsules are considered would add up a cost of $85/CY. In the case in which SMA reinforcement is used, the cost increase will be $1,398/CY; yet, the increased cost of the SMA fibers will be $3.4/CY. Based

on the cost of the different self-healing additives, it is observed that the initial cost per cubic yard increases considerably in cases where SMA reinforcement is considered.

Table 5.2. Cost of self-healing additives

Microencapsulation procedure (laboratory manufacture cost)			
Material description	Quantity (grams)	$/batch (30 g yield)	$/CY of concrete (0.5% by weight of cement)
Urea	5.0	0.2	7.8
Formaldehyde	12.7	0.7	26.0
Calcium Nitrate	10.0	0.7	25.5
Total		2.3	59.3
Shape-memory alloy cost			
Material description	Reinforcement (%)	$/CY	$/CY in Pavement
SMA Bar (ø=0.3 inch)	0.65	215190.9	7,381
SMA Fibers	0.00325	1059.4	7.52

5.4.3 Rehabilitation Cost

Rehabilitation cost calculation was estimated in a similar manner to the initial cost. The rehabilitation alternative considered in this study is a full depth repair and asphalt overlay. Both full depth repair and asphalt overlay costs are based on the Texas state wide average bid prices [19]. Rehabilitation costs are based in terms of percentage of the area to be repaired. It was assumed that the total area needing to be repaired for both first and second rehabilitations represented 10% of the total pavement area. For first rehabilitation procedures, a full depth rehabilitation was considered, while for the second rehabilitation, an asphalt overlay was considered. Assumptions were that the effect of the microcapsules would importantly impact the percentage area which needed to be repaired [7, 17]. This effect could be considered by decreasing the area of repair from 10% of the base alternative to 0%. Moreover, the effect of the SMA reinforcement and fibers was considered to have the same effect on the second rehabilitation procedure. The healing effect of the microcapsules would be diminished for a second rehabilitation

procedure. Since the healing products inside microcapsules are limited, these can only be used for a single rehabilitation event. The effect of self-healing microcapsules was assumed to diminish the cost of the first rehabilitation, while the effect of the SMA was assumed to eliminate the cost for a second rehabilitation. Table 5.3 shows a summary of the cost of the rehabilitation procedures for all alternatives.

Table 5.3. Rehabilitation cost [19]

Pavement type	**Unit**	**Rehabilitation #1 cost (21 +/- 6 years)**	**Rehabilitation #2 cost (13 +/- 4 years)**
Steel	Per mile	$244,274	$385,074
	Per CY	$69.39	$109.40
Steel+MC	Per mile	$0	$385,074
	Per CY	$0	$109.40
SMA and SMA fibers	Per mile	$244,274	$0
	Per CY	$69.39	0
SMA+MC and SMA fibers +MC	Per mile	$0	$0
	Per CY	$0	0

5.4.4 Probability Distribution of Rehabilitation Time

Frangapol [9] proposed a formulation to calculate the present value of the expected rehabilitation cost, based on the probabilistic distribution of the rehabilitation time of application. If the probabilistic distribution of the first and second rehabilitation times are combined on an absolute time scale, it is possible to estimate the combined probability at a certain point in time. This can be represented by the following decision tree (Figure 5.2)

The general formulation for the cost rehabilitation based on this method is as follows [9]:

$$E\left[C_{ri,pj}(t)\right] = \frac{C_{ri}}{(1+v)^{t_{ti,j}}} \quad \text{(Eq. 5.2)}$$

where:

E=Expected cost
p_j=the j-th path in the decision tree,
v=discount rate, (3% will be used in this study)
C_{ri}=undiscounted cost of the i-th rehabilitation
$t_{i,j}$=time (absolute time scale)

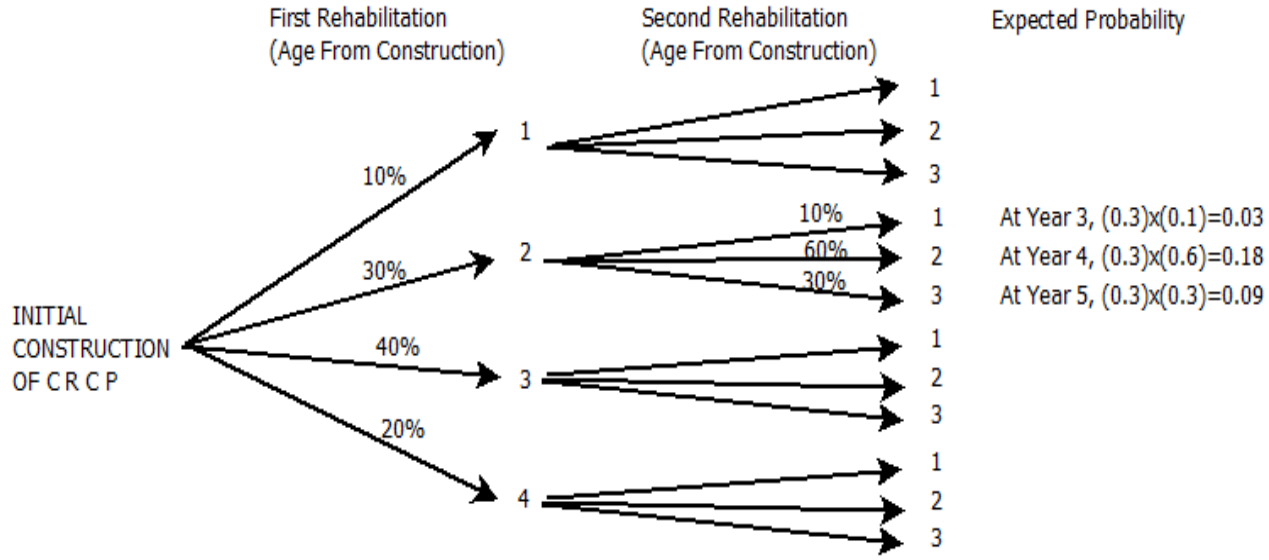

Figure 5.2. Decision tree of two rehabilitation procedures

This general formulation was used in the study where the probability of the rehabilitation is estimated from a nation-wide dataset of concrete pavement rehabilitation procedures [20]. Figure 5.3 shows the rehabilitation times for continuously reinforced concrete pavement. The effect of self-healing concrete will have a positive impact on the cost of rehabilitation. As mentioned before, the ideal self-healing mechanism (figure 5.1b) will provide the structure with the ability to repair itself. Taking this into account for this model, the rehabilitation cost was taken into consideration when the rehabilitation procedure was conducted.

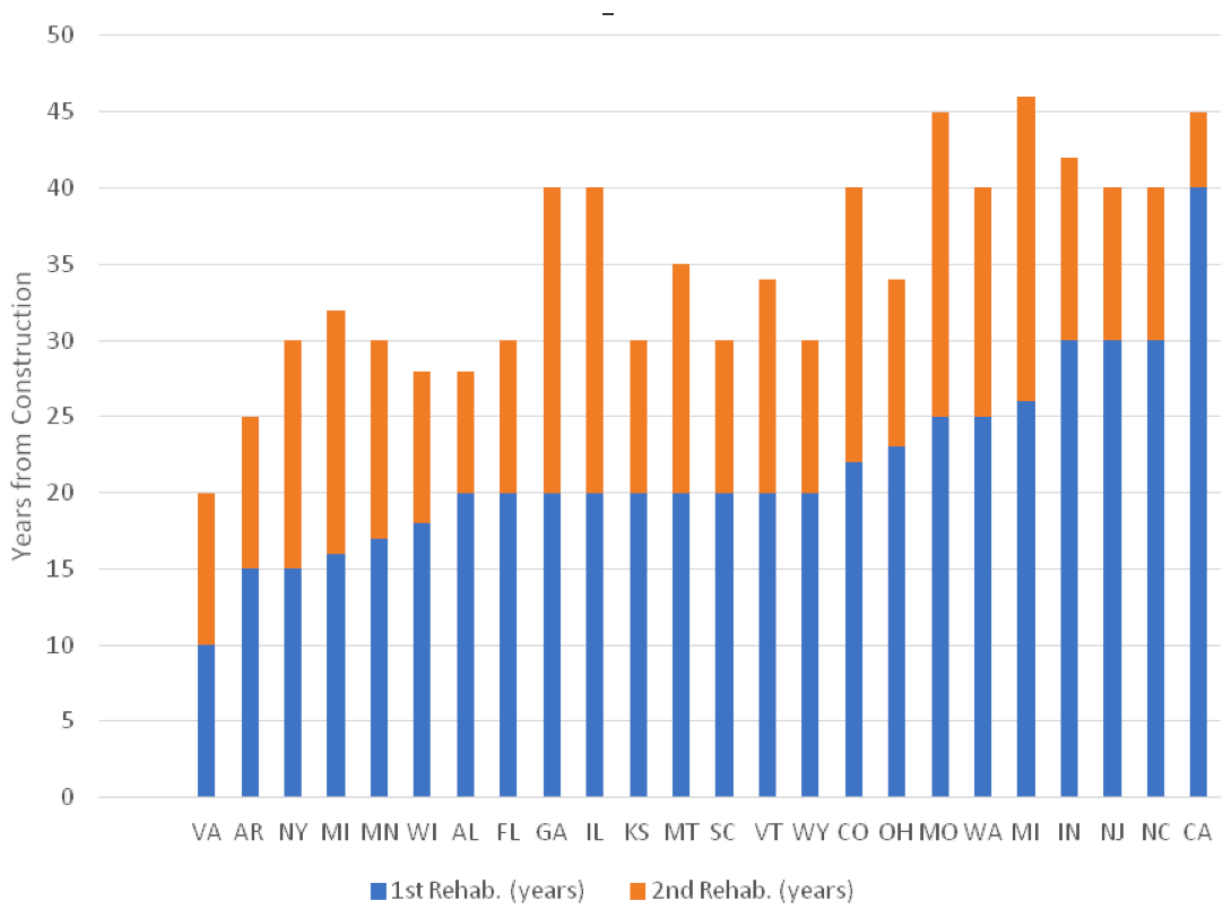

Figure 5.3. Relative time of concrete pavement at rehabilitation [20]

5.5 Results and Analysis

The probability of first rehabilitation and the second rehabilitation occurrence in a specific time (age) can be obtained by adding the probabilities of all the paths in the decision tree with a common age of occurrence. Figure 5.4 shows the probability normal distribution of two time cycles (1st and 2nd rehabilitation) for all pavement alternatives (i.e., Steel, Steel+MC, etc.). Figure 5.4 also shows the probability normal distribution for the second rehabilitation time (years from first rehabilitation procedure). The second rehabilitation probability distribution shows a distribution probability for all pavement scenarios. Figure 5.5 shows a combined probability of first rehabilitation and second rehabilitation, relative to the construction time.

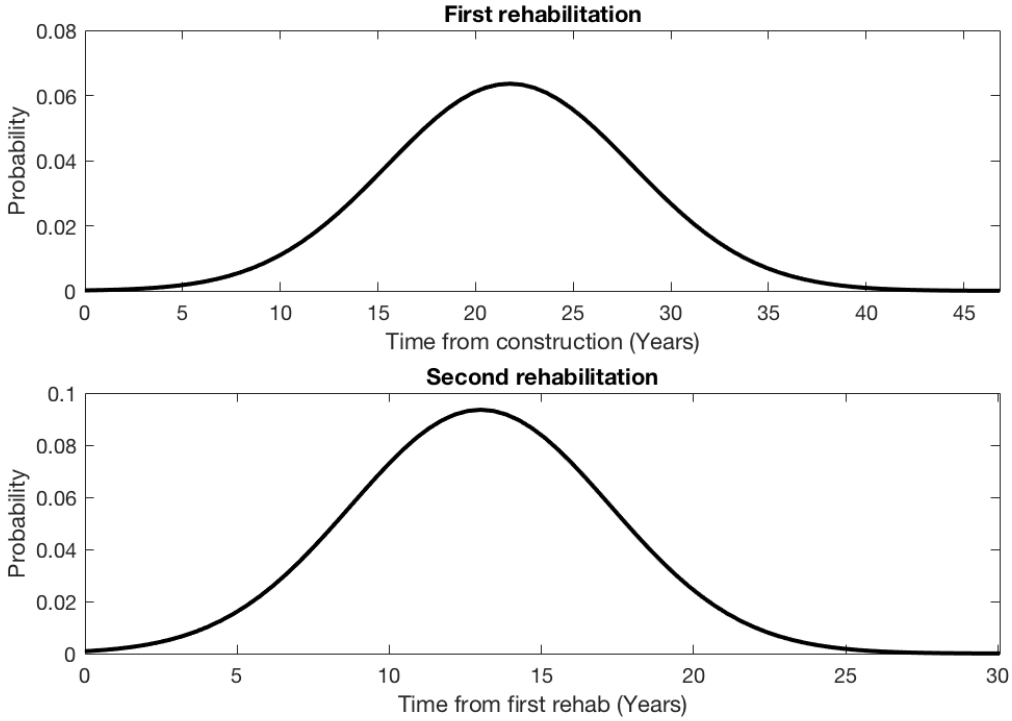

Figure 5.4. Distribution of rehabilitation time of two cycle (relative time scale)

Figure 5.5. Sum of probabilities of annual rehabilitation

The example presented in Figure 5.2 shows each path in the decision tree, with its corresponding probability. Similarly, this procedure may be scaled up for all pavement alternatives. The number of branches in the decision tree (paths) rises higher as the time of

rehabilitation procedures time increases. Lower path numbers means that the total rehabilitation probability is distributed in less branches. For this study, around 1600 paths in the decision tree were obtained, based on the distribution time of rehabilitation procedures. Figure 5.6 shows the decision tree-path number and its respective probability. Each probability path is correspondent to a year (age) of expected rehabilitation procedure. By adding probabilities of common years, a cumulative probability distribution of rehabilitation can be calculated. In order to obtain a better representation of the occurrence probability of rehabilitation (relative to the construction time), a distribution chart is presented in Figure 5.7. The maximum rehabilitation procedures that this study considers is two (Rehab. 1+ Rehab 2).

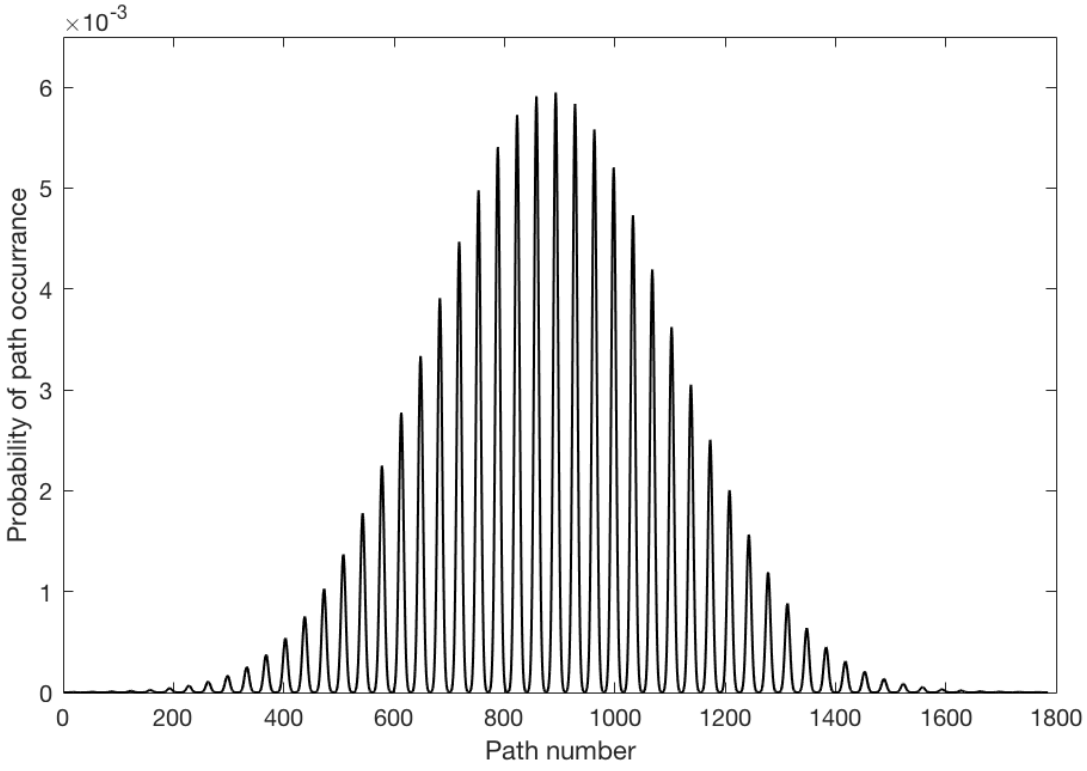

Figure 5.6. Probability of paths in the decision tree

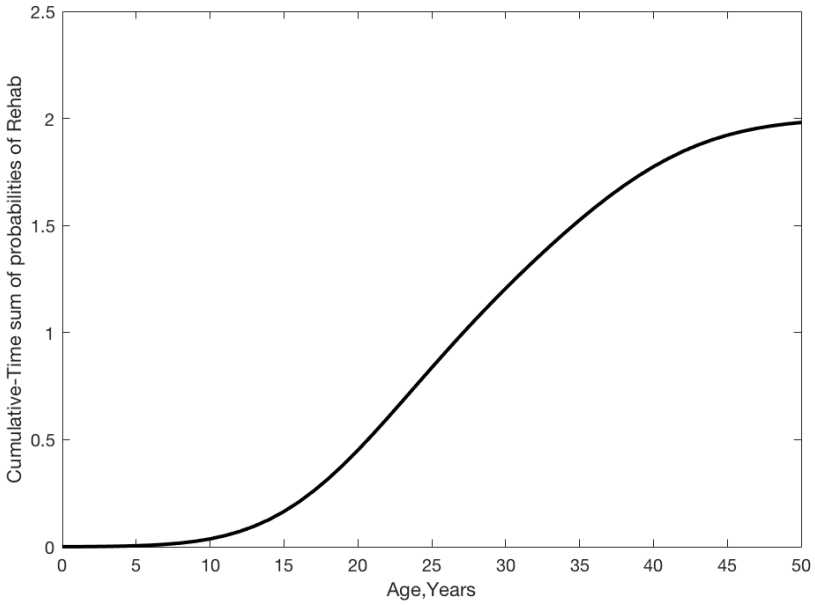

Figure 5.7. Expected number of cumulative rehabilitation

Using Equation 5.2, in which each probability in the decision tree is multiplied by the present value cost of the corresponding rehabilitation procedure, we get the present value cost at a certain year. The resulted calculation values are presented in Figure 5.8. In Figure 5.8, the present value of expected rehabilitation cost is calculated per cubic yard.

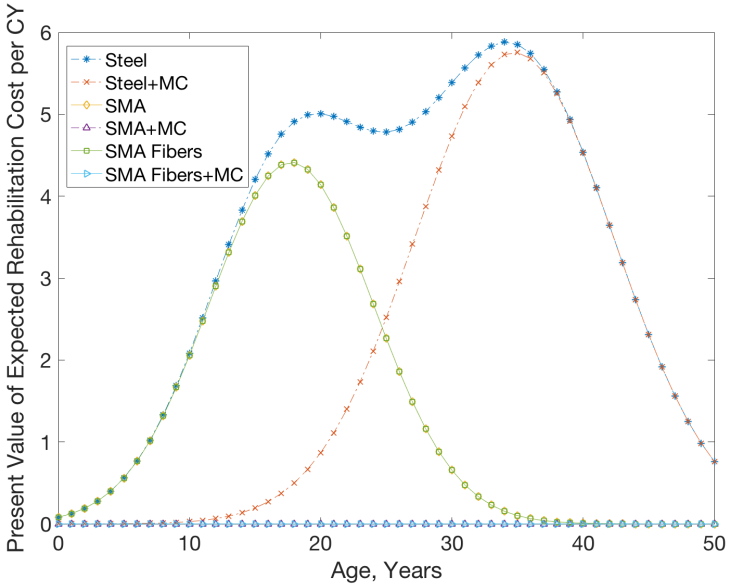

Figure 5.8. Present value of expected rehabilitation cost

As expected, in the case of the base pavement (*Steel*), this present value cost goes higher as the occurrence rehabilitation probability increases. On the other hand, the present value cost of the self-healing pavement alternatives tends to be lower that the based pavement. It is observed that from year 0 to year 11, the *Steel* case shares similar present value costs as the *SMA* and *SMA fibers*. However, starting from year 11, the present value cost of *SMA* and *SMA fibers* start to decrease at a noticeably lower rate than steel. On the other hand, the *Steelco* case does not experience an expected increase in its present value rehabilitation cost until year 11. *Steel+MC* reaches its maximum rehabilitation cost at year 35. Moreover, the expected rehabilitation cost for the pavement that contains both self-healing treatments (*SMA+MC and SMA fibers+MC*) does not experience any increase in the expected rehabilitation cost.

The cumulative present value of the expected rehabilitation cost is presented in figure 5.9. The final net present value cost at year 50 of the *Steel* alternative is $178/CY. On the other hand, the final net present values of *SMA* and *SMA fibers* are $65/CY, which constitutes a decrease of 63.5% from the base alternative (*Steel*). For the *SMA* and *SMA fibers,* the present value cost becomes more cost effective than the *Steel* case at year 18. This is due to the self-healing capabilities that SMAs are expected to have. Present values costs continue to increase until year 30, where the full benefits of SMAs are considered. The cost of *Steel+MC* on the other hand, do not experience an increase in cost for the first 15 years. From this point on, its present value costs start to rise, reaching a final present value cost of $107/CY. Nevertheless, this is a decrease of 39.8% from the base case of *Steel*. The cumulative present value cost of SMA+MC and SMA fibers+MC remains at constant zero dollars over the pavement services life, which is expected from the combined self-healing abilities of such pavement alternatives. For these pavement cases, the total in savings is 100% from the base case *Steel*.

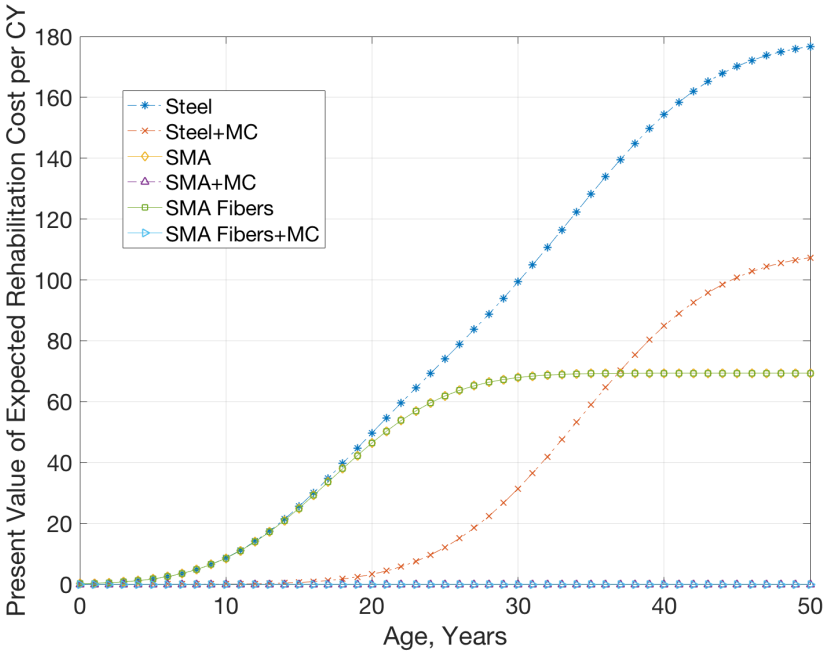

Figure 5.9. Expected cumulative rehabilitation cost

The final step in the LCCA is to take into account the initial cost of each alternative. Figure 5.10 shows the net present value of the expected cumulative cost over time. The effect of the initial costs on both *SMA and SMA+MC* will drastically increase the cumulative cost over time. At year 50, the present values costs of *SMA* and *SMA+MC* is $1710/CY and $1695/CY, respectively. On the other hand, the present value of the base pavement (*Steel*) is $430/CY. The increase of cost for *SMA* and *SMA+MC* is 297% and 294%, respectively. Moreover, the present value cost of *Steel* is consistently cheaper than the rest of the alternatives; However, at year 23, the present value cost of *Steel* and *SMA fibers* are the same ($325/CY). From year 23, the present value of *Steel* starts to increase at a higher rate that *SMA fibers and SMA*. At year 50, the present value of *SMA fibers* and *SMA* is $335, which constitutes a decrease of 22% from the base pavement. Lastly, the present values of *SMA fibers*+MC and *Steel+MC* at year 50 is $325/CY and $425/CY, respectively. This represents an increase in the final present value cost of 24.4% and 1.2%, respectively.

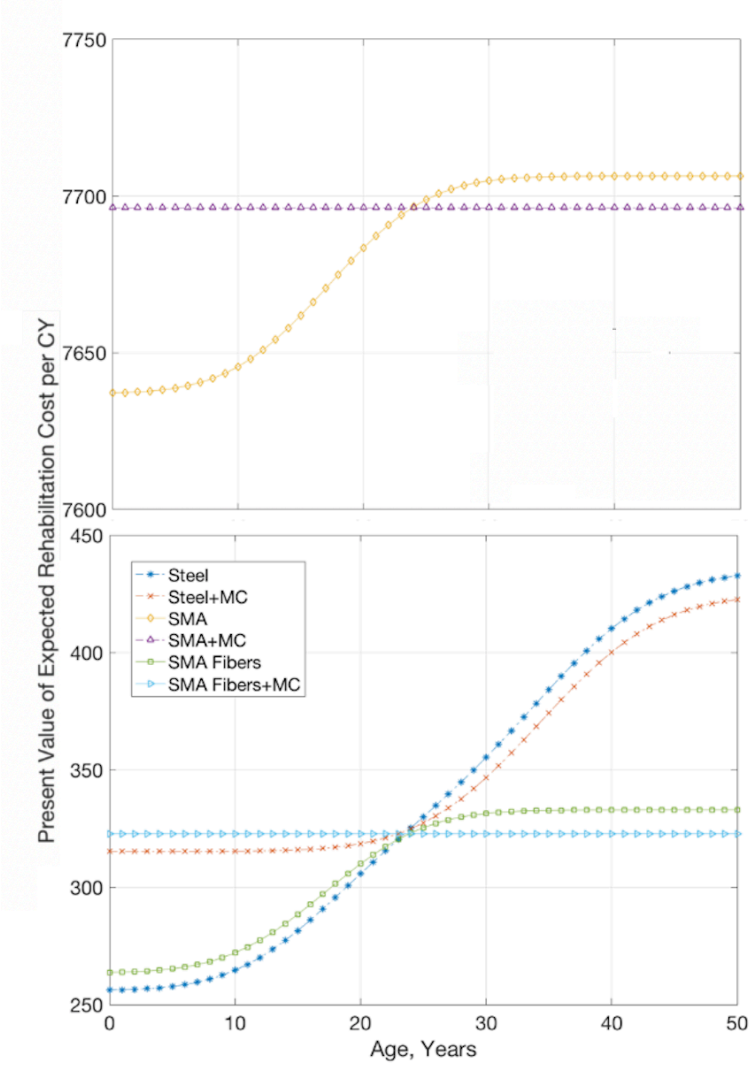

Figure 5.10. Expected cumulative life cycle cost

5.6 Conclusions

Based on the results obtained by implementing a life cycle cost analysis using a probabilistic approach, the following conclusion can be made:

- The effects of combining self-healing microcapsules combined with SMA reinforcement or SMA fibers have the potential to significantly reduce the life cycle cost on pavements. Results showed that the effects of these alternatives (SMA+MC and SMA fiber+MC)

have a noticeable impact on the rehabilitation cost at an early age in the life cycle. The reduction on rehabilitation cost for a 50-year period time showed a potential decrease of 100% from the base alternative (*Steel*).

- The initial cost required for implementing *SMA* and *SMA+MC* alternatives would drastically diminish the overall potential benefits of these alternatives. On the other hand, the initial cost added for the rest of the self-healing alternatives (*Steel+MC, SMA fibers, and SMA fibers+MC*) was not significant. The calculation was that at year 23, that *SMA fibers+MC* would start to be more cost-effective than the base pavement.

5.7 References

[1] D. Cusson, Z. Lounis and L. Daigle., "Benefits of internal curing on service life and life-cycle cost of high-performance concrete bridge decks–A case study.," Cement and Concrete Composites 32, no. 5, pp. 339-350., 2010.

[2] M. R. De Rooij, K. V. Tittelboom, N. D. Belie and E. Schlangen., Self-healing phenomena in cement-based materials, Draft of State-of-the-Art report of RILEM Technical Committee, 2011.

[3] V. Breugel, "Is there a market for self-healing cement-based materials," Proceedings of the first international conference on self-healing materials, 2007.

[4] Z. Yang, J. Hollar, X. He and X. Shi., A self-healing cementitious composite using oil core/silica gel shell microcapsules, vol. 33, Cement and Concrete Composites, 2011, pp. 506-512.

[5] E. Cailleux and V. Pollet, Investigations on the development of self-healing properties in protective coatings for concrete and repair mortars, Chivago: 2nd International Conference on Self-healing Materials, 2009, p. 120.

[6] F. Xing, Z. Ni, N. Han, B. Dong, X. Du, Z. Huang and M. Zhang., Self-healing mechanism of a novel cementitious composite using microcapsules, vol. 2627, Hangzhou: Proceedings of the International Conference on Durability of Concrete Structures, 2008.

[7] M. M. Hassan, J. Milla, T. Rupnow, M. Al-Ansari and W. H. Daly., Microencapsulation of Calcium Nitrate for Concrete Applications, vol. 2577,

Transportation Research Record: Journal of the Transportation Research Board, 2016, pp. 8-16.

[8] Y. Sakai, Y. Kitagawa, T. Fukuta and M. Iiba., "Experimental study on enhancement of self-restoration of concrete beams using SMA wire," Smart Structures and Materials, pp. 178-186, 2003.

[9] D. M. Frangopol and J. S. Kong., Expected maintenance cost of deteriorating civil infrastructures, Life-Cycle Cost Analysis and Design of Civil Infrastructure Systems, 2001, pp. 22-47.

[10] W. I. James and M. R. Smith., "Life-cycle cost analysis in pavement design-interim technical bulletin," No. FHWA-SA-98-079, 1998.

[11] A. Tinni, "Cautions with Life Cycle Cost Analysis for Optimal Pavement Selection," 2013.

[12] State of California Department of transportation pavement standards team & division of, Life-Cycle Cost Analysis Procedures Manual, 2007.

[13] S. Rahman and D. J. Vanier., "Life cycle cost analysis as a decision support tool for managing municipal infrastructure," CIB 2004 triennial congress, vol. 2, no. 1, pp. 11-8, 2004.

[14] H. Hawk, Bridge life-cycle cost analysis, 483 ed., Transportation Research Board, 2003.

[15] K. T. Hall, C. E. Correa, S. H. Carpenter and R. P. Elliot, "Rehabilitation Strategies for Highway Pavements.," 2001.

[16] E. Schlangen and S. Sangadji., "Addressing infrastructure durability and sustainability by self healing Mechanisms-Recent advances in self healing concrete and asphalt," Procedia Engineering, vol. 54, pp. 39-57, 2013.

[17] J. Milla, M. M. Hassan, T. Rupnow, M. Al-Ansari and G. Arce., "Effect of Self-Healing Calcium Nitrate Microcapsules on Concrete Properties," pp. 69-77, 2016.

[18] American Association of State Highway, and Transportation Officials, AASHTO Guide for Design of Pavement Structures, AASHTO, 1993 ed., vol. 1, 1993.

[19] Texas A&M Transportation Institute, "Rehabilitation Cost," [Online]. Available: https://tti.tamu.edu/search/?q=Rehabilitation+Cost. [Accessed 2017].

[20] J. Mack, "Improving Rehabilitation Selection for Pavement Life Cycle Cost Analysis," in ACPA Mid Year Meeting.

CHAPTER 6: CONCLUSION AND FUTURE WORK

6.1 Summary

The main objective of the dissertation was to investigate the combined self-healing effect and economic effectiveness of calcium nitrate microcapsules and low-cost shape memory alloys for concrete applications. In order to achieve these objectives, the dissertation was divided into three phases. The first phase was dedicated to evaluate the self-healing effect of calcium nitrate microcapsules on plain and steel reinforcement concrete beams. The second phase consisted of evaluating the self healing effect of shape memory alloys as a flexural reinforcement for concrete beams. Lastly, the third phase evaluated the cost effectiveness of the combined self healing effect of microcapsules and shape memory alloys by conducting a probabilistic life cycle cost analysis.

6.2 Conclusions

Base on this study, the following conclusion may be drawn,

- Addition of microcapsules lowered the flexural strength of concrete beams in comparison to those of the control samples. The results showed that microcapsules had a direct effect on reducing the flexural strength of the concrete beams, due to the high air content.
- A positive stiffness recovery was recorded for all groups, with and without microcapsules or steel. Control samples showed the lowest stiffness recovery, with a 2% recovery after being damaged. An incorporation of microcapsules and steel increased the stiffness recovery by 5% and 6%, respectively. However, the use of steel with microcapsules presented a superior healing efficiency and improved stiffness recovery significantly by 38%.
- Results from an image analysis showed that crack widths did not completely heal for the control samples, while utilizing microcapsules allowed the cracked widths to heal more

efficiently. The best observed performance was for the microcapsules-steel group, which yielded 100% healing of the crack.

- Even though microcapsules lowered the flexural strength of the beams, it was observed that the stiffness recovery values were higher for the samples with microcapsules in steel reinforced beams, followed directly by the samples containing microcapsules and SMAs.
- Atomic ratio plots suggested the possible presence of hydration products, due to the healing agents inside the beams with microcapsules. In contrast, the control group revealed the formation of calcium hydroxide (CH) as a healing product; however, the study did not find any C-S-H product or any points on the S/Ca vs. Al/Ca atomic ratio plots for the control group suggesting that no phases were formed for this group.
- The effects of combining self-healing microcapsules, combined with SMA reinforcement, have the potential to significantly reduce the life cycle cost on pavements. Results showed that the effect alternatives with both SMAs and microcapsules have a big impact on the rehabilitation cost at an early age in the life cycle. The reduction on rehabilitation cost for a 50-year period time showed a potential decrease of 100% from the control alternative (Steel reinforcement without self-healing treatment).
- The initial cost required for implementing SMA alternatives will drastically diminish the overall self-healing potential benefits. On the other hand, alternatives where SMA fibers combined with microcapsules were considered, showed to be more cost effective starting from year 23.

6.3 Future work

Based on the above conclusions of this study, the author recommends the following future research:

- Optimization of the microencapsulation procedure should be conducted to diminish the microcapsules effect on decreasing in overall compressive strength.
- Conduct a life cycle assessment to quantify the environmental impact of self-healing concrete for infrastructures.
- Long term-permeability testing of self-healing concrete should be conducted to evaluate the long-term effect of both microcapsules and SMAs.

APPENDIX. MATLAB CODE FOR LLCA

```
clear all; close all; clc;
%%%%%%%%%%%%%%%%%%%%%%%%%%%%%%%%%%%%%%%%%%%%%%%%%%%%%%%%%%%%%%%%%%%%%%%%%%%%%%%
%%%%%%%%%%%%%%%%%% STEEL REINFORCED CONCRETE %%%%%%%%%%%%%%%%%%%%%%%%%%%%%%%%%%
%%%%%%%%%%%%%%%%%%%%%%%%%%%%%%%%%%%%%%%%%%%%%%%%%%%%%%%%%%%%%%%%%%%%%%%%%%%%%%%
%obtain the database for the rehabilitiation information from excel file
data = xlsread('lcc.xlsx','Input2');
onerehab = data(:,1);% 1st rehabilitation information
secondrehab=data(:,2);% 2nd rehabilitation information

%mean and std rehab 1
mean1= mean(onerehab);
std1=std(onerehab);

%mean and std rehab 2
mean2= mean(secondrehab);
std2=std(secondrehab);

%z values
z= transpose(linspace(4,-4,81));

% z values times std of 1sr rehab plus mean
newz1=z*std1+mean1;
newz2=z*std2+mean2;

%Probability distribution values
p1=normpdf(newz1,mean1,std1);
p2=normpdf(newz2,mean2,std2);

%Plot PDF
figure (1)
ax1=subplot(2,1,1);
ax2=subplot(2,1,2);

plot(ax1,newz1,p1,'-*','DisplayName','Steel')
title(ax1,'First rehabilitation');
ylabel(ax1,'Probability')
xlabel(ax1,'Time from construction (Years)')
legend('show')
subplot(2,1,1); hold on

plot(ax2,newz2,p2,'-.*','DisplayName','Steel');
title(ax2,'Second rehabilitation');
ylabel(ax2,'Probability')
xlabel(ax2,'Time from first rehab (Years)')
legend('show')
subplot(2,1,2); hold on

%get years for the rehabilitation descision tree
newz1= transpose([round(min(newz1)):round(max(newz1))]);
newz2= transpose([round(min(newz2)):round(max(newz2))]);

%for First rehabilitation
newp1=normpdf(newz1,mean1,std1);
figure(2)
plot(newz1,newp1,'-.*','DisplayName','Steel');
% text(newz1,newp1,num2str(newp1,'%0.2f'),...
%     'HorizontalAlignment','center',...
%     'VerticalAlignment','bottom')
title('First Rehabilitation')
xlabel('Time from Construction (Years)');
ylabel('Probability, absolute time (years)');
xlim([0 max(newz1)])
legend('show')
hold on

%Second Rehabilitiation
newp2=normpdf(newz2,mean2,std2);

%Desicion tree calculations
```

```
[r1,c1]=size(newz1);
[r2,c2]=size(newz2);

z3=zeros(r1*r2,2);
column1=1;
column2=2;

z4=zeros(r2,1);
z4(1)=r2;

for i=2:r2
    z4(i) = z4(i-1)-1;
end

for i=1:r1
    for a=r2-1:-1:0
        z3(i*r2-a,column1)=newz1(i);
    end
end

for i=1:r1
    for b=r2-1:-1:0
        z3(i*r2-b,column2)=newz2(z4(b+1));
    end
end
% second rehabilitation absolute time
r2a=zeros(size(z3,1),1);
for i=1:size(r2a,1)
    r2a(i)= sum(z3(i,:));
end
%Probability of second rehabilitation
p1r2=zeros(size(z3,1),1);
for i=1:size(p1r2,1)
    p1r2(i)= normpdf(z3(i),mean1,std1);
end
p2r2=zeros(size(z3,1),1);
for i=1:size(p2r2,1)
    p2r2(i)= normpdf(z3(i,2),mean2,std2);
end
cummp2=times(p1r2,p2r2);
%summary table for second rehab
table2=[z3,r2a,cummp2];
X=[r2a,cummp2];
[a,~,c] = unique(X(:,1));
finalp2 = [a, accumarray(c,X(:,2))];
x1=finalp2(:,1);
y1=finalp2(:,2);

figure (3)
plot(x1,y1,'-.*','DisplayName','Steel');
%  text(x1,y1,num2str(y1,'%0.2f'),...
%      'HorizontalAlignment','center',...
%      'VerticalAlignment','bottom')
 title('Second Rehabilitation')
 xlabel('Time from Construction (Years)');
 ylabel('Probability, absolute time (years)');
 xlim([0 max(x1)])
 legend('show')
 hold on

 %cummulative
 cummyear= zeros(size(newz1,1)+size(x1,1),1);
 for i=1:size(newz1,1)
    cummyear(i)= newz1(i);
    for j=1:size(x1,1)
        cummyear((size(newz1,1))+j)=x1(j);
    end
 end

cummprob=zeros(size(newp1,1)+size(y1,1),1);
 for i=1:size(newp1,1)
    cummprob(i)= newp1(i);
    for j=1:size(y1,1)
        cummprob((size(newp1,1))+j)=y1(j);
    end
```

```
 end

Y=[cummyear,cummprob];
[a,~,c] = unique(Y(:,1));
finalp2 = [a, accumarray(c,Y(:,2))];
x2=finalp2(:,1);
y2=finalp2(:,2);

figure (4)
plot(x2,y2,'-.*','DisplayName','Steel');
%  text(x2,y2,num2str(y2,'%0.2f'),...
%      'HorizontalAlignment','center',...
%      'VerticalAlignment','bottom')
 title('P1,A + P2,A')
 xlabel('Age,Years');
 ylabel('Sum of probabilities of annual rehabilitation');
 xlim([0 max(x2)])
 legend('show')
 hold on

cummabsolute=cumsum(y2);
figure (5)
plot(x2,cummabsolute,'-.*','DisplayName','Steel');
title('P1,A + P2,A')
xlabel('Age,Years');
ylabel('Cumulative-Time sum of probabilities of Rehab');
xlim([0 max(x2)])
legend('show')
hold on

%Probability of paths in the descision tree
paths=zeros(size(z3,1),2);
for i=1:size(z3,1)
       paths(i,1)= i;
       paths(i,2)=cummp2(i);
end
figure (6)
plot(paths(:,1),paths(:,2),'-.*','DisplayName','Steel')
%  text(paths(:,1),paths(:,2),num2str(paths(:,2),'%0.2f'),...
%      'HorizontalAlignment','center',...
%      'VerticalAlignment','bottom')
 title('Probability of paths in the descicion tree')
 xlabel('Path number');
 ylabel('Probability of path occurrance');
 legend('show')
 hold on

%EXPECTED REHABILITATION COST
data2 = xlsread('lcc.xlsx','imputcostrehab2');
v = data2(1,1);% discount rate
cost1=data2(1,3);% Undiscounted cost of 1st rehab
cost2=data2(1,4);% Undiscounted cost of 2nd rehab
table3=[newz1,newp1];
costrehab1= zeros(size(newz1,1),1);
for i=1:size(newz1,1)
    costrehab1(i)=(cost1/((1+v)^(table3(i,1))))*table3(i,2);
end

table4=[x1,y1];
costrehab2=zeros(size(x1,1),1);
for i=1:size(x1,1)
    costrehab2(i)=(cost2/((1+v)^(table4(i,1))))*table4(i,2);
end

sumarytable=zeros(size(x2,1),3);
for i=1:size(x2,1)
     sumarytable(i,1)=x2(i);
     for j=1:size(costrehab1,1)
         sumarytable(j,2)=costrehab1(j);
        for k=1:size(costrehab2,1)
            sumarytable(k+(abs(min(table4(:,1))-min(x2(:,1)))),3)=costrehab2(k);
        end
     end
end
```

```
col1=sumarytable(:,1);
col2=sumarytable(:,2);
col3=sumarytable(:,3);

T=table;
T.Age_Years=col1;
T.First_Rehab_Cost=col2;
T.Secod_Rehab_Cost=col3;

figure (7)
uitable('Data',T{:,:},'ColumnName',T.Properties.VariableNames,...
      'RowName',T.Properties.RowNames,'Units', 'Normalized', 'Position',[0, 0, 1, 1]);

%Cummulative cost
C=zeros(size(T,1),2);
for  i=1:size(T,1)
    C(i,1)=col1(i);
    C(i,2)=col2(i)+col3(i);
end

figure(8)
plot(C(:,1),C(:,2),'-.*','DisplayName','Steel');
%  text(paths(:,1),paths(:,2),num2str(paths(:,2),'%0.2f'),...
%      'HorizontalAlignment','center',...
%      'VerticalAlignment','bottom')
 title('Present Value of Expected Rehabilitation Cost')
 xlabel('Age, Years');
 ylabel('Present Value of Expected Rehabilitation Cost');
 xlim([0 max(C(:,1))])
 legend('show')
 hold on

figure(9)
plot(C(:,1),cumsum(C(:,2)),'-.*','DisplayName','Steel');
%  text(paths(:,1),paths(:,2),num2str(paths(:,2),'%0.2f'),...
%      'HorizontalAlignment','center',...
%      'VerticalAlignment','bottom')
 title('Present Value of Expected Cumulative Rehabilitation Cost')
 xlabel('Age, Years');
 ylabel('Present Value of Expected Rehabilitation Cost');
 xlim([0 max(C(:,1))])
 legend('show')
 hold on

%TAKING INTO ACCOUNT INITIAL COST

data3 = xlsread('lcc.xlsx','initialcost');
C2=cumsum(C(:,2));
C3=C2+data3(1,1);

figure(13)
plot(C(:,1),C3,'-.*','DisplayName','Steel');
%  text(paths(:,1),paths(:,2),num2str(paths(:,2),'%0.2f'),...
%      'HorizontalAlignment','center',...
%      'VerticalAlignment','bottom')
 title('Initial Cost and Present Value of Expected Cumulative Rehabilitation Cost')
 xlabel('Age, Years');
 ylabel('Present Value of Expected Rehabilitation Cost');
 xlim([0 max(C(:,1))])
 legend('show')
 hold on
 npvsteel=max(C3);
%%%%%%%%%%%%%%%%%%%%%%%%%%%%%%%%%%%%%%%%%%%%%%%%%%%%%%%%%%%%%%%%%%%%%%%%%%%%%%%
%%%%%%%%%%%%%%%%%%%%%%%%%%%%%%%% STEEL+MC %%%%%%%%%%%%%%%%%%%%%%%%%%%%%%%%%%%%
%%%%%%%%%%%%%%%%%%%%%%%%%%%%%%%%%%%%%%%%%%%%%%%%%%%%%%%%%%%%%%%%%%%%%%%%%%%%%%%

data = xlsread('lcc.xlsx','Input2');
onerehab = data(:,4);% 1st rehabilitation information
secondrehab=data(:,5);% 2nd rehabilitation information

%mean and std rehab 1
mean1= mean(onerehab);
std1=std(onerehab);

%mean and std rehab 2
```

```
mean2= mean(secondrehab);
std2=std(secondrehab);

%z values
z= transpose(linspace(4,-4,81));

% z values times std of 1sr rehab plus mean
newz1=z*std1+mean1;
newz2=z*std2+mean2;

%Probability distribution values
p1=normpdf(newz1,mean1,std1);
p2=normpdf(newz2,mean2,std2);

%Plot PDF
figure (1)
ax1=subplot(2,1,1);
ax2=subplot(2,1,2);

plot(ax1,newz1,p1,'-.x','DisplayName','Steel+MC')
title(ax1,'First rehabilitation');
ylabel(ax1,'Probability')
xlabel(ax1,'Time from construction (Years)')
legend('show')
subplot(2,1,1); hold on

plot(ax2,newz2,p2,'-.x','DisplayName','Steel+MC');
title(ax2,'Second rehabilitation');
ylabel(ax2,'Probability')
xlabel(ax2,'Time from first rehab (Years)')
legend('show')
hold on

subplot(2,1,2); hold on
%get years for the rehabilitation descision tree
newz1= transpose([round(min(newz1)):round(max(newz1))]);
newz2= transpose([round(min(newz2)):round(max(newz2))]);

%for First rehabilitation
newp1=normpdf(newz1,mean1,std1);
figure(2)
plot(newz1,newp1,'-.x','DisplayName','Steel+MC');
% text(newz1,newp1,num2str(newp1,'%0.2f'),...
%     'HorizontalAlignment','center',...
%     'VerticalAlignment','bottom')
title('First Rehabilitation')
xlabel('Time from Construction (Years)');
ylabel('Probability, absolute time (years)');
xlim([0 max(newz1)])
legend('show')
hold on


%Second Rehabilitiation
newp2=normpdf(newz2,mean2,std2);

%Desicion tree calculations

[r1,c1]=size(newz1);
[r2,c2]=size(newz2);

z3=zeros(r1*r2,2);
column1=1;
column2=2;

z4=zeros(r2,1);
z4(1)=r2;

for i=2:r2
    z4(i) = z4(i-1)-1;
end

for i=1:r1
    for a=r2-1:-1:0
        z3(i*r2-a,column1)=newz1(i);
```

```
    end
end

for i=1:r1
    for b=r2-1:-1:0
        z3(i*r2-b,column2)=newz2(z4(b+1));
    end
end
% second rehabilitation absolute time
r2a=zeros(size(z3,1),1);
for i=1:size(r2a,1)
    r2a(i)= sum(z3(i,:));
end
%Probability of second rehabilitation
p1r2=zeros(size(z3,1),1);
for i=1:size(p1r2,1)
    p1r2(i)= normpdf(z3(i),mean1,std1);
end
p2r2=zeros(size(z3,1),1);
for i=1:size(p2r2,1)
    p2r2(i)= normpdf(z3(i,2),mean2,std2);
end
cummp2=times(p1r2,p2r2);
%summary table for second rehab
table2=[z3,r2a,cummp2];
X=[r2a,cummp2];
[a,~,c] = unique(X(:,1));
finalp2 = [a, accumarray(c,X(:,2))];
x1=finalp2(:,1);
y1=finalp2(:,2);

figure (3)
plot(x1,y1,'-.x','DisplayName','Steel+MC');
%  text(x1,y1,num2str(y1,'%0.2f'),...
%      'HorizontalAlignment','center',...
%      'VerticalAlignment','bottom')
 title('Second Rehabilitation')
 xlabel('Time from Construction (Years)');
 ylabel('Probability, absolute time (years)');
 xlim([0 max(x1)])
 legend('show')
 hold on


 %cummulative
 cummyear= zeros(size(newz1,1)+size(x1,1),1);
 for i=1:size(newz1,1)
    cummyear(i)= newz1(i);
    for j=1:size(x1,1)
        cummyear((size(newz1,1))+j)=x1(j);
    end
 end

cummprob=zeros(size(newp1,1)+size(y1,1),1);
 for i=1:size(newp1,1)
    cummprob(i)= newp1(i);
    for j=1:size(y1,1)
        cummprob((size(newp1,1))+j)=y1(j);
    end
 end

Y=[cummyear,cummprob];
[a,~,c] = unique(Y(:,1));
finalp2 = [a, accumarray(c,Y(:,2))];
x2=finalp2(:,1);
y2=finalp2(:,2);

figure (4)
plot(x2,y2,'-.x','DisplayName','Steel+MC');
%  text(x2,y2,num2str(y2,'%0.2f'),...
%      'HorizontalAlignment','center',...
%      'VerticalAlignment','bottom')
 title('P1,A + P2,A')
 xlabel('Age,Years');
 ylabel('Sum of probabilities of annual rehabilitation');
```

```
 xlim([0 max(x2)])
 legend('show')
 hold on

cummabsolute=cumsum(y2);
figure (5)
plot(x2,cummabsolute,'-.x','DisplayName','Steel+MC');
title('P1,A + P2,A')
xlabel('Age,Years');
ylabel('Cumulative-Time sum of probabilities of Rehab');
xlim([0 max(x2)])
legend('show')
hold on

%Probability of paths in the descision tree
paths=zeros(size(z3,1),2);
for i=1:size(z3,1)
       paths(i,1)= i;
       paths(i,2)=cummp2(i);
end
figure (6)
plot(paths(:,1),paths(:,2),'-.x','DisplayName','Steel+MC')
%  text(paths(:,1),paths(:,2),num2str(paths(:,2),'%0.2f'),...
%      'HorizontalAlignment','center',...
%      'VerticalAlignment','bottom')
 title('Probability of paths in the descicion tree')
 xlabel('Path number');
 ylabel('Probability of path occurrance');
 legend('show')
 hold on

%EXPECTED REHABILITATION COST
data2 = xlsread('lcc.xlsx','imputcostrehab2');
v = data2(1,1);% discount rate
cost1=data2(1,6);% Undiscounted cost of 1st rehab
cost2=data2(1,7);% Undiscounted cost of 2nd rehab
table3=[newz1,newp1];
costrehab1= zeros(size(newz1,1),1);
for i=1:size(newz1,1)
    costrehab1(i)=(cost1/((1+v)^(table3(i,1))))*table3(i,2);
end

table4=[x1,y1];
costrehab2=zeros(size(x1,1),1);
for i=1:size(x1,1)
    costrehab2(i)=(cost2/((1+v)^(table4(i,1))))*table4(i,2);
end

sumarytable=zeros(size(x2,1),3);
for i=1:size(x2,1)
     sumarytable(i,1)=x2(i);
     for j=1:size(costrehab1,1)
         sumarytable(j,2)=costrehab1(j);
        for k=1:size(costrehab2,1)
            sumarytable(k+(abs(min(table4(:,1))-min(x2(:,1)))),3)=costrehab2(k);
        end
     end
end

col1=sumarytable(:,1);
col2=sumarytable(:,2);
col3=sumarytable(:,3);

T=table;
T.Age_Years=col1;
T.First_Rehab_Cost=col2;
T.Secod_Rehab_Cost=col3;

figure (10)
uitable('Data',T{:,:},'ColumnName',T.Properties.VariableNames,...
      'RowName',T.Properties.RowNames,'Units', 'Normalized', 'Position',[0, 0, 1, 1]);

%Cummulative cost
C=zeros(size(T,1),2);
for  i=1:size(T,1)
```

```
    C(i,1)=col1(i);
    C(i,2)=col2(i)+col3(i);
end

figure(8)
plot(C(:,1),C(:,2),'-.x','DisplayName','Steel+MC');
%  text(paths(:,1),paths(:,2),num2str(paths(:,2),'%0.2f'),...
%      'HorizontalAlignment','center',...
%      'VerticalAlignment','bottom')
 title('Present Value of Expected Rehabilitation Cost')
 xlabel('Age, Years');
 ylabel('Present Value of Expected Rehabilitation Cost');
 xlim([0 max(C(:,1))])
 legend('show')
 hold on

figure(9)
plot(C(:,1),cumsum(C(:,2)),'-.x','DisplayName','Steel+MC');
%  text(paths(:,1),paths(:,2),num2str(paths(:,2),'%0.2f'),...
%      'HorizontalAlignment','center',...
%      'VerticalAlignment','bottom')
 title('Present Value of Expected Cumulative Rehabilitation Cost')
 xlabel('Age, Years');
 ylabel('Present Value of Expected Rehabilitation Cost');
 xlim([0 max(C(:,1))])
 legend('show')
 hold on
 %TAKING INTO ACCOUNT INITIAL COST

data3 = xlsread('lcc.xlsx','initialcost');
C2=cumsum(C(:,2));
C4=C2+data3(1,2);

figure(13)
plot(C(:,1),C4,'-.x','DisplayName','Steel+MC');
%  text(paths(:,1),paths(:,2),num2str(paths(:,2),'%0.2f'),...
%      'HorizontalAlignment','center',...
%      'VerticalAlignment','bottom')
 title('Initial Cost and Present Value of Expected Cumulative Rehabilitation Cost')
 xlabel('Age, Years');
 ylabel('Present Value of Expected Rehabilitation Cost');
 xlim([0 max(C(:,1))])
 legend('show')
 hold on

 npvsteelmc=max(C4);
 %%%%%%%%%%%%%%%%%%%%%%%%%%%%%%%%%%%%%%%%%%%%%%%%%%%%%%%%%%%%%%%%%%%%%%%%%%%%
%%%%%%%%%%%%%%%%%%%%%%%%%%%%% SMA %%%%%%%%%%%%%%%%%%%%%%%%%%%%%%%%%%%%%%%%%%
%%%%%%%%%%%%%%%%%%%%%%%%%%%%%%%%%%%%%%%%%%%%%%%%%%%%%%%%%%%%%%%%%%%%%%%%%%%%

data = xlsread('lcc.xlsx','Input2');
onerehab = data(:,7);% 1st rehabilitation information
secondrehab=data(:,8);% 2nd rehabilitation information

%mean and std rehab 1
mean1= mean(onerehab);
std1=std(onerehab);

%mean and std rehab 2
mean2= mean(secondrehab);
std2=std(secondrehab);

%z values
z= transpose(linspace(4,-4,81));

% z values times std of 1sr rehab plus mean
newz1=z*std1+mean1;
newz2=z*std2+mean2;

%Probability distribution values
p1=normpdf(newz1,mean1,std1);
p2=normpdf(newz2,mean2,std2);

%Plot PDF
figure (1)
```

```
ax1=subplot(2,1,1);
ax2=subplot(2,1,2);

plot(ax1,newz1,p1,'-d','DisplayName','SMA')
title(ax1,'First rehabilitation');
ylabel(ax1,'Probability')
xlabel(ax1,'Time from construction (Years)')
legend('show')
subplot(2,1,1); hold on

plot(ax2,newz2,p2,'-d','DisplayName','SMA');
title(ax2,'Second rehabilitation');
ylabel(ax2,'Probability')
xlabel(ax2,'Time from first rehab (Years)')
legend('show')
subplot(2,1,2); hold on

%get years for the rehabilitation descision tree
newz1= transpose([round(min(newz1)):round(max(newz1))]);
newz2= transpose([round(min(newz2)):round(max(newz2))]);

%for First rehabilitation
newp1=normpdf(newz1,mean1,std1);
figure(2)
plot(newz1,newp1,'-d','DisplayName','SMA');
% text(newz1,newp1,num2str(newp1,'%0.2f'),...
%     'HorizontalAlignment','center',...
%     'VerticalAlignment','bottom')
title('First Rehabilitation')
xlabel('Time from Construction (Years)');
ylabel('Probability, absolute time (years)');
xlim([0 max(newz1)])
legend('show')
hold on



%Second Rehabilitiation
newp2=normpdf(newz2,mean2,std2);

%Desicion tree calculations

[r1,c1]=size(newz1);
[r2,c2]=size(newz2);

z3=zeros(r1*r2,2);
column1=1;
column2=2;

z4=zeros(r2,1);
z4(1)=r2;

for i=2:r2
    z4(i) = z4(i-1)-1;
end

for i=1:r1
    for a=r2-1:-1:0
        z3(i*r2-a,column1)=newz1(i);
    end
end

for i=1:r1
    for b=r2-1:-1:0
        z3(i*r2-b,column2)=newz2(z4(b+1));
    end
end
% second rehabilitation absolute time
r2a=zeros(size(z3,1),1);
for i=1:size(r2a,1)
    r2a(i)= sum(z3(i,:));
end
%Probability of second rehabilitation
p1r2=zeros(size(z3,1),1);
for i=1:size(p1r2,1)
```

```
    p1r2(i)= normpdf(z3(i),mean1,std1);
end
p2r2=zeros(size(z3,1),1);
for i=1:size(p2r2,1)
    p2r2(i)= normpdf(z3(i,2),mean2,std2);
end
cummp2=times(p1r2,p2r2);
%summary table for second rehab
table2=[z3,r2a,cummp2];
X=[r2a,cummp2];
[a,~,c] = unique(X(:,1));
finalp2 = [a, accumarray(c,X(:,2))];
x1=finalp2(:,1);
y1=finalp2(:,2);

figure (3)
plot(x1,y1,'-d','DisplayName','SMA');
%  text(x1,y1,num2str(y1,'%0.2f'),...
%      'HorizontalAlignment','center',...
%      'VerticalAlignment','bottom')
 title('Second Rehabilitation')
 xlabel('Time from Construction (Years)');
 ylabel('Probability, absolute time (years)');
 xlim([0 max(x1)])
 legend('show')
 hold on


 %cummulative
 cummyear= zeros(size(newz1,1)+size(x1,1),1);
 for i=1:size(newz1,1)
    cummyear(i)= newz1(i);
    for j=1:size(x1,1)
        cummyear((size(newz1,1))+j)=x1(j);
    end
 end

cummprob=zeros(size(newp1,1)+size(y1,1),1);
 for i=1:size(newp1,1)
    cummprob(i)= newp1(i);
    for j=1:size(y1,1)
        cummprob((size(newp1,1))+j)=y1(j);
    end
 end

Y=[cummyear,cummprob];
[a,~,c] = unique(Y(:,1));
finalp2 = [a, accumarray(c,Y(:,2))];
x2=finalp2(:,1);
y2=finalp2(:,2);

figure (4)
plot(x2,y2,'-d','DisplayName','SMA');
%  text(x2,y2,num2str(y2,'%0.2f'),...
%      'HorizontalAlignment','center',...
%      'VerticalAlignment','bottom')
 title('P1,A + P2,A')
 xlabel('Age,Years');
 ylabel('Sum of probabilities of annual rehabilitation');
 xlim([0 max(x2)])
 legend('show')
 hold on

cummabsolute=cumsum(y2);
figure (5)
plot(x2,cummabsolute,'-d','DisplayName','SMA');
title('P1,A + P2,A')
xlabel('Age,Years');
ylabel('Cumulative-Time sum of probabilities of Rehab');
xlim([0 max(x2)])
legend('show')
hold on

%Probability of paths in the descision tree
paths=zeros(size(z3,1),2);
```

```
for i=1:size(z3,1)
       paths(i,1)= i;
       paths(i,2)=cummp2(i);
end
figure (6)
plot(paths(:,1),paths(:,2),'-d','DisplayName','SMA')
%  text(paths(:,1),paths(:,2),num2str(paths(:,2),'%0.2f'),...
%      'HorizontalAlignment','center',...
%      'VerticalAlignment','bottom')
 title('Probability of paths in the descicion tree')
 xlabel('Path number');
 ylabel('Probability of path occurrance');
 legend('show')
 hold on

%EXPECTED REHABILITATION COST
data2 = xlsread('lcc.xlsx','imputcostrehab2');
v = data2(1,1);% discount rate
cost1=data2(1,9);% Undiscounted cost of 1st rehab
cost2=data2(1,10);% Undiscounted cost of 2nd rehab
table3=[newz1,newp1];
costrehab1= zeros(size(newz1,1),1);
for i=1:size(newz1,1)
    costrehab1(i)=(cost1/((1+v)^(table3(i,1))))*table3(i,2);
end

table4=[x1,y1];
costrehab2=zeros(size(x1,1),1);
for i=1:size(x1,1)
    costrehab2(i)=(cost2/((1+v)^(table4(i,1))))*table4(i,2);
end

sumarytable=zeros(size(x2,1),3);
for i=1:size(x2,1)
     sumarytable(i,1)=x2(i);
     for j=1:size(costrehab1,1)
         sumarytable(j,2)=costrehab1(j);
        for k=1:size(costrehab2,1)
            sumarytable(k+(abs(min(table4(:,1))-min(x2(:,1)))),3)=costrehab2(k);
        end
     end
end

col1=sumarytable(:,1);
col2=sumarytable(:,2);
col3=sumarytable(:,3);

T=table;
T.Age_Years=col1;
T.First_Rehab_Cost=col2;
T.Secod_Rehab_Cost=col3;

figure (11)
uitable('Data',T{:,:},'ColumnName',T.Properties.VariableNames,...
      'RowName',T.Properties.RowNames,'Units', 'Normalized', 'Position',[0, 0, 1, 1]);

%Cummulative cost
C=zeros(size(T,1),2);
for  i=1:size(T,1)
    C(i,1)=col1(i);
    C(i,2)=col2(i)+col3(i);
end

figure(8)
plot(C(:,1),C(:,2),'-d','DisplayName','SMA');
%  text(paths(:,1),paths(:,2),num2str(paths(:,2),'%0.2f'),...
%      'HorizontalAlignment','center',...
%      'VerticalAlignment','bottom')
 title('Present Value of Expected Rehabilitation Cost')
 xlabel('Age, Years');
 ylabel('Present Value of Expected Rehabilitation Cost');
 xlim([0 max(C(:,1))])
 legend('show')
 hold on
```

```
figure(9)
plot(C(:,1),cumsum(C(:,2)),'-d','DisplayName','SMA');
%  text(paths(:,1),paths(:,2),num2str(paths(:,2),'%0.2f'),...
%      'HorizontalAlignment','center',...
%      'VerticalAlignment','bottom')
 title('Present Value of Expected Cumulative Rehabilitation Cost')
 xlabel('Age, Years');
 ylabel('Present Value of Expected Rehabilitation Cost');
 xlim([0 max(C(:,1))])
 legend('show')
 hold on

%TAKING INTO ACCOUNT INITIAL COST
data3 = xlsread('lcc.xlsx','initialcost');
C2=cumsum(C(:,2));
C5=C2+data3(1,3);

figure(13)
plot(C(:,1),C5,'-d','DisplayName','SMA');
%  text(paths(:,1),paths(:,2),num2str(paths(:,2),'%0.2f'),...
%      'HorizontalAlignment','center',...
%      'VerticalAlignment','bottom')
 title('Initial Cost and Present Value of Expected Cumulative Rehabilitation Cost')
 xlabel('Age, Years');
 ylabel('Present Value of Expected Rehabilitation Cost');
 xlim([0 max(C(:,1))])
 legend('show')
 hold on

 npvsma=max(C5);

%%%%%%%%%%%%%%%%%%%%%%%%%%%%%%%%%%%%%%%%%%%%%%%%%%%%%%%%%%%%%%%%%%%%%%%%%%%%%%%
%%%%%%%%%%%%%%%%%%%%%%%%%%%%%%%% SMA+MC %%%%%%%%%%%%%%%%%%%%%%%%%%%%%%%%%%%%%%
%%%%%%%%%%%%%%%%%%%%%%%%%%%%%%%%%%%%%%%%%%%%%%%%%%%%%%%%%%%%%%%%%%%%%%%%%%%%%%%

data = xlsread('lcc.xlsx','Input2');
onerehab = data(:,10);% 1st rehabilitation information
secondrehab=data(:,11);% 2nd rehabilitation information

%mean and std rehab 1
mean1= mean(onerehab);
std1=std(onerehab);

%mean and std rehab 2
mean2= mean(secondrehab);
std2=std(secondrehab);

%z values
z= transpose(linspace(4,-4,81));

% z values times std of 1sr rehab plus mean
newz1=z*std1+mean1;
newz2=z*std2+mean2;

%Probability distribution values
p1=normpdf(newz1,mean1,std1);
p2=normpdf(newz2,mean2,std2);

%Plot PDF
figure (1)
ax1=subplot(2,1,1);
ax2=subplot(2,1,2);

plot(ax1,newz1,p1,'-.^','DisplayName','SMA+MC')
title(ax1,'First rehabilitation');
ylabel(ax1,'Probability')
xlabel(ax1,'Time from construction (Years)')
legend('show')
xlim(ax1,[0 inf])
subplot(2,1,1); hold on

plot(ax2,newz2,p2,'-.^','DisplayName','SMA+MC');
title(ax2,'Second rehabilitation');
ylabel(ax2,'Probability')
xlabel(ax2,'Time from first rehab (Years)')
```

```
hold on
legend('show')
xlim(ax2,[0 inf])
subplot(2,1,2); hold on

%get years for the rehabilitation descision tree
newz1= transpose([round(min(newz1)):round(max(newz1))]);
newz2= transpose([round(min(newz2)):round(max(newz2))]);

%for First rehabilitation
newp1=normpdf(newz1,mean1,std1);
figure(2)
plot(newz1,newp1,'-.^','DisplayName','SMA+MC');
% text(newz1,newp1,num2str(newp1,'%0.2f'),...
%     'HorizontalAlignment','center',...
%     'VerticalAlignment','bottom')
title('First Rehabilitation')
xlabel('Time from Construction (Years)');
ylabel('Probability, absolute time (years)');
%xlim([0 max(newz1)])
legend('show')
hold on



%Second Rehabilitiation
newp2=normpdf(newz2,mean2,std2);

%Desicion tree calculations

[r1,c1]=size(newz1);
[r2,c2]=size(newz2);

z3=zeros(r1*r2,2);
column1=1;
column2=2;

z4=zeros(r2,1);
z4(1)=r2;

for i=2:r2
    z4(i) = z4(i-1)-1;
end

for i=1:r1
    for a=r2-1:-1:0
        z3(i*r2-a,column1)=newz1(i);
    end
end

for i=1:r1
    for b=r2-1:-1:0
        z3(i*r2-b,column2)=newz2(z4(b+1));
    end
end
% second rehabilitation absolute time
r2a=zeros(size(z3,1),1);
for i=1:size(r2a,1)
    r2a(i)= sum(z3(i,:));
end
%Probability of second rehabilitation
p1r2=zeros(size(z3,1),1);
for i=1:size(p1r2,1)
    p1r2(i)= normpdf(z3(i),mean1,std1);
end
p2r2=zeros(size(z3,1),1);
for i=1:size(p2r2,1)
    p2r2(i)= normpdf(z3(i,2),mean2,std2);
end
cummp2=times(p1r2,p2r2);
%summary table for second rehab
table2=[z3,r2a,cummp2];
X=[r2a,cummp2];
[a,~,c] = unique(X(:,1));
finalp2 = [a, accumarray(c,X(:,2))];
```

```
x1=finalp2(:,1);
y1=finalp2(:,2);

figure (3)
plot(x1,y1,'-.^','DisplayName','SMA+MC');
%  text(x1,y1,num2str(y1,'%0.2f'),...
%      'HorizontalAlignment','center',...
%      'VerticalAlignment','bottom')
 title('Second Rehabilitation')
 xlabel('Time from Construction (Years)');
 ylabel('Probability, absolute time (years)');
 xlim([0 max(x1)])
 legend('show')
 hold on


 %cummulative
 cummyear= zeros(size(newz1,1)+size(x1,1),1);
 for i=1:size(newz1,1)
    cummyear(i)= newz1(i);
    for j=1:size(x1,1)
        cummyear((size(newz1,1))+j)=x1(j);
    end
 end

cummprob=zeros(size(newp1,1)+size(y1,1),1);
 for i=1:size(newp1,1)
    cummprob(i)= newp1(i);
    for j=1:size(y1,1)
        cummprob((size(newp1,1))+j)=y1(j);
    end
 end

Y=[cummyear,cummprob];
[a,~,c] = unique(Y(:,1));
finalp2 = [a, accumarray(c,Y(:,2))];
x2=finalp2(:,1);
y2=finalp2(:,2);

figure (4)
plot(x2,y2,'-.^','DisplayName','SMA+MC');
%  text(x2,y2,num2str(y2,'%0.2f'),...
%      'HorizontalAlignment','center',...
%      'VerticalAlignment','bottom')
title(' ')
%title('P1,A + P2,A')
 xlabel('Age,Years');
 ylabel('Sum of probabilities of annual rehabilitation');
 xlim([0 max(x2)])
 legend('show')
 hold on

cummabsolute=cumsum(y2);
figure (5)
plot(x2,cummabsolute,'-.^','DisplayName','SMA+MC');
title(' ')
xlabel('Age/Service Life, Years');
ylabel('Cumulative-Time sum of probabilities of Rehab');
xlim([0 max(x2)])
ylim([0 2.5])
legend('show')
legend('Location','southeast')
hold on

%Probability of paths in the descision tree
paths=zeros(size(z3,1),2);
for i=1:size(z3,1)
       paths(i,1)= i;
       paths(i,2)=cummp2(i);
end
figure (6)
plot(paths(:,1),paths(:,2),'-.^','DisplayName','SMA+MC')
%  text(paths(:,1),paths(:,2),num2str(paths(:,2),'%0.2f'),...
%      'HorizontalAlignment','center',...
%      'VerticalAlignment','bottom')
```

```
 title(' ')
 xlabel('Path number');
 ylabel('Probability of Path occurrance');
 legend('show')
 hold on

%EXPECTED REHABILITATION COST
data2 = xlsread('lcc.xlsx','imputcostrehab2');
v = data2(1,1);% discount rate
cost1=data2(1,12);% Undiscounted cost of 1st rehab
cost2=data2(1,13);% Undiscounted cost of 2nd rehab
table3=[newz1,newp1];
costrehab1= zeros(size(newz1,1),1);
for i=1:size(newz1,1)
    costrehab1(i)=(cost1/((1+v)^(table3(i,1))))*table3(i,2);
end

table4=[x1,y1];
costrehab2=zeros(size(x1,1),1);
for i=1:size(x1,1)
    costrehab2(i)=(cost2/((1+v)^(table4(i,1))))*table4(i,2);
end

sumarytable=zeros(size(x2,1),3);
for i=1:size(x2,1)
     sumarytable(i,1)=x2(i);
     for j=1:size(costrehab1,1)
         sumarytable(j,2)=costrehab1(j);
        for k=1:size(costrehab2,1)
            sumarytable(k+(abs(min(table4(:,1))-min(x2(:,1)))),3)=costrehab2(k);
        end
     end
end

col1=sumarytable(:,1);
col2=sumarytable(:,2);
col3=sumarytable(:,3);

T=table;
T.Age_Years=col1;
T.First_Rehab_Cost=col2;
T.Secod_Rehab_Cost=col3;

figure (12)
uitable('Data',T{:,:},'ColumnName',T.Properties.VariableNames,...
      'RowName',T.Properties.RowNames,'Units', 'Normalized', 'Position',[0, 0, 1, 1]);

%Cummulative cost
C=zeros(size(T,1),2);
for  i=1:size(T,1)
    C(i,1)=col1(i);
    C(i,2)=col2(i)+col3(i);
end

figure(8)
plot(C(:,1),C(:,2),'-.^','DisplayName','SMA+MC');
%  text(paths(:,1),paths(:,2),num2str(paths(:,2),'%0.2f'),...
%      'HorizontalAlignment','center',...
%      'VerticalAlignment','bottom')
title(' ')
%title('Present Value of Expected Rehabilitation Cost')
 xlabel('Age, Years');
 ylabel('Present Value of Expected Rehabilitation Cost');
 xlim([0 max(C(:,1))])
 legend('show')
 hold on

figure(9)
plot(C(:,1),cumsum(C(:,2)),'-.^','DisplayName','SMA+MC');
%  text(paths(:,1),paths(:,2),num2str(paths(:,2),'%0.2f'),...
%      'HorizontalAlignment','center',...
%      'VerticalAlignment','bottom')
 title(' ')
%title('Present Value of Expected Cumulative Rehabilitation Cost')
 xlabel('Age, Years');
```

```
 ylabel('Present Value of Expected Rehabilitation Cost');
 xlim([0 max(C(:,1))])
 legend('show')
 grid on
 legend('Location','southeast')
 hold on

 %TAKING INTO ACCOUNT INITIAL COST
data3 = xlsread('lcc.xlsx','initialcost');
C2=cumsum(C(:,2));
C6=C2+data3(1,4);

figure(13)
plot(C(:,1),C6,'-.^','DisplayName','SMA+MC');
%  text(paths(:,1),paths(:,2),num2str(paths(:,2),'%0.2f'),...
%      'HorizontalAlignment','center',...
%      'VerticalAlignment','bottom')
 title(' ')
 %title('Initial Cost and Present Value of Expected Cumulative Rehabilitation Cost')
 xlabel('Age, Years');
 ylabel('Present Value Cost');
 xlim([0 max(C(:,1))])
 ylim([0 max(union(union(max(C3),max(C4)),union(max(C5),max(C6))))*1.1])
 legend('show')
 legend('Location','southeast')
 grid on
 hold on

 %%%%%%%%%%%%%%%%%%%%%%%%%%%%%%%%%%%%%%%%%%%%%%%%%%%%%%%%%%%%%%%%%%%%%%%%%%%%%%%
%%%%%%%%%%%%%%%%%% SMA Fibers %%%%%%%%%%%%%%%%%%%%%%%%%%%%%%%%
%%%%%%%%%%%%%%%%%%%%%%%%%%%%%%%%%%%%%%%%%%%%%%%%%%%%%%%%%%%%%%%%%%%%%%%%%%%%%%%
%obtain the database for the rehabilitiation information from excel file
data = xlsread('lcc.xlsx','Input2');
onerehab = data(:,13);% 1st rehabilitation information
secondrehab=data(:,14);% 2nd rehabilitation information

%mean and std rehab 1
mean1= mean(onerehab);
std1=std(onerehab);

%mean and std rehab 2
mean2= mean(secondrehab);
std2=std(secondrehab);

%z values
z= transpose(linspace(4,-4,81));

% z values times std of 1sr rehab plus mean
newz1=z*std1+mean1;
newz2=z*std2+mean2;

%Probability distribution values
p1=normpdf(newz1,mean1,std1);
p2=normpdf(newz2,mean2,std2);

%Plot PDF
figure (1)
ax1=subplot(2,1,1);
ax2=subplot(2,1,2);

plot(ax1,newz1,p1,'-s','DisplayName','SMA Fibers')
title(ax1,'First rehabilitation');
ylabel(ax1,'Probability')
xlabel(ax1,'Time from construction (Years)')
legend('show')
subplot(2,1,1); hold on

plot(ax2,newz2,p2,'-s','DisplayName','SMA Fibers');
title(ax2,'Second rehabilitation');
ylabel(ax2,'Probability')
xlabel(ax2,'Time from first rehab (Years)')
legend('show')
subplot(2,1,2); hold on

%get years for the rehabilitation descision tree
```

```
newz1= transpose([round(min(newz1)):round(max(newz1))]);
newz2= transpose([round(min(newz2)):round(max(newz2))]);

%for First rehabilitation
newp1=normpdf(newz1,mean1,std1);
figure(2)
plot(newz1,newp1,'-s','DisplayName','SMA Fibers');
% text(newz1,newp1,num2str(newp1,'%0.2f'),...
%     'HorizontalAlignment','center',...
%     'VerticalAlignment','bottom')
title('First Rehabilitation')
xlabel('Time from Construction (Years)');
ylabel('Probability, absolute time (years)');
xlim([0 max(newz1)])
legend('show')
hold on


%Second Rehabilitiation
newp2=normpdf(newz2,mean2,std2);

%Desicion tree calculations

[r1,c1]=size(newz1);
[r2,c2]=size(newz2);

z3=zeros(r1*r2,2);
column1=1;
column2=2;

z4=zeros(r2,1);
z4(1)=r2;

for i=2:r2
    z4(i) = z4(i-1)-1;
end

for i=1:r1
    for a=r2-1:-1:0
        z3(i*r2-a,column1)=newz1(i);
    end
end

for i=1:r1
    for b=r2-1:-1:0
        z3(i*r2-b,column2)=newz2(z4(b+1));
    end
end
% second rehabilitation absolute time
r2a=zeros(size(z3,1),1);
for i=1:size(r2a,1)
    r2a(i)= sum(z3(i,:));
end
%Probability of second rehabilitation
p1r2=zeros(size(z3,1),1);
for i=1:size(p1r2,1)
    p1r2(i)= normpdf(z3(i),mean1,std1);
end
p2r2=zeros(size(z3,1),1);
for i=1:size(p2r2,1)
    p2r2(i)= normpdf(z3(i,2),mean2,std2);
end
cummp2=times(p1r2,p2r2);
%summary table for second rehab
table2=[z3,r2a,cummp2];
X=[r2a,cummp2];
[a,~,c] = unique(X(:,1));
finalp2 = [a, accumarray(c,X(:,2))];
x1=finalp2(:,1);
y1=finalp2(:,2);

figure (3)
plot(x1,y1,'-s','DisplayName','SMA Fibers');
%  text(x1,y1,num2str(y1,'%0.2f'),...
%      'HorizontalAlignment','center',...
```

```
%      'VerticalAlignment','bottom')
 title('Second Rehabilitation')
 xlabel('Time from Construction (Years)');
 ylabel('Probability, absolute time (years)');
 xlim([0 max(x1)])
 legend('show')
 hold on


 %cummulative
 cummyear= zeros(size(newz1,1)+size(x1,1),1);
 for i=1:size(newz1,1)
    cummyear(i)= newz1(i);
    for j=1:size(x1,1)
        cummyear((size(newz1,1))+j)=x1(j);
    end
 end

cummprob=zeros(size(newp1,1)+size(y1,1),1);
 for i=1:size(newp1,1)
    cummprob(i)= newp1(i);
    for j=1:size(y1,1)
        cummprob((size(newp1,1))+j)=y1(j);
    end
 end

Y=[cummyear,cummprob];
[a,~,c] = unique(Y(:,1));
finalp2 = [a, accumarray(c,Y(:,2))];
x2=finalp2(:,1);
y2=finalp2(:,2);

figure (4)
plot(x2,y2,'-s','DisplayName','SMA Fibers');
%  text(x2,y2,num2str(y2,'%0.2f'),...
%      'HorizontalAlignment','center',...
%      'VerticalAlignment','bottom')
 title('P1,A + P2,A')
 xlabel('Age,Years');
 ylabel('Sum of probabilities of annual rehabilitation');
 xlim([0 max(x2)])
 legend('show')
 hold on

cummabsolute=cumsum(y2);
figure (5)
plot(x2,cummabsolute,'-s','DisplayName','SMA Fibers');
title('P1,A + P2,A')
xlabel('Age,Years');
ylabel('Cumulative-Time sum of probabilities of Rehab');
xlim([0 max(x2)])
legend('show')
hold on

%Probability of paths in the descision tree
paths=zeros(size(z3,1),2);
for i=1:size(z3,1)
       paths(i,1)= i;
       paths(i,2)=cummp2(i);
end
figure (6)
plot(paths(:,1),paths(:,2),'-s','DisplayName','SMA Fibers')
%  text(paths(:,1),paths(:,2),num2str(paths(:,2),'%0.2f'),...
%      'HorizontalAlignment','center',...
%      'VerticalAlignment','bottom')
 title('Probability of paths in the descicion tree')
 xlabel('Path number');
 ylabel('Probability of path occurrance');
 legend('show')
 hold on

%EXPECTED REHABILITATION COST
data2 = xlsread('lcc.xlsx','imputcostrehab2');
v = data2(1,1);% discount rate
cost1=data2(1,15);% Undiscounted cost of 1st rehab
```

```
cost2=data2(1,16);% Undiscounted cost of 2nd rehab
table3=[newz1,newp1];
costrehab1= zeros(size(newz1,1),1);
for i=1:size(newz1,1)
    costrehab1(i)=(cost1/((1+v)^(table3(i,1))))*table3(i,2);
end

table4=[x1,y1];
costrehab2=zeros(size(x1,1),1);
for i=1:size(x1,1)
    costrehab2(i)=(cost2/((1+v)^(table4(i,1))))*table4(i,2);
end

sumarytable=zeros(size(x2,1),3);
for i=1:size(x2,1)
     sumarytable(i,1)=x2(i);
     for j=1:size(costrehab1,1)
         sumarytable(j,2)=costrehab1(j);
        for k=1:size(costrehab2,1)
            sumarytable(k+(abs(min(table4(:,1))-min(x2(:,1)))),3)=costrehab2(k);
        end
     end
end

col1=sumarytable(:,1);
col2=sumarytable(:,2);
col3=sumarytable(:,3);

T=table;
T.Age_Years=col1;
T.First_Rehab_Cost=col2;
T.Secod_Rehab_Cost=col3;

figure (20)
uitable('Data',T{:,:},'ColumnName',T.Properties.VariableNames,...
      'RowName',T.Properties.RowNames,'Units', 'Normalized', 'Position',[0, 0, 1, 1]);

%Cummulative cost
C=zeros(size(T,1),2);
for  i=1:size(T,1)
    C(i,1)=col1(i);
    C(i,2)=col2(i)+col3(i);
end

figure(8)
plot(C(:,1),C(:,2),'-s','DisplayName','SMA Fibers');
%  text(paths(:,1),paths(:,2),num2str(paths(:,2),'%0.2f'),...
%      'HorizontalAlignment','center',...
%      'VerticalAlignment','bottom')
 title('Present Value of Expected Rehabilitation Cost')
 xlabel('Age, Years');
 ylabel('Present Value of Expected Rehabilitation Cost');
 xlim([0 max(C(:,1))])
 legend('show')
 hold on

figure(9)
plot(C(:,1),cumsum(C(:,2)),'-s','DisplayName','SMA Fibers');
%  text(paths(:,1),paths(:,2),num2str(paths(:,2),'%0.2f'),...
%      'HorizontalAlignment','center',...
%      'VerticalAlignment','bottom')
 title('Present Value of Expected Cumulative Rehabilitation Cost')
 xlabel('Age, Years');
 ylabel('Present Value of Expected Rehabilitation Cost');
 xlim([0 max(C(:,1))])
 legend('show')
 hold on

%TAKING INTO ACCOUNT INITIAL COST

data3 = xlsread('lcc.xlsx','initialcost');
C2=cumsum(C(:,2));
C3=C2+data3(1,5);

figure(13)
```

```
plot(C(:,1),C3,'-s','DisplayName','SMA Fibers');
%  text(paths(:,1),paths(:,2),num2str(paths(:,2),'%0.2f'),...
%      'HorizontalAlignment','center',...
%      'VerticalAlignment','bottom')
 title('Initial Cost and Present Value of Expected Cumulative Rehabilitation Cost')
 xlabel('Age, Years');
 ylabel('Present Value of Expected Rehabilitation Cost');
 xlim([0 max(C(:,1))])
 legend('show')
 hold on

%%%%%%%%%%%%%%%%%%%%%%%%%%%%%%%%%%%%%%%%%%%%%%%%%%%%%%%%%%%%%%%%%%%%%%%%%%%%%%%
%%%%%%%%%%%%%%%%%% SMA Fibers + MC %%%%%%%%%%%%%%%%%%%%%%%%%%%%%%%%
%%%%%%%%%%%%%%%%%%%%%%%%%%%%%%%%%%%%%%%%%%%%%%%%%%%%%%%%%%%%%%%%%%%%%%%%%%%%%%%
%obtain the database for the rehabilitiation information from excel file
data = xlsread('lcc.xlsx','Input2');
onerehab = data(:,16);% 1st rehabilitation information
secondrehab=data(:,17);% 2nd rehabilitation information

%mean and std rehab 1
mean1= mean(onerehab);
std1=std(onerehab);

%mean and std rehab 2
mean2= mean(secondrehab);
std2=std(secondrehab);

%z values
z= transpose(linspace(4,-4,81));

% z values times std of 1sr rehab plus mean
newz1=z*std1+mean1;
newz2=z*std2+mean2;

%Probability distribution values
p1=normpdf(newz1,mean1,std1);
p2=normpdf(newz2,mean2,std2);

%Plot PDF
figure (1)
ax1=subplot(2,1,1);
ax2=subplot(2,1,2);

plot(ax1,newz1,p1,'->','DisplayName','SMA Fibers+MC')
title(ax1,'First rehabilitation');
ylabel(ax1,'Probability')
xlabel(ax1,'Time from construction (Years)')
legend('show')
subplot(2,1,1); hold on

plot(ax2,newz2,p2,'->','DisplayName','SMA Fibers+MC');
title(ax2,'Second rehabilitation');
ylabel(ax2,'Probability')
xlabel(ax2,'Time from first rehab (Years)')
legend('show')
subplot(2,1,2); hold on

%get years for the rehabilitation descision tree
newz1= transpose([round(min(newz1)):round(max(newz1))]);
newz2= transpose([round(min(newz2)):round(max(newz2))]);

%for First rehabilitation
newp1=normpdf(newz1,mean1,std1);
figure(2)
plot(newz1,newp1,'->','DisplayName','SMA Fibers+MC');
% text(newz1,newp1,num2str(newp1,'%0.2f'),...
%     'HorizontalAlignment','center',...
%     'VerticalAlignment','bottom')
title('First Rehabilitation')
xlabel('Time from Construction (Years)');
ylabel('Probability, absolute time (years)');
xlim([0 max(newz1)])
legend('show')
hold on
```

```
%Second Rehabilitiation
newp2=normpdf(newz2,mean2,std2);

%Desicion tree calculations

[r1,c1]=size(newz1);
[r2,c2]=size(newz2);

z3=zeros(r1*r2,2);
column1=1;
column2=2;

z4=zeros(r2,1);
z4(1)=r2;

for i=2:r2
    z4(i) = z4(i-1)-1;
end

for i=1:r1
    for a=r2-1:-1:0
        z3(i*r2-a,column1)=newz1(i);
    end
end

for i=1:r1
    for b=r2-1:-1:0
        z3(i*r2-b,column2)=newz2(z4(b+1));
    end
end
% second rehabilitation absolute time
r2a=zeros(size(z3,1),1);
for i=1:size(r2a,1)
    r2a(i)= sum(z3(i,:));
end
%Probability of second rehabilitation
p1r2=zeros(size(z3,1),1);
for i=1:size(p1r2,1)
    p1r2(i)= normpdf(z3(i),mean1,std1);
end
p2r2=zeros(size(z3,1),1);
for i=1:size(p2r2,1)
    p2r2(i)= normpdf(z3(i,2),mean2,std2);
end
cummp2=times(p1r2,p2r2);
%summary table for second rehab
table2=[z3,r2a,cummp2];
X=[r2a,cummp2];
[a,~,c] = unique(X(:,1));
finalp2 = [a, accumarray(c,X(:,2))];
x1=finalp2(:,1);
y1=finalp2(:,2);

figure (3)
plot(x1,y1,'->','DisplayName','SMA Fibers+MC');
%  text(x1,y1,num2str(y1,'%0.2f'),...
%      'HorizontalAlignment','center',...
%      'VerticalAlignment','bottom')
 title('Second Rehabilitation')
 xlabel('Time from Construction (Years)');
 ylabel('Probability, absolute time (years)');
 xlim([0 max(x1)])
 legend('show')
 hold on


 %cummulative
 cummyear= zeros(size(newz1,1)+size(x1,1),1);
 for i=1:size(newz1,1)
    cummyear(i)= newz1(i);
    for j=1:size(x1,1)
        cummyear((size(newz1,1))+j)=x1(j);
    end
 end
```

```
cummprob=zeros(size(newp1,1)+size(y1,1),1);
 for i=1:size(newp1,1)
    cummprob(i)= newp1(i);
    for j=1:size(y1,1)
        cummprob((size(newp1,1))+j)=y1(j);
    end
 end

Y=[cummyear,cummprob];
[a,~,c] = unique(Y(:,1));
finalp2 = [a, accumarray(c,Y(:,2))];
x2=finalp2(:,1);
y2=finalp2(:,2);

figure (4)
plot(x2,y2,'->','DisplayName','SMA Fibers+MC');
%  text(x2,y2,num2str(y2,'%0.2f'),...
%      'HorizontalAlignment','center',...
%      'VerticalAlignment','bottom')
 title('P1,A + P2,A')
 xlabel('Age,Years');
 ylabel('Sum of probabilities of annual rehabilitation');
 xlim([0 max(x2)])
 legend('show')
 hold on

cummabsolute=cumsum(y2);
figure (5)
plot(x2,cummabsolute,'->','DisplayName','SMA Fibers+MC');
title('P1,A + P2,A')
xlabel('Age,Years');
ylabel('Cumulative-Time sum of probabilities of Rehab');
xlim([0 max(x2)])
legend('show')
hold on

%Probability of paths in the descision tree
paths=zeros(size(z3,1),2);
for i=1:size(z3,1)
       paths(i,1)= i;
       paths(i,2)=cummp2(i);
end
figure (6)
plot(paths(:,1),paths(:,2),'->','DisplayName','SMA Fibers+MC')
%  text(paths(:,1),paths(:,2),num2str(paths(:,2),'%0.2f'),...
%      'HorizontalAlignment','center',...
%      'VerticalAlignment','bottom')
 title('Probability of paths in the descicion tree')
 xlabel('Path number');
 ylabel('Probability of path occurrance');
 legend('show')
 hold on

%EXPECTED REHABILITATION COST
data2 = xlsread('lcc.xlsx','imputcostrehab2');
v = data2(1,1);% discount rate
cost1=data2(1,18);% Undiscounted cost of 1st rehab
cost2=data2(1,19);% Undiscounted cost of 2nd rehab
table3=[newz1,newp1];
costrehab1= zeros(size(newz1,1),1);
for i=1:size(newz1,1)
    costrehab1(i)=(cost1/((1+v)^(table3(i,1))))*table3(i,2);
end

table4=[x1,y1];
costrehab2=zeros(size(x1,1),1);
for i=1:size(x1,1)
    costrehab2(i)=(cost2/((1+v)^(table4(i,1))))*table4(i,2);
end

sumarytable=zeros(size(x2,1),3);
for i=1:size(x2,1)
     sumarytable(i,1)=x2(i);
     for j=1:size(costrehab1,1)
```

```
         sumarytable(j,2)=costrehab1(j);
        for k=1:size(costrehab2,1)
            sumarytable(k+(abs(min(table4(:,1))-min(x2(:,1)))),3)=costrehab2(k);
        end
    end
end

col1=sumarytable(:,1);
col2=sumarytable(:,2);
col3=sumarytable(:,3);

T=table;
T.Age_Years=col1;
T.First_Rehab_Cost=col2;
T.Secod_Rehab_Cost=col3;

figure (21)
uitable('Data',T{:,:},'ColumnName',T.Properties.VariableNames,...
      'RowName',T.Properties.RowNames,'Units', 'Normalized', 'Position',[0, 0, 1, 1]);

%Cummulative cost
C=zeros(size(T,1),2);
for  i=1:size(T,1)
    C(i,1)=col1(i);
    C(i,2)=col2(i)+col3(i);
end

figure(8)
plot(C(:,1),C(:,2),'->','DisplayName','SMA Fibers+MC');
%  text(paths(:,1),paths(:,2),num2str(paths(:,2),'%0.2f'),...
%      'HorizontalAlignment','center',...
%      'VerticalAlignment','bottom')
 title('Present Value of Expected Rehabilitation Cost')
 xlabel('Age, Years');
 ylabel('Present Value of Expected Rehabilitation Cost');
 xlim([0 max(C(:,1))])
 legend('show')
 hold on

figure(9)
plot(C(:,1),cumsum(C(:,2)),'->','DisplayName','SMA Fibers+MC');
%  text(paths(:,1),paths(:,2),num2str(paths(:,2),'%0.2f'),...
%      'HorizontalAlignment','center',...
%      'VerticalAlignment','bottom')
 title('Present Value of Expected Cumulative Rehabilitation Cost')
 xlabel('Age, Years');
 ylabel('Present Value of Expected Rehabilitation Cost');
 xlim([0 max(C(:,1))])
 legend('show')
 hold on

%TAKING INTO ACCOUNT INITIAL COST

data3 = xlsread('lcc.xlsx','initialcost');
C2=cumsum(C(:,2));
C3=C2+data3(1,6);

figure(13)
plot(C(:,1),C3,'->','DisplayName','SMA Fibers+MC');
%  text(paths(:,1),paths(:,2),num2str(paths(:,2),'%0.2f'),...
%      'HorizontalAlignment','center',...
%      'VerticalAlignment','bottom')
 title('Initial Cost and Present Value of Expected Cumulative Rehabilitation Cost')
 xlabel('Age, Years');
 ylabel('Present Value of Expected Rehabilitation Cost');
 xlim([0 max(C(:,1))])
 legend('show')
 hold on
npvsteel=max(C3);
npvsmamc=max(C6);

T=table;
T.NPVSteel=npvsteel;
T.NPVSteelMc=npvsteelmc;
T.NPVSMA=npvsma;
```

```
T.NPVSMAMc=npvsmamc;
figure (14)
uitable('Data',T{:,:},'ColumnName',T.Properties.VariableNames,'RowName',T.Properties.RowNames,'Units',
'Normalized', 'Position',[0, 0, 1, 1]);
```

VITA

Luis Bonilla was born in1992 in San Salvador, El Salvador. In 2013, he finished his Bachelor of Science in Civil Engineering from Louisiana State University. He obtained his Master of Science in 2016 from Louisiana State University. He is a candidate for the Doctor of Philosophy degree in engineering science.